Application of Sparse Feedback Control Strategies to Civil Structures

A THESIS
SUBMITTED TO THE FACULTY OF THE GRADUATE SCHOOL
OF THE UNIVERSITY OF MINNESOTA
BY

Reuben D. Verdoljak

IN PARTIAL FULFILLMENT OF THE REQUIREMENTS
FOR THE DEGREE OF
MASTER OF SCIENCE

Dr. Lauren E. Linderman

May, 2016

Acknowledgements

I would like to express my gratitude to Professor Lauren Linderman for her encouragement, knowledge, and guidance, which were instrumental in both my graduate education and in the research that comprises this thesis. Without her, I would not have been introduced to structural control and a variety of other topics that will undoubtedly prove useful in my future as a structural engineer.

I would also like to thank my thesis committee, Prof. Mihailo Jovanovic and Prof. Arturo Schultz, for their willingness to share their knowledge and time in the thesis process. Prof. Schultz has instructed me on a variety of subjects within Structural Engineering, sharing his wealth of knowledge from masonry to seismic events, and Prof. Jovanovic has helped me to expand my knowledge into the realm of Control Theory, while always being happy to answer any of my questions.

I am particularly grateful to the people of the department of Civil, Environmental, and Geo-Engineering for accepting me and instructing me in both undergraduate and graduate degree programs, and especially to Prof. Joe Labuz and Prof. Cathy French, who pushed me to complete a masters degree when I was hesitant to do so. I am also thankful to all of the professors and staff within CEGE that have helped and encouraged me for the last seven years. My special thanks are extended to Paul Bergson, who helped greatly in the shake table and specimen design processes.

When I started looking at colleges, my parents encouraged me to pursue a degree in Civil Engineering. I am thankful for their advice, but I am especially thankful for their continuing love and support as I continue on from graduate school.

Finally, I would like to thank my wife, Annie, for her love, constancy, and patience, which are the foundations of my life and education, Briar, who is the definition of unconditional love, and Joule, I guess.

Abstract

Modern structural control systems use centralized, wired sensor feedback to impart counter forces based on measurement of the response. However, centralized systems can be sensitive to sensor failure, controller failure, and the reliability of sensor links. The recent study of wireless control systems has encouraged decentralized control approaches to overcome wireless structural control challenges, including limiting the wireless communication required and the associated slow sampling rate and time delays in the control system. Decentralized control offers the additional advantages of multiple independent controllers and small subsets of measurement feedback. Previous decentralized structural control algorithms, both Ad-Hoc and Heuristic, enforce a spatial sparsity pattern during the design, which is assumed *a priori*. Therefore, the optimal feedback structure is not considered in the design. This work explores a decentralized optimal LQR design algorithm (LQRSP) where the sparsity of the feedback gain is incorporated into the objective function. The control approach is compared to previous decentralized control techniques on 5- and 20-Story control benchmark structures fitted with active or semi-active systems. Additionally, the sparsity and control requirements are compared to centralized designs to gain insight on the overall performance of sparse feedback systems. The LQRSP program and its additional parameters are explored more fully to make informed control decisions, further enhancing the decentralized control design. The optimal sparse feedback design offers the best balance of performance, measurement feedback, and control effort, while clearly highlighting important feedback control measurements. Additionally, the feedback structure identified is not easily identifiable *a priori* in the reduced order model of the 20-story structure, highlighting the significance of particular measurements in this feedback framework. To bridge the gap between simulation and reality, the LQRSP design is extended to a discrete time simulation system to incorporate wireless transmission time as well as sensor and estimation noise. A 5-Story specimen with semi-active control devices is designed for a uniaxial shake table for future physical testing of various centralized and decentralized control algorithms during seismic excitations.

Contents

List of Tables

List of Figures

Chapter 1

Introduction

1.1 Motivation

Dynamic loading of structures, especially from earthquakes, can be extremely dangerous to building occupants and costly to society. Earthquakes are both unpredictable and potentially damaging to civil infrastructure, which makes mitigating their risks a goal of building codes and source of research. Current design codes in the United States aim to prevent collapse in large seismic events through controlled damage, which results in fewer deaths, but may still require significant repairs or demolition of the structure.

Structural control is an attractive option for limiting structural response to dynamic loading in these events. Rather than dissipating energy through damage of the structure, control systems limit the vibration response of the structure by altering its mass or stiffness, or by introducing counter forces through a supplemental damping device. Control approaches can be divided into four categories: passive, active, semi-active, and hybrid. Some prevailing passive control options are base isolation systems or tuned mass dampers (TMDs), which decrease response of the structure at the predominant natural frequency, and viscous dampers, which dissipate energy. However, these passive systems can be ineffective in seismic events due to the broadband frequency content of earthquakes. Active and semi-active systems take real-time measurements of the structural response in order to prescribe a desired counter-force in the structural control system. Active control achieves this force through an active control device, such as an active mass driver (AMD), while semi-active control uses passive dampers with variable properties, such as semi-active hydraulic dampers (SHDs) or magnetorheological (MR)

dampers. The passive SHDs and MR dampers dissipate energy and provide forces dependent on the response of the system, rendering them inherently stable, while active devices are capable of inputting additional energy to the system, potentially leading to structural instability. Therefore, semi-active devices provide the best path forward for acceptance in future building codes provided they are capable of supplying the desired level of control force.

To prescribe counter forces in real-time, classical control techniques rely on full-state feedback, where all sensor measurements return to a single centralized controller. While these centralized control systems offer theoretically optimal results, they can be costly to install in large structures and have a single point of failure. With the advent of wireless sensors and controllers, decentralized control techniques, which only rely on local or nearby sensor information, become more attractive. A centralized control system may not be feasible when utilizing wireless sensors due to potential problems with latency, sampling rate, and data loss when sending information wirelessly. On the other hand, decentralized control prioritizes information at each controller, limiting the required feedback and the associated challenges of centralized control.

The challenge with decentralized control lies in the feedback control calculation. Centralized control has a clear globally optimal solution, while decentralized control is necessarily suboptimal. Therefore, several decentralized control approaches have been proposed to search for the global minimum solution in the structured feedback gain space. The two main frameworks for both centralized and decentralized control lie within H_2/LQR control, where the system response is minimized over all frequencies, or H_∞ control, where the maximum system response is minimized. This work will focus on optimal decentralized control within the LQR framework. A heuristic method presented by Lunze (1992) provides a searching algorithm for optimizing an H_2 structured feedback control design; however, to use the heuristic method, the most important measurement feedback information must be determined in an ad-hoc manner. In order to optimize the structure of the gain matrix, Lin et al. (2013) have proposed a decentralized control design algorithm (LQRSP) in which the sparsity of the feedback gain matrix is incorporated into the objective cost function. By determining the most important information links within a decentralized control system in an optimized routine, LQRSP provides the control designer with the ability to optimize the decentralized structure as well as the final feedback gains. Because of its ability to find important feedback

links, LQRSP is particularly powerful in computing structured feedback gains where the optimal feedback gain structure is not immediately apparent.

Benchmark structures are used to compare the different control design approaches. By using standardized benchmark structures for modeling and earthquake simulations, the results gleaned from any research can be compared to other researchers using the same benchmark structures. The two steel structures chosen to compare the LQRSP and Heuristic decentralized approaches to LQR, passive, and uncontrolled approaches are the 5-Story Kajima-Shizuoka building as presented by Kurata et al. (1999) and modified by Wang (2007), and the 20-Story SAC Phase II Steel Project building, as designed by Brandow & Johnston Associates and laid out by Ohtori (2000). The 5-Story structure is modeled as a shear structure with collocated sensors and control devices to provide a relatively simple and intuitive optimal feedback gain structure, while the 20-Story structure requires a model reduction, obscuring the optimal feedback gain structure.

1.2 Overview of Research

The objective of this research is to evaluate the performance of decentralized controllers on civil structures. The LQRSP algorithm, which makes no assumptions *a priori*, will be compared to classical centralized and decentralized LQR approaches. This comparison will be done through numerical simulations of benchmark control structures. In addition, a specimen design with semi-active control devices will be presented for the physical testing of the control algorithms during uniaxial shake table excitations. The result of the research will be the validation of a new decentralized control approach for the control of civil structural systems.

- Chapter 2 presents a brief overview of structural control and various approaches for reducing structural response to place the techniques in context. The overview includes different approaches to control theory, different control devices and their challenges, and the movement of research toward wireless control systems and decentralized control. The recent advances in decentralized control are presented in this chapter. Two benchmark structures used as comparison tools for control design approaches are presented, along with their applications and challenges. Review of theory to be considered in the specimen design is also considered.

- Chapter 3 provides the theory and derivations of the control systems used in the

research. The basis of structural control, including the dynamics of structures, the state-space system conventions, and the LQR theory, is presented. The extension of LQR to the Heuristic and LQRSP methods is outlined, and all systems are extended to discrete time to incorporate time delay into the design. Finally, the semi-active damper model used in simulations is defined.

- Chapter 4 compares the various control methods in the continuous-time domain. The H_2 norm calculated with each control design is compared at varying levels of feedback gain sparsity, while the additional parameters in LQRSP are used to refine the control design. The 5- and 20-Story benchmark structures with active and semi-active control are then used to compare the earthquake responses of the structures equipped with different control approaches, and steady-state results are calculated to verify the earthquake simulation results. In addition, the discrepancies between the LQRSP and Heuristic optimizations are determined.

- Chapter 5 extends the LQRSP evaluation to the discrete-time domain. This allows the simulations to take into account further physical limitations, including time delay and measurement noise. Various degrees of decentralization are compared to determine the effect of time delay as subsystem size increases. Potential loss of information during a seismic event is also considered.

- Chapter 6 provides the design of a physical specimen to be used for uniaxial shake table tests. Design considerations and calculations are presented, as well as the final drawings for the main specimen features.

- Chapter 7 presents the conclusions of the thesis and direction of future research.

Chapter 2

Literature Review

This chapter presents a background of structural control and various approaches for reducing structural response. Different approaches to control theory and different control devices are reviewed, two benchmark structures are presented for control comparison, similitude studies and earthquake records for physical specimens are considered, and model reduction techniques are investigated.

2.1 Structural Control

Structural control is an attractive approach to limiting structural response to natural hazards. Transient events, such as earthquakes, are difficult to design for due to their large effective lateral forces and unknown frequency characteristics. Some buildings may escape unscathed from a given earthquake, while others are heavily damaged due to their modal characteristics. The prevailing design approach in the United States encourages ductility and energy dissipation in the structure through localized damage during large events to ensure life safety.

Control systems, on the other hand, alter the mass, stiffness, or add a supplemental damping device in the structural system to limit its vibration response (Yao 1972). The field of structural control evolved out of aerospace control, and gained popularity gradually until the Northridge and Kobe earthquakes in 1994 and 1995, respectively, showed a great need for improved structural performance in earthquakes (Housner et al. 1997).

There are four types of structural control: passive, active, semi-active, and hybrid

(Housner et al. 1997). Passive control systems are more widely used due to their stability and lack of need for external power, of which the tuned mass damper (TMD) and base isolation are the most prevalent. Additional passive damping systems are also an option, in which the damage to the structure is either relocated to a specific replaceable yield point, or dampers without adaptable charateristics are added, such as viscoelastic, metallic yield, friction, or viscous fluid dampers. Often, the passive dampers are employed for vibration mitigation, such as in wind loading. However, most earthquakes are broadband excitations, affecting multiple natural frequencies of the structure. While passive dampers dissipate energy from a structural system, they are sometimes unable to appreciably decrease response to broadband excitations. If the dampers are too soft, the natural frequencies of a system remain the same while the peak frequency response is decreased slightly, but if the dampers have higher viscosity, the natural frequencies of the structure may increase to a frequency where the earthquake has higher energy, offsetting the energy dissipation of the dampers.

As many destructive earthquakes have a similar range of frequency content, increasing the natural frequencies of the building can be effective in mitigating some damage, but the system may need to be made unreasonably stiff for this to be effective in more destructive earthquakes. Control systems that impart forces based on feedback of measurement of the response—active, semi-active, and hybrid systems—offer adaptability and can be effective over a broader frequency range (Soong and Chen 1990). Active systems add or dissipate energy from a structural system using an active mass driver (AMD) or similar device (Housner et al. 1997). An example of a current active control system is the Kyobashi Seiwa building, which has multiple AMDs controlling building sway and torsion installed in 1989 (Kobori 1990). This ability to add energy to the system allows a control system to prescribe internal forces regardless of the current building response. While this is advantageous in a controlled structure when the desired control force is in the same direction as the current velocity, this also makes it possible for active control to destabilize a system. Therefore, uncertainty in the system may lead to system instability, and robustness of the active control system is then of great importance (Housner et al. 1997). In addition, the power requirements for the system make active control less practical for large-scale implementation.

Semi-active control, on the other hand, has guaranteed bounded input, bounded output (BIBO) stability and very low power requirements (Housner et al. 1997). Because

semi-active control combines the best features of both passive and active control it is the most likely feedback control technique to be accepted by practitioners in the United States (Housner et al. 1997). A semi-active system is guaranteed to only dissipate energy from the structural system, guaranteeing stability. Semi-active control devices include SHD, variable orifice, variable friction, and magnetorheological (MR) dampers. They are also able to operate on battery power during seismic events, which is critical due to the likelihood of interrupted power supply during an earthquake. For example, a 70 W power supply can power a semi-active hydraulic damper (SHD) with a maximum force of 1000 kN [225 kip] (Kurata et al. 1999). The concern with semi-active control is the uncertainty of the available counter force; the desired feedback control force can be much greater than or in the opposite direction of the force the damper can provide given the current location and velocity of the damper. However, Dyke et al. (1996) showed that semi-active control systems perform better than passive systems and even approach the effectiveness of active systems. While passive systems affect smaller bands of the frequency response of a structural system, semi-active (and active) control is able to effectively reduce the peak frequency reponses of the system over broad bands of frequency content.

The growing use of structural control systems in the world is outlined by Spencer and Nagarajaiah (2003). Most of the buildings outfitted with structural control systems are in Japan or Taiwan, showing the difficulties this technology has in being adopted in the United States. In addition, the vast majority of installed systems at the time of publishing were either active or hybrid systems, while semi-active systems were still in their infancy. The authors acknowledged the fact that semi-active systems were less used, but they also considered semi-active control to be the answer to many of the problems that keep active control from widespread acceptance: cost of installation and maintenance, large external power requirements, and potential for system instability.

In order to prescribe counter forces in an active or semi-active system, LQR/H_2 or H_∞ theory can be used to compute feedback gains. Traditional LQR/H_2 control design relies on a centralized feedback control system, where all measurements taken throughout the structure must be passed to a single controller, often through wired connections (Sandell et al. 1978). In this case, all sensors affect every actuator input and all measurements are fed back to a single point, which makes the system vulnerable

to both sensor and controller failure. To mitigate the risks of centralized control, decentralized control has been proposed to prioritize information passed between sensors and actuators, or between groups thereof.

Specific to civil infrastructure is the large scale of the system, which can lead to costly and time-consuming instrumentation and cable installation (Wang 2007). Due to advancement in wireless technology, wireless sensors have been increasing in popularity and have been subject to much research in the feasibility of wireless sensors and controllers in civil systems (Linderman and Spencer 2014, Lynch et al. 2008, Wang and Law 2011). Because of their low costs, wireless sensors provide a cost-effective alternative to traditional tethered control systems. However, due to wireless communication being much slower than wired communication, communication time must be considered and restricted in wireless controller design. If full-state feedback is desired, the size of the system may cause the wireless controllers to run prohibitively slowly; wireless sensors therefore are likely more compatible with decentralized control methods in which fewer communication links are required.

Wireless decentralized control has been shown to be an effective control approach, but there are still challenges to be addressed beyond controller design. Wireless transceivers can use a significant amount of power, beyond what potential energy harvesting techniques can provide; therefore, a battery is necessary (Lynch et al. 2004). The more battery power required in a structural control system, the greater the need for additional maintenance. By their nature, wireless systems also have an associated sampling rate that depends on data transmission size and distance (Wang 2007). The sampling rate can also be affected by time delays due to lost or blocked data, or due to clock imprecision (Lei et al. 2005). These challenges of wireless control must be considered by taking sampling rate into consideration and designing robust systems for the case of lost or delayed data.

Another challenge to be considered in structural control is in the building model. Larger structures may have complex models, so a reduced model will need to be considered (Soong and Chen 1990). While the input-output behavior of a reduced system model remains the same, the decentralized feedback control design becomes more complicated and less intuitive. Ad-Hoc decentralized control methods become difficult to use because the states used to describe the system no longer have a physical meaning.

This makes decentralized control design especially difficult in systems where state estimation is used, which is a common approach in determining the response of a building from limited measurements.

2.2 Decentralized Control

Centralized LQR/H_2 control has been proven to have an analytical solution, while decentralized control has no true optimal solution. However, the issues of potential system failure and system deployment in centralized control, especially as they pertain to civil structural systems, make decentralized control a more attractive choice (Sandell et al. 1978). The basic idea behind decentralized control is to somehow restrict the information passed between sensors and controllers while maintaining a desired level of control. However, the methods of restricting the feedback gain structure and tuning the resulting gains have no clear optimal solution.

There are three types of decentralized control: fully decentralized control, partially decentralized control, and hierarchically decentralized control (Lynch and Law 2002). In the fully decentralized case, local state knowledge is only shared with the local controller. Partially decentralized control allows some communication between nearby controllers, which should improve the system control, but may also result in worsened control due to increased communication time between controllers. Finally, hierarchically decentralized control adds another higher level of controllers that ensure separate controllers are not working against each other to degrade global performance. This work will focus on fully and partially decentralized control.

2.2.1 Ad-Hoc and Structured Optimal Control Methods

The simplest way to create a decentralized architecture is to calculate the optimal centralized LQR gain matrix and zero out terms that correspond to unwanted communication links (Lynch and Law 2002). Determining the decentralized gain matrix this way is termed an Ad-Hoc approach. Desired communication links can be selected by looking at the magnitude of the gains; the larger a gain value, the more important that measurement is to the given controller. This approach is appealing for idealized systems due to its own simplicity, and it can be applied somewhat effectively to a lumped mass system. However, stability is not guaranteed in this approach, and just because

the values were pulled directly from the optimal LQR gain matrix does not make it an optimal solution.

The Ad-Hoc approach can be extended to implement a heuristic tuning to determine a structured optimal decentralized controller (Lynch and Law 2002). The iterative approach proposed by Lunze (1992) can be used to calculate the optimal heuristic gain matrix by searching the solution space for the minimum H_2 norm. Similar to the LQR solution, the quadratic cost of the gain matrix is determined from the trace of the Riccati solution matrix, except now the gain matrix has a decentralized architecture, and the cost must be determined at each solution step (Wang 2007). In each solution step, an auxiliary matrix and the Lagrangian multiplier matrix are calculated for the current gain matrix with sparsity constraints imposed. These matrices are used to calculate the search gradient for the quadratic cost of the decentralized gain matrix. Stability is enforced at each time step, and as the search gradient goes to zero, the solution converges to a minimum H_2 norm. As this is a heuristic tuning, the final solution is dependent on search step size and initial guess, so the calculated gain matrix is sometimes a sub-optimal local minimum of the solution space. However, it is implementable on any system where the gain matrix can easily be determined *a priori* and provides a marked improvement over the Ad-Hoc method (Lynch and Law 2002). Lynch and Law (2002) were able to significantly improve performance of a 20-Story lumped mass structure during simulated continuous-time earthquake excitations with the Heuristic technique, and Wang (2007) also was able to improve performance of a physical 3-Story steel structure with a discrete-time Heuristic controller.

The optimal design of structured feedback gains has a long history in controls community and was recently revisited by Fardad et al. (2009) and Lin et al. (2011). Rather than using the auxiliary and Lagrangian multiplier matrices within the optimal structured feedback gain calculation, the closed-loop observability and controllability gramians are utilized. Lin et al. (2011) have also employed the augmented Lagrangian approach to determine the stabilizing optimal feedback gain matrix with the desired sparsity patterns.

2.2.2 LQRSP

A new approach for optimal sparse control called the Sparsity-Promoting Linear Quadratic Regulator (LQRSP) has been proposed by Lin et al. (2013). It uses the LQR

framework, but no gain matrix structure is assumed *a priori* as with the Ad-Hoc Methods. Instead of minimizing only the LQR quadratic cost function, a sparsity cost function is added to the objective function. Both are combined and the new objective function is minimized. A sparsity multiplier is used to specify the desired level of sparsity in the gain matrix. If the sparsity multiplier is zero, the LQR cost equation is recovered. As the sparsity multiplier is increased, more weight is placed on the sparsity cost, and additional entries in the gain matrix are zeroed to lower the sparsity cost function contribution (Fardad et al. 2011).

LQRSP uses the Alternating Direction Method of Multipliers (ADMM) to step slowly from the LQR gain matrix structure to the optimal decentralized gain matrix structure (Lin et al. 2013). The ADMM is able to provide a good starting guess for the polishing step used to optimize the structured feedback gain matrix. LQRSP has shown to be effective in both a simple mass-spring system, where the expected diagonal gain matrix structure was uncovered, and in a randomly and uniformly distributed network of nodes with unstable dynamics, where the decentralized feedback gain matrix with only 20% of the non-zero elements relative to the LQR feedback gain matrix corresponded to less than a 10% decrease in control performance. Therefore, both the decentralized feedback gain structure and the feedback gain tuning are seen to be improved with LQRSP.

In addition to the computation of the optimal feedback gain, the LQRSP framework has proved useful in other applications. The optimization program can be used alongside a framework that optimizes sensor and actuator locations, further optimizing the feedback control system (Dhingra et al. 2014). LQRSP has also been useful in technological applications, especially in the sparse control of power systems (Dörfler et al. 2013, Dörfler et al. 2014, Wu et al. 2016). With a wide range of potential applications and successful implementation on other control problems, the LQRSP approach offers a clear extension into the control of civil structures.

The LQRSP software that is utilized for continuous-time analysis in this thesis is available for download at `http://www.ece.umn.edu/users/mihailo/software/lqrsp/index.html`. The discrete-time software, though not currently available for download, is also provided by the same research group.

2.3 Benchmark Structures

The use of benchmark structures is common in evaluating new structural control techniques (Kurata et al. 1999, Ohtori et al. 2000, Spencer et al. 1998). By using common structures and similar ground motions, comparisons can be made more consistently between different control designs and control devices.

2.3.1 5-Story Benchmark

One benchmark structure of interest is the Kajima-Shizuoka building, a 5-Story benchmark steel structure with 8 semi-active hydraulic dampers (SHDs) in the direction of interest (Kurata et al. 1999). A modified Kajima-Shizuoka building with 10 SHDs as presented by Wang (2007) is considered, as seen in Figure 2.1 with parameters in Table 2.1. With relatively simple floor plans, large masses lumped at each story height, and a low-rise profile, the Kajima-Shizuoka building is analyzed as a shear building. This simplifies the dynamic analysis of the structure—while horizontal degrees of freedom are measured and controlled, vertical and rotational degrees of freedom are negligible. If sensors and control devices are assumed to be collocated as in Wang (2007), the LQR framework is very intuitive and easy to implement. As such, even decentralized feedback gains where the decentralized structure is assumed *a priori* perform well compared to the centralized LQR approach (Wang et al. 2006). With a collocated shear building, the feedback gain matrix naturally reduces to a fully decentralized architecture, where only local information is needed. This allows the 5-Story Kajima-Shizuoka building to be a natural first step in analyzing and verifying new control designs.

Table 2.1: Kajima-Shizuoka Building model parameters (Wang 2007).

Floor	**Seismic Mass [kg]**	**Interstory Stiffness [kN/m]**
1	215.2 x 10^3	147 x 10^3
2	209.2 x 10^3	113 x 10^3
3	207.0 x 10^3	99 x 10^3
4	204.8 x 10^3	89 x 10^3
5	266.1 x 10^3	84 x 10^3
Damping: 5% Natural Damping		

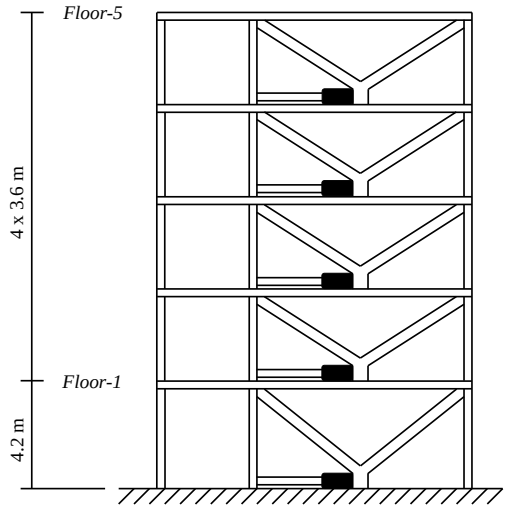

Figure 2.1: Kajima-Shizuoka building elevation (Wang 2007). There are two dampers at each story, collocated with a sensor. The five natural frequencies are 1.01 Hz, 2.82 Hz, 4.49 Hz, 5.80 Hz, and 6.77 Hz.

2.3.2 20-Story Benchmark

The second benchmark structure considered is a 20-Story steel building, as designed by Brandow & Johnston Associates for the SAC Phase II Steel Project and laid out by Ohtori et al. (2000). It is a typical high-rise structure for the Los Angeles area with five bays and two basement stories. The first three natural frequencies are 0.26 Hz, 0.75 Hz, and 1.30 Hz. Various damper layouts are considered (Lynch and Law 2002, Ohtori et al. 2000, Wang 2007), but the results in the following sections rely on the damper layout proposed by Wang (2007). The full model of the 20-Story benchmark structure requires 291 degrees of freedom, and some of the natural frequencies are up to 10^8 Hz, which are too fast and unnecessary for the simulations considered. Therefore, a model reduction that preserves the input-output behavior of the structure is required.

One way to reduce the model for in-plane excitations is to use a lumped-mass model, similar to the 5-Story benchmark analysis (Kurata et al. 1999). While this method retains all of the states of interest, the input-output behavior in the system is not necessarily preserved when vertical and rotational degrees of freedom are also considered. A Guyan reduction is also considered, which eliminates states where no force is applied (Guyan 1965). The Guyan approach is useful for reducing states with very low energies

and very high natural frequencies, as is done by Ohtori et al. (2000). The final model reduction approach considered is balanced reduction, where the lowest energy states are eliminated from the system. The energy of each state can be computed with the Hankel singular values of the system, which gives a measure of the energy of a given state in the input-output behavior of the system.

2.3.3 Specimen Design

Due to the relatively simple nature of the Kajima-Shizuoka building, it was also chosen to be a basis for the scale model used for physical testing on a uniaxial shake table. In order to match the dynamic characteristics of the roughly 1/10 scale model, dynamic similitude is considered.

Dynamic Similitude

Two key scaling numbers in similitude studies are the Cauchy and the Froude numbers (Harris and Sabnis 1999, Williams and Blakeborough 2001). The Cauchy number gives a ratio of the inertial forces and the elastic restoring forces, and the Froude number gives a ratio of the inertial forces and the gravity forces. True Replica models match the Cauchy and Froude numbers of the full scale structure, which means that the inertial, gravitational, and restoring forces will be duplicated in the model (Harris and Sabnis 1999). These scaling ratios are particularly useful for structures where the stress-strain behavior of the structure is investigated. However, the true replica models are difficult to build and test due to mass scaling requirements.

Matching the Cauchy and Froude numbers of the full scale structure also implies that the mass-scale factor will be the inverse of the length-scale factor, while the time-scale factor will be the square root of the length-scale factor (Williams and Blakeborough 2001). For example, if the scale model is 1/10 scale, the specific mass would increase by a factor of 10 and the time scale will be decreased by a factor of 3.16. However, the compression of the time scale leads to larger earthquake content at higher frequencies.

As both Harris and Sabnis (1999) and Williams and Blakeborough (2001) noted, it is extremely difficult to match both the Froude and Cauchy numbers, especially for a small structure. At 1/10 scale, the time scaling would result in ground motions that are not achievable by a shake table, especially when running earthquakes with large high-frequency content. Therefore, the first step to creating a suitable scale model should be

to simply match the eigenvalues and eigenvectors of the system.

Wang (2007) and Wang et al. (2006) verified their control algorithm through physical testing by scaling the earthquake ground records to a peak ground acceleration (PGA) of 1 m/s^2. The safety of the structure was ensured by lessening column stresses through scaling the accelerations of the earthquake records rather than scaling the time. Their three story structure has natural frequencies of 1.18Hz, 3.26Hz, and 4.84Hz, which are similar to the natural frequencies of the Kajima-Shizuoka building. By verifying the numerical simulation with the physical testing at low accelerations, the numerical simulations can be extended to larger systems and ground motions, leading to verification of the effectiveness of new control algorithms.

2.4 Summary

In this chapter, an overview of structural control is presented. Advantages and challenges of centralized and decentralized control are investigated, and two frameworks for providing optimized decentralized control are explored. Two benchmark structures used for comparison of control techniques are presented, and their uses in control literature are documented. Finally, a study of dynamic similitude and physical testing is done with the purpose of designing a specimen for physical comparison and verification of control designs.

Chapter 3

Theory

In this chapter, the theory used in creating optimal controllers is laid out for both centralized and decentralized systems.

3.1 Lumped Mass System

For a building such as the Kajima-Shizuoka building (Figure 2.1), it is convenient to write the equations of motion as a lumped mass system with j stories as:

$$\mathbf{M}\ddot{\mathbf{x}}_{abs} + \mathbf{C}\dot{\mathbf{x}} + \mathbf{K}\mathbf{x} = \mathbf{u} \tag{3.1}$$

where $\mathbf{M}$ is the lumped mass matrix of the building, $\mathbf{C}$ is the damping matrix of the building, $\mathbf{K}$ is the stiffness matrix of the building. $\mathbf{x}$ is the displacement of each story relative to the ground, $\dot{\mathbf{x}}$ is the velocity of each story relative to the ground, $\ddot{\mathbf{x}}_{abs}$ is the absolute global acceleration of each story, and $\mathbf{u}$ is the force input at each story. In a lumped mass system, $\mathbf{M}$ is diagonal and $\mathbf{K}$ is tridiagonal. All of the matrices of the system are $j \times j$ matrices and all of the vectors are $j \times 1$ vectors. To simplify the system, the absolute accelerations can be broken into ground accelerations $\ddot{\mathbf{x}}_g$ and accelerations relative to the ground $\ddot{\mathbf{x}}$

$$\ddot{\mathbf{x}}_{abs} = \ddot{\mathbf{x}}_g + \ddot{\mathbf{x}} \tag{3.2}$$

and Equation 3.1 can be rewritten as

$$\ddot{\mathbf{x}} = -\ddot{\mathbf{x}}_g - \mathbf{M}^{-1}\mathbf{K}\mathbf{x} - \mathbf{M}^{-1}\mathbf{C}\dot{\mathbf{x}} + \mathbf{M}^{-1}\mathbf{u} \tag{3.3}$$

Within this framework, it becomes convenient to solve this second order differential equation as two first order differential equations in state-space format with $\dot{\mathbf{x}}_1 = \dot{\mathbf{x}}$ and $\dot{\mathbf{x}}_2 = \ddot{\mathbf{x}}$.

$$\begin{Bmatrix} \dot{\mathbf{x}}_1 \\ \dot{\mathbf{x}}_2 \end{Bmatrix} = \begin{bmatrix} \mathbf{0} & \mathbf{1} \\ -\mathbf{M}^{-1}\mathbf{K} & -\mathbf{M}^{-1}\mathbf{C} \end{bmatrix} \begin{Bmatrix} \mathbf{x}_1 \\ \mathbf{x}_2 \end{Bmatrix} + \begin{bmatrix} \mathbf{0} \\ \mathbf{M}^{-1} \end{bmatrix} \Big\{ \mathbf{u} \Big\} + \begin{bmatrix} \mathbf{0} \\ -\mathbf{1} \end{bmatrix} \Big\{ \ddot{\mathbf{x}}_g \Big\} \tag{3.4}$$

From the same format, desired output measurements can be calculated in the vector $\mathbf{y}$.

$$\Big\{ \mathbf{y} \Big\} = \begin{Bmatrix} \mathbf{x} \\ \dot{\mathbf{x}} \\ \ddot{\mathbf{x}}_{abs} \end{Bmatrix} = \begin{bmatrix} \mathbf{1} & \mathbf{0} \\ \mathbf{0} & \mathbf{1} \\ -\mathbf{M}^{-1}\mathbf{K} & -\mathbf{M}^{-1}\mathbf{C} \end{bmatrix} \begin{Bmatrix} \mathbf{x}_1 \\ \mathbf{x}_2 \end{Bmatrix} + \begin{bmatrix} \mathbf{0} \\ \mathbf{0} \\ \mathbf{M}^{-1} \end{bmatrix} \Big\{ \mathbf{u} \Big\} + \begin{bmatrix} \mathbf{0} \\ \mathbf{0} \\ \mathbf{0} \end{bmatrix} \Big\{ \ddot{\mathbf{x}}_g \Big\} \tag{3.5}$$

This architecture has a number of convenient characteristics for numerical simulation of control schemes, using tools such as MATLAB and Simulink: the two first-order differential equations can be solved numerically within Simulink, feedback control forces can be calculated easily using system outputs, semi-active and passive control devices can be simulated, and the damping matrix need not be modal. Equations 3.4 and 3.5 can be simplified as follows:

$$\dot{\mathbf{x}} = \mathbf{A}\mathbf{x} + \mathbf{B}\mathbf{u} + \mathbf{E}\ddot{\mathbf{x}}_g \tag{3.6}$$

$$\mathbf{y} = \mathbf{C}\mathbf{x} + \mathbf{D}\mathbf{u} + \mathbf{F}\ddot{\mathbf{x}}_g \tag{3.7}$$

The states of the structure are defined by the matrix $\mathbf{x}$, the prescribed control forces are defined by the matrix $\mathbf{u}$, the measurements of the structure are contained in the matrix $\mathbf{y}$, and the ground motion is $\ddot{\mathbf{x}}_g$. $\mathbf{A}$ is the $n \times n$ state transition matrix, $\mathbf{B}$ and $\mathbf{E}$ are the $n \times p$ control and $n \times 1$ ground input matrices, respectively, $\mathbf{C}$ is the $q \times n$ measurement output matrix, and $\mathbf{D}$ and $\mathbf{F}$ are the $q \times p$ control and $q \times 1$ ground feedforward matrices, respectively. In addition to its ease of use for numerical

simulations, the state-space framework is very convenient for optimal control designs explored in the following sections.

3.2 Linear Quadratic Regulator (LQR)

In centralized structural control design, one method for optimizing the feedback gain matrix is a Linear Quadratic Regulator (LQR) design, which aims to minimize the H_2 norm of a closed loop system. The time-invariant, infinite-horizon LQR control is easily calculated for a state-space system as in Equations 3.6 and 3.7, where the standard assumptions are held that $(\mathbf{A}, \mathbf{B})$ is controllable and $(\mathbf{A}, \mathbf{C})$ is observable.

Two matrix parameters $\mathbf{Q}$ and $\mathbf{R}$ are defined in LQR control, where $\mathbf{Q}$ is a positive semi-definite matrix weighting the cost of the structural response and $\mathbf{R}$ is the positive definite matrix weighting the cost of control effort.

$$\mathbf{Q} = \mathbf{Q}^T \geq 0, \quad \mathbf{R} = \mathbf{R}^T > 0 \tag{3.8}$$

The larger the cost of response relative to the cost of control effort, the more control will be exerted in the structure. The closed loop H_2 norm of the system is then defined as J in the standard LQR equation

$$J = \int_0^\infty \mathbf{x}^T \mathbf{Q} \mathbf{x} + \mathbf{u}^T \mathbf{R} \mathbf{u} \, dt \tag{3.9}$$

which is minimized subject to the control law:

$$\mathbf{u} = -\mathbf{K}\mathbf{x} \tag{3.10}$$

LQR uses the solution, $\mathbf{P}$, of the continuous time algebraic Riccati equation

$$\mathbf{A}^T\mathbf{P} + \mathbf{P}\mathbf{A} + \mathbf{P}\mathbf{B}\mathbf{R}^{-1}\mathbf{B}^T\mathbf{P} + \mathbf{Q} = 0 \tag{3.11}$$

to solve for the optimal feedback gain matrix $\mathbf{K}$:

$$\mathbf{K} = \mathbf{R}^{-1}\mathbf{B}^T\mathbf{P} \tag{3.12}$$

The fully populated feedback control gain matrix $\mathbf{K}$ allows for all measurement information to be passed to one central controller, which then computes and prescribes

damper forces. In this state-space framework, the gain matrix will be $p \times n$, where each row corresponds to the control device on each story, and each column corresponds to the feedback information of a state. In this work, full-state feedback is assumed to simplify the comparison of the different methods.

In civil structural control, damage is associated with large interstory drifts. Therefore, it is a common control objective to minimize interstory drifts. The states of a lumped mass building model are displacements and velocities relative to the ground, therefore the interstory states of story i ($x_{int,i}$) are a function of the state of the story (x_i) and that of the story below (x_{i-1})

$$x_{int,i} = x_i - x_{i-1} \tag{3.13}$$

Within the state-space framework, interstory components can be calculated with a coordinate transformation matrix $\mathbf{T}$ from states relative to the ground to interstory states.

$$\mathbf{x}_{int} = \mathbf{T}\mathbf{x} \tag{3.14}$$

where

$$\mathbf{T} = \begin{bmatrix} 1 & 0 & 0 & \dots \\ -1 & 1 & 0 & \ddots \\ 0 & -1 & 1 & \ddots \\ \vdots & \ddots & \ddots & \ddots \end{bmatrix} \tag{3.15}$$

If the control goal is to weight interstory drifts to minimize damage, Equation 3.9 then becomes

$$J = \int_0^\infty \mathbf{x}_{int}^T \mathbf{Q}_{int} \mathbf{x}_{int} + \mathbf{u}^T \mathbf{R} \mathbf{u} \, dt \tag{3.16}$$

with $\mathbf{Q}_{int}$ as an identity matrix. In order to limit only interstory drift, $\mathbf{T}_1$ takes the form

$$\mathbf{T}_1 = \begin{bmatrix} \mathbf{T} & \mathbf{0} \\ \mathbf{0} & \mathbf{0} \end{bmatrix} \tag{3.17}$$

and the new weighting matrix for Equation 3.9 becomes

$$\mathbf{Q} = \mathbf{T}_1^T \mathbf{Q}_{int} \mathbf{T}_1 \tag{3.18}$$

In this work, $\mathbf{R}$ is assumed an identity matrix. The $\mathbf{Q}$ and $\mathbf{R}$ matrices are multiplied by constants to achieve the desired level of control; the larger $\mathbf{Q}$ is relative to $\mathbf{R}$, the greater the control effort. While only the relative values of $\mathbf{Q}$ and $\mathbf{R}$ are important in the LQR calculation, the iterative methods in sections ahead can be sensitive to the absolute values of the constant multipliers.

The LQR gain matrix represents the optimal feedback gain to minimize the H_2 norm of the closed loop system. Therefore, if time delay is not an issue, as in a wired centralized system, LQR as laid out above will compute the globally optimal continuous-time feedback control gain matrix. Even if time delay is considered, as in a decentralized system with wireless full-state feedback sharing, the discrete time dynamics can be considered to compute the optimal solution from the discrete time algebraic Riccati equation. However, both continuous-time and discrete-time LQR controllers require full-state feedback, which may not always be feasible or cost-effective. Therefore, the following sections will present options for computing decentralized feedback controllers.

3.3 Ad-Hoc and Heuristic Methods

The LQR gain matrix solution relies on full state feedback to a central controller, which is difficult to provide in practice. Centralized systems are also subject to potential system failure due to their single point of failure, and using LQR can be prohibitively slow in a full-state feedback wireless system. Therefore, decentralized control systems with wireless sensors and controllers are an attractive alternative.

The Ad-Hoc method is used to decentralize an LQR gain matrix $\mathbf{K}_{LQR}$ by zeroing out values associated with less important communication links, where each link's importance is decided by the control designer. Important values are decided by examining the LQR feedback gain matrix and finding the values with the largest magnitude or by keeping information that is intuitively important, such as local information. A convenient way to write the Ad-Hoc gain matrix is by introducing the structural identity $\mathbf{I}_S$, a matrix of ones that the same size as $\mathbf{K}_{LQR}$. When a gain matrix value is chosen for elimination in the Ad-Hoc method, its corresponding value in $\mathbf{I}_S$ is made zero. Therefore, the Ad-Hoc

gain matrix $\mathbf{K}$ can be written as an element-wise multiplication of the LQR gain matrix and the structural identity:

$$\mathbf{K} = \mathbf{K}_{LQR} \circ \mathbf{I}_S \tag{3.19}$$

The Heuristic Method (Lunze 1992, Wang 2007) is an iterative procedure that takes an already decentralized gain matrix $\mathbf{K}$ and tunes it to minimize the cost, J, of the system, which is taken as the trace of the Riccati solution matrix, $\mathbf{P}$.

$$min[J = trace(\mathbf{P})] \tag{3.20}$$

In order to minimize $trace(\mathbf{P})$ with the decentralized gain matrix $\mathbf{K}$, an iterative procedure is initialized with $\mathbf{P}$ calculated using a modified version of Equation 3.11.

$$(\mathbf{A} - \mathbf{BKC})^T\mathbf{P} + \mathbf{P}(\mathbf{A} - \mathbf{BKC}) + \mathbf{C}^T\mathbf{K}^T\mathbf{RKC} + \mathbf{Q} = 0 \tag{3.21}$$

For lumped mass system with full-state feedback, which is assumed, $\mathbf{C}$ becomes an identity. Next, a Lagrange Multiplier matrix, $\mathbf{L}$, is calculated by solving the equation

$$\frac{\partial J}{\partial \mathbf{P}} = (\mathbf{A} - \mathbf{BKC})\mathbf{L} + \mathbf{L}(\mathbf{A} - \mathbf{BKC})^T + \mathbf{I} = 0 \tag{3.22}$$

$\mathbf{P}$ and $\mathbf{L}$ are then used to calculate the gradient of the cost with respect to the decentralized gain matrix

$$\Delta = \frac{\partial J}{\partial \mathbf{K}} = 2(\mathbf{RKC} - \mathbf{B}^T\mathbf{P})\mathbf{LC}^T \tag{3.23}$$

A scalar multiplier, s, is used to calculate the next gain matrix iteration

$$\mathbf{K}_{i+1} = \mathbf{K}_i - s\Delta \tag{3.24}$$

The following optimality and stability constraints are checked to ensure the current solution is better than the previous solution and stable:

$$trace(\mathbf{P}_{i+1}) \leq trace(\mathbf{P}) \quad and \quad max(\mathrm{Re}(eig(\mathbf{A} - \mathbf{BK}))) \leq 0 \tag{3.25}$$

If these constraints are met, $\mathbf{K}_{i+1}$ is kept and the process is repeated starting with Equation 3.21, otherwise the multiplier, s, is halved and Equation 3.24 is solved again. Once the difference of the H_2 norm of $\mathbf{K}_{i+1}$ and $\mathbf{K}$ reaches a threshold value set by the

control designer, the process is completed.

Because an iterative process is used, it is not guaranteed that the Heuristic algorithm will find the global minimum of J. Therefore, the initial guess and search step size can affect the final result. In addition, as is the assumption in LQR design, the input is assumed to be an unshaped random white noise.

3.4 LQRSP

A new approach for optimal sparse control called the Sparsity-Promoting Linear Quadratic Regulator (LQRSP) has been proposed by Lin et al. (2013). It also uses the LQR framework, but no gain matrix structure is assumed *a priori* as with the Ad-Hoc and Heuristic Methods. Instead of minimizing only the LQR cost function J from Equation 3.9, a sparsity cost function (g) is added to the objective function. Both are combined as

$$J(\mathbf{K}) + \gamma g(\mathbf{K}) \tag{3.26}$$

and this new objective function is minimized. A sparsity multiplier, γ, is used to increase the level of sparsity in the gain matrix. If γ is zero, the LQR cost equation is recovered. As γ increases, more weight is placed on the sparsity, and additional entries in the gain matrix are zeroed to lower the sparsity cost function contribution until no gain matrix remains as γ increases toward $+\infty$.

LQRSP divides the problem by representing the gain matrix as both matrices $\mathbf{F}$ and $\mathbf{G}$, which allows for the use of the Alternating Direction Method of Multipliers (ADMM). The resulting problem formulation is:

$$minimize\ J(\mathbf{F}) + \gamma g(\mathbf{G}) \tag{3.27}$$

subject to

$$\mathbf{F} - \mathbf{G} = 0 \tag{3.28}$$

The LQR cost function is solved first, and for each discrete value of γ specified by the control designer, the ADMM process is executed. An augmented Lagrangian $\mathcal{L}_\rho$

$$\mathcal{L}_\rho(\mathbf{F}, \mathbf{G}, \mathbf{\Lambda}) = J(\mathbf{F}) + \gamma g(\mathbf{G}) + trace(\mathbf{\Lambda}^T(\mathbf{F} - \mathbf{G})) + \frac{\rho}{2}\|\mathbf{F} - \mathbf{G}\|_F^2 \tag{3.29}$$

is introduced, where $\mathbf{\Lambda}$ is the Lagrange multiplier matrix and ρ is a parameter that scales the solution path. The initial values of $\mathbf{F}^k$, $\mathbf{G}^k$, and $\mathbf{\Lambda}^k$ are

$$\mathbf{F}^0 = \mathbf{K}_{LQR}, \quad \mathbf{G}^0 = \mathbf{0}, \quad \mathbf{\Lambda}^0 = \mathbf{0} \tag{3.30}$$

Two additional matrices are calculated

$$\mathbf{U}^{k+1} = \mathbf{G}^k - \frac{\mathbf{\Lambda}^k}{\rho} \tag{3.31}$$

$$\mathbf{V}^{k+1} = \mathbf{F}^{k+1} + \frac{\mathbf{\Lambda}^k}{\rho} \tag{3.32}$$

for the F-minimization and G-minimization steps in the ADMM process, which iterates as follows:

1. $\mathbf{F}^{k+1}$ is solved by using the Anderson-Moore method to minimize the objective function Φ of the F-minimization step:

$$\Phi = trace(\mathbf{L}(\mathbf{Q} + \mathbf{F}^T\mathbf{R}\mathbf{F})) + \frac{\rho}{2}\|\mathbf{F} - \mathbf{U}\|_F^2 \tag{3.33}$$

   This minimization is done by calculating two Lyapunov equations for initial guess $\mathbf{F}_0 = \mathbf{F}^k$.

$$(\mathbf{A} - \mathbf{B}\mathbf{F})\mathbf{L} + \mathbf{L}(\mathbf{A} - \mathbf{B}\mathbf{F})^T + \mathbf{E}\mathbf{E}^T = 0 \tag{3.34}$$

$$(\mathbf{A} - \mathbf{B}\mathbf{F})^T\mathbf{P} + \mathbf{P}(\mathbf{A} - \mathbf{B}\mathbf{F}) + \mathbf{Q} + \mathbf{F}^T\mathbf{R}\mathbf{F} = 0 \tag{3.35}$$

   $\mathbf{L}$ is the closed-loop controllability gramian and $\mathbf{P}$ is the closed-loop observability gramian. With new solutions $\mathbf{L}_1$ and $\mathbf{P}_1$ as functions of $\mathbf{F}_0$, the next solution $\mathbf{F}_1$ is solved through the Sylvester equation

$$\mathbf{F}\mathbf{L} + \rho(2\mathbf{R})^{-1}\mathbf{F} = \mathbf{R}^{-1}\mathbf{B}^T\mathbf{P}\mathbf{L} + \rho(2\mathbf{R})^{-1}\mathbf{U} \tag{3.36}$$

   The process is repeated until Φ is minimized, at which point $\mathbf{F}^{k+1}$ is reached.

2. Next, using the separability of $\mathbf{F}$ and $\mathbf{G}$, $\mathbf{G}^{k+1}$ is calculated element-wise by

minimizing

$$\gamma g(G_{ij}) + \frac{\rho}{2}(G_{ij} - V_{ij})^2 \tag{3.37}$$

The function $g(G_{ij})$ can take a variety of forms within the LQRSP framework, but the two used in this work are

$$g(G_{ij}) = \mathbf{card}(G_{ij}), \quad \mathbf{card}(G_{ij}) = \left\{ \begin{array}{ll} 1, & G_{ij} \neq 0 \\ 0, & G_{ij} = 0 \end{array} \right\} \tag{3.38}$$

and

$$g(G_{ij}) = W_{ij}|G_{ij}|, \quad W_{ij} = \left\{ \begin{array}{ll} \frac{1}{|G_{ij}|}, & |G_{ij}| \neq 0 \\ \epsilon, & |G_{ij}| = 0 \end{array} \right\} \tag{3.39}$$

The cardinality function from Equation 3.38 leads to the truncation of the smallest gain matrix values. This leads to a non-convex optimization problem, so the weighted l_1 approach in Equation 3.39 is used to shrink the gain matrix and maintain a convex optimization problem. When the cardinality function is used, the gain matrix values are truncated as follows:

$$G_{ij} = \left\{ \begin{array}{ll} Gij, & |Vij| > \sqrt{\frac{2\gamma}{\rho}} \\ 0, & |Vij| \leq \sqrt{\frac{2\gamma}{\rho}} \end{array} \right\} \tag{3.40}$$

When the weighted l_1 norm is used, shrinkage is applied to the gain matrix values as follows:

$$G_{ij} = \left\{ \begin{array}{ll} Gij - (\frac{\gamma}{\rho})W_{ij}, & |Vij| > (\frac{\gamma}{\rho})W_{ij} \\ 0, & |Vij| \leq (\frac{\gamma}{\rho})W_{ij} \end{array} \right\} \tag{3.41}$$

3. Last, the Lagrange multiplier matrix is updated for the current iteration:

$$\mathbf{\Lambda}^{k+1} = \mathbf{\Lambda}^k + \rho(\mathbf{F}^{k+1} - \mathbf{G}^{k+1}) \tag{3.42}$$

The entire process iterates, and as $\mathbf{\Lambda}^{k+1}$ approaches zero, the ADMM process is completed and the gain matrix structure is fixed as $\mathbf{I}_S$. The final gain matrix $\mathbf{F}^{k+1}$ is used as an initial guess of $\mathbf{K}$ for the polishing step, which solves the same three equations as the Heuristic method with some modifications. The three equations solved are:

$$(\mathbf{A} - \mathbf{BK})^T\mathbf{P} + \mathbf{P}(\mathbf{A} - \mathbf{BK}) + \mathbf{K}^T\mathbf{RK} + \mathbf{Q} = 0 \tag{3.43}$$

$$(\mathbf{A}-\mathbf{BK})\mathbf{L}+\mathbf{L}(\mathbf{A}-\mathbf{BK})^T+\mathbf{EE}^T=0 \tag{3.44}$$

$$[(\mathbf{RK}-\mathbf{B}^T\mathbf{P})\mathbf{L}]\circ\mathbf{I}_S \tag{3.45}$$

Rather than solve Equation 3.45 to simply find the gradient of the cost function as the Heuristic method does, the polishing step uses Equation 3.45 within Newton's method and the conjugate gradient scheme to find the Newton direction. The most important difference between the Heuristic and LQRSP polishing algorithms is the cost function which is minimized. Equation 3.20 minimizes the trace of the matrix $\mathbf{P}$, while Equation 3.44 shows that LQRSP has the goal

$$min[J=trace(\mathbf{E}^T\mathbf{PE})] \tag{3.46}$$

The Heuristic method assumes that the inputs are random variables uniformly distributed on a unit sphere, while the LQRSP method uses the closed-loop controllability gramian and the matrix $\mathbf{E}$ to gain insight into the nature of the external input signal.

When used in conjunction with the ADMM method, the LQRSP polishing step is able to quickly converge to the global minimum of the decentralized solution space. The ADMM method provides a good starting guess for the polishing step, and the conjugate gradient scheme is less likely to find a local minimum than the Heuristic method, which only relies on the gradient of the cost function. When computing a homotopic path of optimal decentralized gain matrices for a range of increasing γ, the LQRSP method can quickly and efficiently find optimal decentralized gain matrices at varying levels of sparsity.

In the LQRSP framework, the sparsity weights in the weighted l_1 approach can also be adjusted to encourage information sharing. For example, to encourage local information to be kept when using the weighted l_1 approach (Equation 3.39), the weights $W_{i,j}$ for $i=j$ can be set to zero. Also, the block sparsity option in LQRSP can be used to link state measurements together that would be simultaneously available. For example, if the wireless transceiver in a partially decentralized system has measurements of two states for its local story, it will be able to send both states to another transceiver without incurring any additional time penalty over only sending one state. LQRSP is then useful to link states together in the optimal control design for a more intuitive representation.

3.5 Discrete Time

The previous sections in this chapter are laid out for a continuous time system. However, time delay must be taken into account for systems that have slower fundamental sampling times. In a discrete time system, the state-space equations become

$$\mathbf{x}[k+1] = \mathbf{A}_d\mathbf{x}[k] + \mathbf{B}_d\mathbf{u}[k] + \mathbf{E}_d\ddot{\mathbf{x}}_g[k] \tag{3.47}$$

$$\mathbf{y}[k+1] = \mathbf{C}_d\mathbf{x}[k] + \mathbf{D}_d\mathbf{u}[k] + \mathbf{F}_d\ddot{\mathbf{x}}_g[k] \tag{3.48}$$

in which the continuous time system is transformed into a discrete time system using a zero order hold. In addition, all of the Riccati, Sylvester, and gradient equations in the previous sections have discrete time counterparts. Therefore, the LQR, Heuristic, and LQRSP methods are all solvable in discrete time.

The largest difference between continuous time and discrete time systems is the sample time. All wireless control schemes must be implemented with a fundamental sample time dependent on the time required to send feedback information wirelessly and the number of communication links in the system; therefore, discrete time systems must be considered when comparing wireless control algorithms. Fewer communication links lead to a faster sample time and less feedback information, while full state feedback will have the slowest sample time and the most feedback information.

3.6 Semi-Active Damper Model

Idealized control simulations assume that any force can be applied at any time by the control system. This is largely possible up to a maximum force if an active control device, such as an active mass driver, is used. However, for practical applications of feedback control in civil structures, semi-active dampers are typically considered because of their low power requirements, large forces, and inherent stability. In this research, a Maxwell model (Equation 3.49) is used to describe the force $u(t)$ in a semi-active hydraulic damper (SHD), based on its stiffness k_{eff}, its damping coefficient c_{SHD}, and the interstory velocity $\Delta\dot{q}$ (Hatada et al. 2000).

$$\dot{u}(t) + \frac{k_{eff}}{c_{SHD}(t)}u(t) = k_{eff}\Delta\dot{q}(t) \tag{3.49}$$

This damper model is implemented alongside the idealized dampers in the simulated feedback control systems in the following chapters. When the SHDs are considered, the feedback gain matrix is used to calculate the desired damper force at each time step, then the desired damping coefficient c_{SHD} is approximated by dividing the desired force by the interstory velocity. The damper parameters are listed in Table 3.1. The dampers and their saturation parameters lead to a nonlinear system; however, the gain matrices are calculated as though the systems are linear.

Table 3.1: Semi-active damper parameters for the 5-story and 20-story simulations.

Damper Parameters	
	Values
k_{eff} [kN/mm]	400
c_{min} [kN-s/mm]	1
c_{max} [kN-s/mm]	200
f_{max} [kN]	1000

A simple way to implement a control system without any feedback is to use passive dampers. Within a passive system, each SHD is set to a particular value of c_{SHD} throughout the entire excitation time history. The two passive systems considered in this work are Passive On, where the damper is set to c_{max}, and Passive Off, where the damper is set to c_{min}. The feedback control algorithms aim to alter c_{SHD} such that the results are better than those any passive system can achieve.

3.7 Summary

Two algorithms for calculating feedback gain matrices for decentralized systems have been presented. The Heuristic method is dependent on a structural identity being imposed on the feedback gain matrix *a priori*, while the LQRSP method incorporates the cost of the feedback structure into the objective cost function. The LQRSP method also has a number of other features, including the ability to lump state feedback information together, the ability to reweight the system to encourage certain communication links, and the ability to compute large families of γ-parameterized gain matrices for easy comparison of various levels of gain matrix sparsity.

Comparisons of the Heuristic and LQRSP algorithms for the two benchmark structures fitted with active and semi-active control devices are examined in the remaining

chapters. The continuous time and discrete time controllers are compared by using theoretical closed-loop cost comparisons, structural response maxima achieved during earthquake simulations, and RMS structural response during band-limited white noise (BLWN) simulations with active and semi-active control devices. The results are also compared to results from LQR, Passive On, and Passive Off control techniques where applicable in order to study the overall effectiveness of the decentralized feedback control techniques.

Chapter 4

Continuous Time Comparison

In this chapter, the Heuristic and LQRSP decentralized control algorithms are compared to centralized LQR control in the continuous time domain on two benchmark structures.

4.1 Closed-Loop Cost

The various control methods are initially examined on the 5-Story Kajima-Shizuoka building (Figure 2.1 and Table 2.1) where the feedback structure can be more clearly identified because it is analyzed as a shear building with collocated sensors and control devices. The analytical model is the lumped mass system used by Wang (2007), which is a modified version of the Kajima-Shizuoka building presented by Kurata et al. (1999). Only horizontal degrees of freedom are measured and controlled, while vertical and rotational degrees of freedom are considered negligible. In this representation, the states are the horizontal displacements and velocities at each story relative to the ground, and ideal actuators are assumed. For LQR, the response weighting matrix $\mathbf{Q}$ is multiplied by 10^9 and the control weighting matrix $\mathbf{R}$ is multiplied by 10^{-6}. The structure of Q is made to limit interstory drifts to prevent damage within the structure.

Due to the collocated sensors and control and the $\mathbf{Q}$ and $\mathbf{R}$ matrix structures, the resulting LQR gain matrix has a distinct pattern in which the diagonals have large magnitudes relative to the off-diagonal values, as seen in Figure 4.1. This pattern allows for an intuitive guess of the desired sparsity pattern of a decentralized gain matrix in the Ad-Hoc method. The Ad-Hoc gain matrix pattern with 10 non-zero (nz) entries, shown in Figure 4.2, is then optimized by the Heuristic method. No

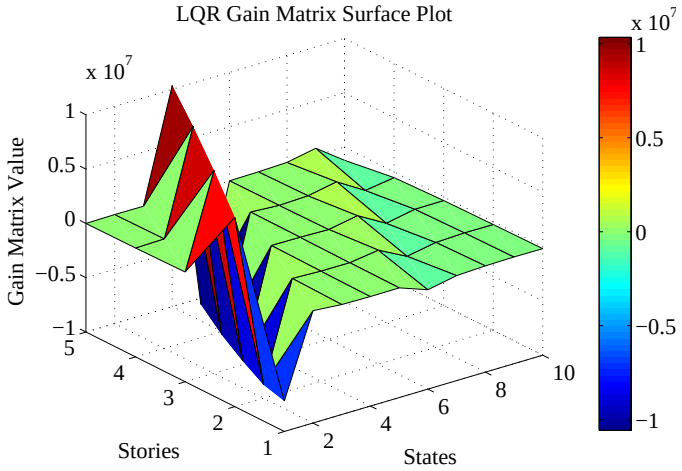

Figure 4.1: LQR gain matrix surface plot.

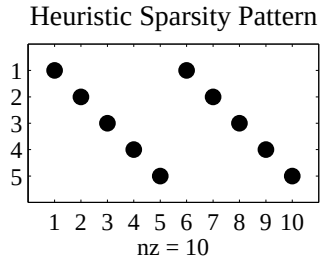

Figure 4.2: Sparsity pattern considered for Heuristic method.

information is passed between nonlocal sensors for the control calculation, so the design is considered to be fully decentralized control (Lynch et al. 2002). While some gain matrix values associated with displacements of the story below are larger than the gain matrix values associated with local velocites, intuition would tell the control designer that local velocity information is important for determining the future response of the system. For this reason, local velocity information is kept, even at the cost of eliminating some larger gain matrix values. Because the Heuristic method is an optimized case of the Ad-Hoc method and guarantees closed-loop stability, only the Heuristic method is evaluated in this thesis.

The Heuristic method is only possible to use if the desired sparse gain matrix structure has been chosen, but when using the LQRSP algorithm of Lin et al. (2013)—downloaded from `http://www.ece.umn.edu/users/mihailo/software/lqrsp/index.`

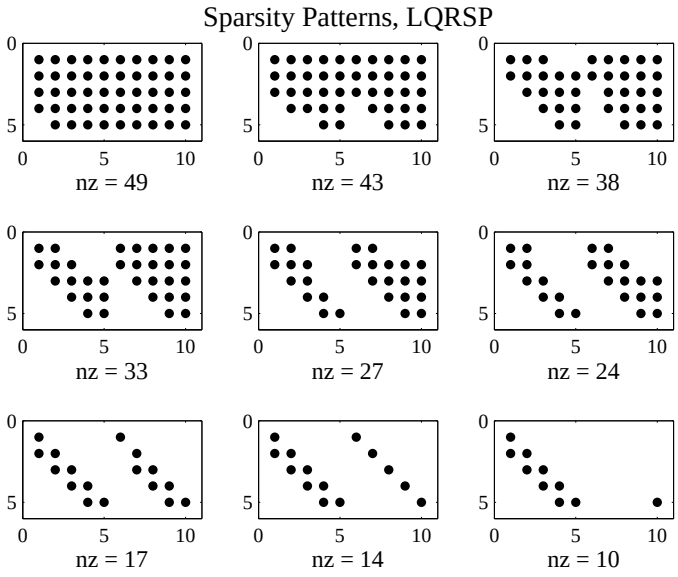

Figure 4.3: Sparsity patterns in LQRSP with increasing γ.

`html`—a set of $\mathbf{A}$, $\mathbf{B}$, $\mathbf{E}$, $\mathbf{Q}$, and $\mathbf{R}$, creates a γ-parameterized family of gain matrices that can be compared at varying levels of sparsity. If a logarithmic spacing of γ over a large range of values is used, the family of gain matrices includes many different sparsity values. Decreasing the spacing between γ values and increasing the number of γ values can increase the number of gain matrices considered and is found to provide the LQRSP polishing step with better initial guesses.

For the Kajima-Shizuoka building, the evolution of the LQRSP gain matrix for increasing γ with the weighted l_1 approach can be seen in Figure 4.3. As γ increases, information from distant sensors is discarded as expected. However, the default parameters of LQRSP lead to a different gain matrix format than that considered for the Heuristic algorithm at a sparsity level of $nz = 10$. Because the $\mathbf{Q}$ and $\mathbf{R}$ matrices weight interstory drifts and not velocities, the absolute value of the LQR gain matrix entries associated with displacement measurements of the story below are larger than the entries associated with local velocity measurements (Figure 4.1). The LQRSP formulation determines that the larger displacement values are more important than the local velocity information.

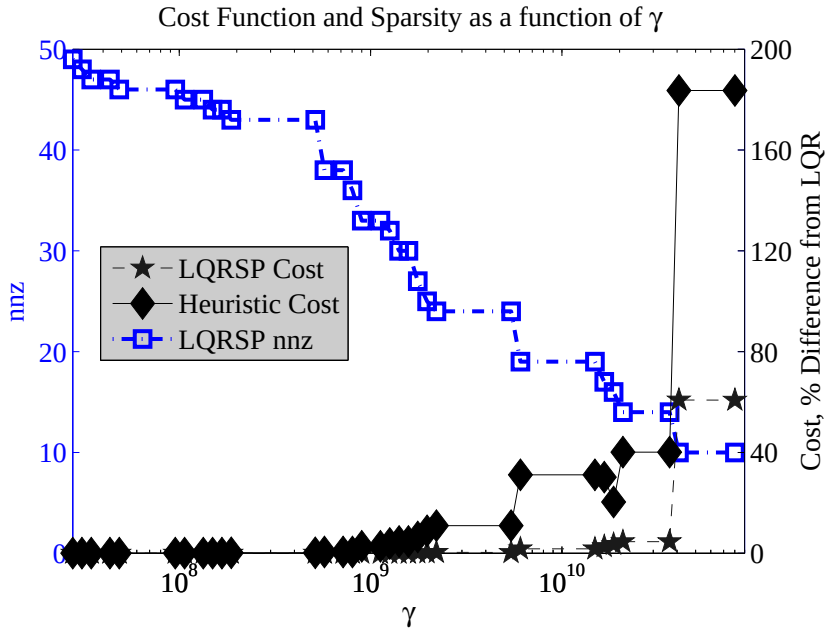

Figure 4.4: Number of non-zero elements in the gain matrix decreasing as γ and the cost of the objective function increases.

The closed-loop cost increase of each LQRSP gain matrix with increasing γ, calculated in Equation 3.46, is plotted normalized to the LQR gain matrix cost in Figure 4.4 on the right y-axis. The Heuristic method is used to calculate its own optimal feedback gain matrices for the sparsity patterns produced by LQRSP, and their closed-loop costs are calculated by Equation 3.46 and plotted alongside the LQRSP values. Finally, the number of non-zeros (nnz) in the gain matrix at each value of γ are plotted on the y-axis. As expcted, the LQR gain matrix is recovered at low values of γ, and the LQR cost is the global minimum of the entire system. As γ and the sparsity of the gain matrix are increased, the closed-loop cost increases slowly for both LQRSP and the Heuristic method. Beyond $\gamma = 2 \times 10^9$, the Heuristic closed-loop cost increases appreciably, and around $\gamma = 4 \times 10^{10}$, both closed-loop costs increase greatly. Although the same gain matrix structures are considered for both LQRSP and Heuristic, the LQRSP gain matrix has the lower closed-loop cost at high sparsity because it is minimizing Equation 3.46 instead of Equation 3.20 as the Heuristic method does.

The most striking part of Figure 4.4 is the large jump in cost for both methods for $\gamma \geq 4 \times 10^{10}$. The number of non-zeros goes from $nz = 14$ to $nz = 10$ in this span, which Figure 4.3 shows eliminates four local velocity measurements. It is clear that the local

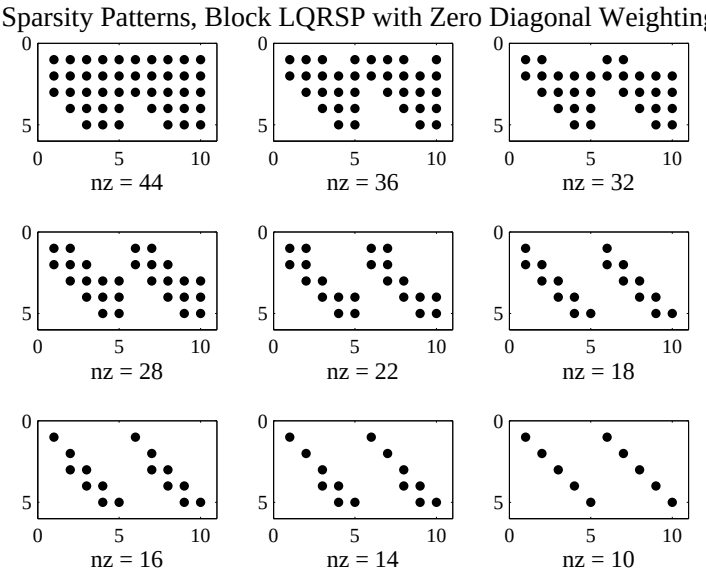

Figure 4.5: Sparsity patterns in LQRSP with increasing γ, when block sparsity and zero diagonal weightings are used.

velocity states provide valuable information and should not be discarded, and in reality, the velocity state is also likely available with its corresponding displacement state. To reflect these facts, the parameters in LQRSP are changed to lump local states together into blocks in the sparsity formulation, e.g. if the fourth story controller asks for third story displacement, the third story velocity will be lumped in for free. Additionally, the weights along the diagonals are made zero—$W_{i,j} = 0$ for $i = j$ in Equation 3.39—in order to guarantee that local information will always be kept. This changes the sparsity patterns for higher levels of sparsity, seen in Figure 4.5. The highest sparsity level is a diagonal gain matrix as expected, where no information is passed between the sensors and the controllers on different stories, which is the same pattern as the Heuristic gain matrix considered in Figure 4.2. If the sparsity constraint is relaxed, the upper stories are given state measurements from the story below before the lower stories are passed any information.

The closed-loop costs for LQRSP and Heuristic block gain matrices with zero diagonal weightings are calculated and plotted in Figure 4.6. The LQRSP method is still much better at minimizing the closed-loop cost than the Heuristic method, and the use of local information and block information completely eliminates the large cost jump

present in the original LQRSP formulation. According to this cost metric, LQRSP only increases the closed-loop cost over LQR by about 2% when local information and information from the story below is used (nz = 18 and $\gamma = 1 \times 10^{10}$) and by about 5% when only local information is kept ($nz = 10$ and $\gamma = 4 \times 10^{12}$). It is easy to use the LQRSP method with the default parameters, but by noting which gain matrix values cause large increases in the cost function when eliminated, the performance at high sparsity levels can be greatly improved. Also, intuition would tell the control designer that local velocity information is important for determining the future response of the system, so any information the designer can add to the system can also improve LQRSP.

By the closed-loop cost metric, the LQRSP polishing step appears to be more powerful than the Heuristic optimization of a structured gain matrix. However, when considering the sparsity level $nz = 10$, the default LQRSP parameters lead to a cost increase more than 60% over the LQR cost (Figure 4.4), which is much worse than the Ad-Hoc/Heuristic gain matrix at less than 45% increase over the LQR cost (Figure 4.6). When the intuition gained from the LQRSP analysis is used to alter the l_1 weights, LQRSP at $nz = 10$ is far better than both at 5% increase (Figure 4.6). Therefore, it is essential to use LQRSP as an analysis tool alongside the intuition of the control designer.

4.2 Ground Motion Simulations

To extend the closed-loop cost analysis to seismic building simulations, the LQR, LQRSP, and Heuristic methods are compared on the 5-Story Kajima-Shizuoka and the 20-Story SAC (Section 2.3.2) benchmark structures equipped with idealized active control devices —where any damper force is assumed to be possible at all times —and semi-active control devices —where the damper force is dependent on its properties and the response of the structure. Four different earthquake ground acceleration records are considered:

- El Centro: El Centro Array #9, Imperial Valley, CA (1940)
- Northridge: Castaic Old Ridge Rt Station (1994)
- Chi-Chi: Station CHY006 (1999)
- Kobe: KJMA Station (1995)

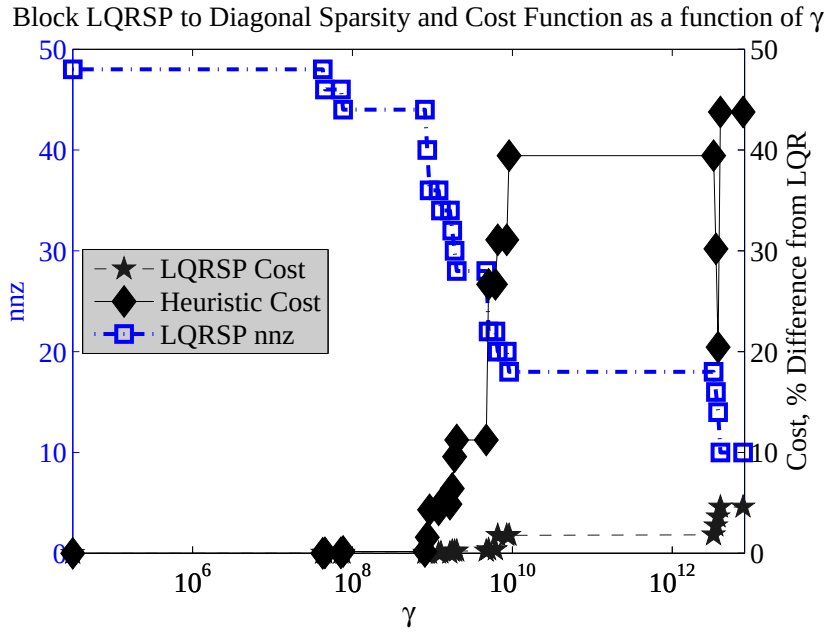

Figure 4.6: Number of non-zero elements in the gain matrix decreasing as γ and the cost of the objective function increases.

In addition, a band-limited white noise (BLWN) shaped by a Kanai-Tajimi filter is used as a ground acceleration record to compute the steady-state response of the structure. MATLAB and Simulink are used to simulate the response of the structure to the considered ground motions, and the displacement, velocity, acceleration, and control time histories are recorded to calculate maximum and root-mean-square (RMS) response quantities. Both displacements and velocities relative to the ground are needed for the feedback control calculations, and both are assumed to be measured despite their difficulty to do so in practice.

4.2.1 Active 5-Story Benchmark

In order to compare the methods further and validate the results found in the theoretical cost analysis for the 5-Story Kajima-Shizuoka building, four different LQRSP gain matrix structures are considered for continuous time ground motion simulations. These are found in Figure 4.7. The two top structures —LQRSP 14 and LQRSP 10 —highlight the large cost jump in Figures 4.3 and 4.4, and the two bottom structures —LQRSP 18 Block and LQRSP 10 Block —highlight whether non-local information is

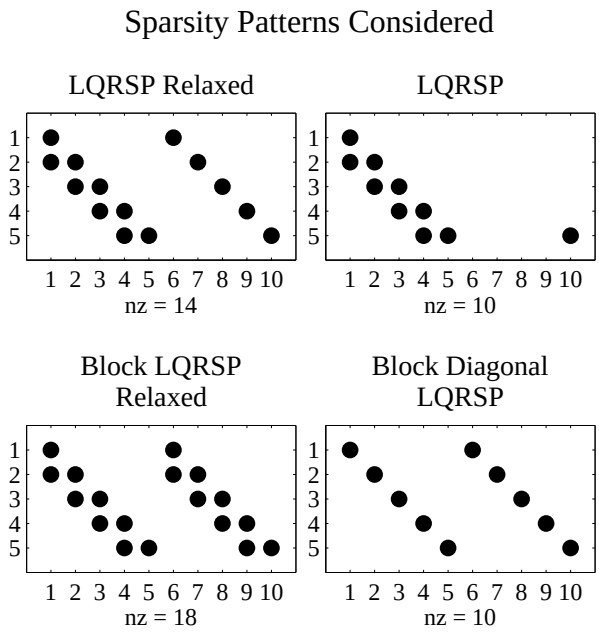

Figure 4.7: Sparsity patterns used for Continuous Time Simulations.

needed in the block sparsity approach in Figures 4.5 and 4.6.

The first two LQRSP gain matrix structures in Figure 4.7 are compared to the fully populated LQR gain matrix and the Heuristic gain matrix seen in Figure 4.2 in the four earthquake ground motion simulations. The maximum interstory drifts, accelerations, and actuator forces at each story for each earthquake are plotted in Figure 4.8. As expected, all control schemes improve on the maximum interstory drift of the uncontrolled structure, with LQR being the best. LQRSP 14 has very similar drift results as the LQR system and only requires information from the local story and the story below. However, the Heuristic system does poorly in controlling the drift of stories 1, 2 and 5, while LQRSP 10 has trouble controlling the bottom four stories. These results largely match the cost analysis in Section 4.1 for each control scheme.

The maximum accelerations of each lumped story mass and maximum control force in each damper are also considered in Figure 4.8. The LQR and LQRSP 14 systems are similar in both accelerations and forces. With only a fraction of the feedback information, the LQRSP 14 feedback gain provides virtually the same level of control as the globally optimal LQR gain matrix. On the other hand, the Heuristic system has very high control forces on the 5^{th} story and often increases the maximum accelerations of the

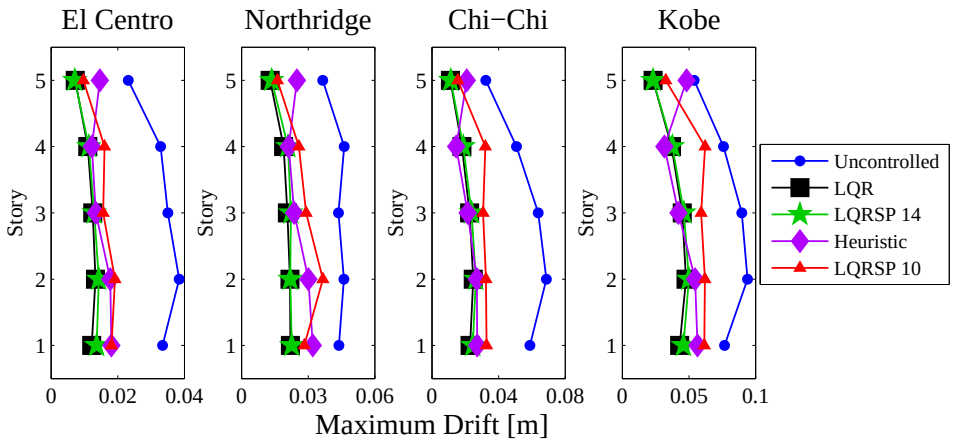

(a) Maximum Drift

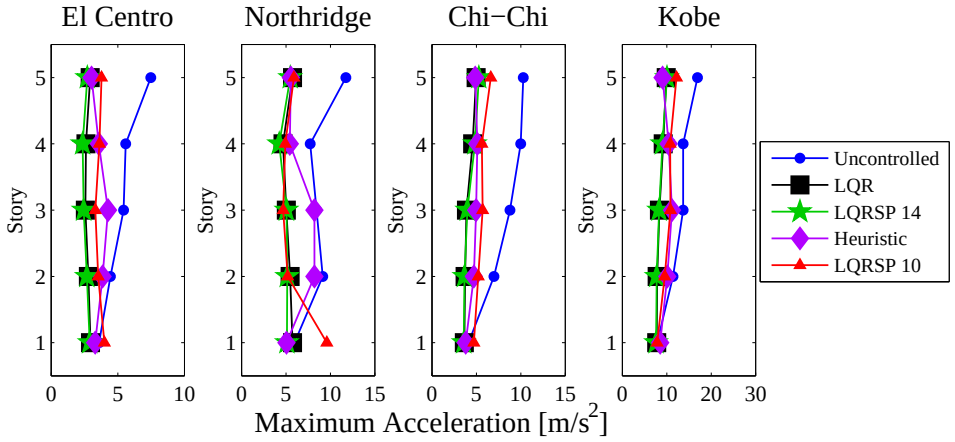

(b) Maximum Acceleration

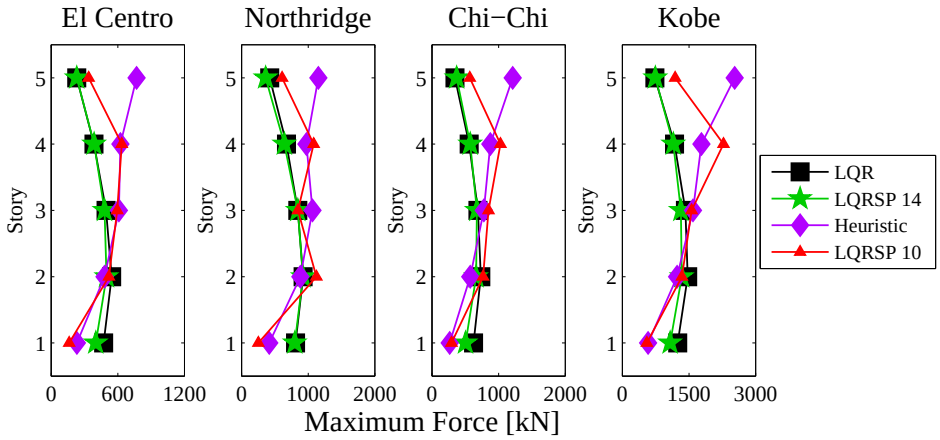

(c) Maximum Force

Figure 4.8: Maximum Responses for Kajima-Shizuoka building with active control during multiple earthquake simulations.

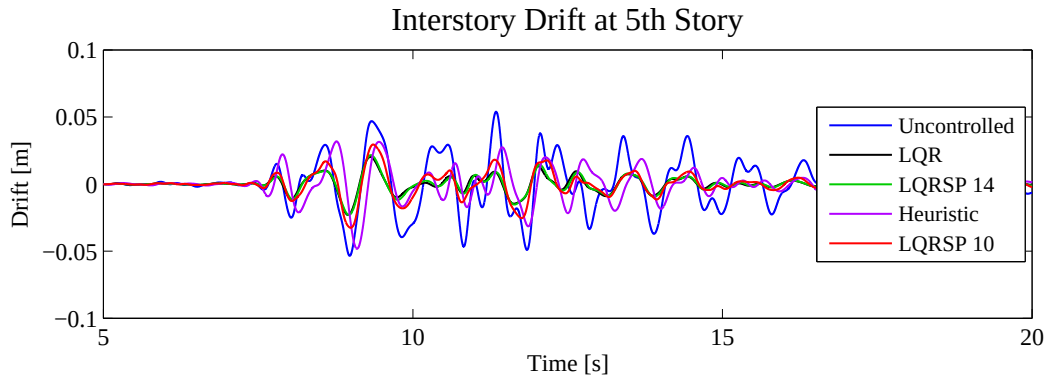

(a) Drift of 5th Story relative to 4th story during Kobe earthquake simulation

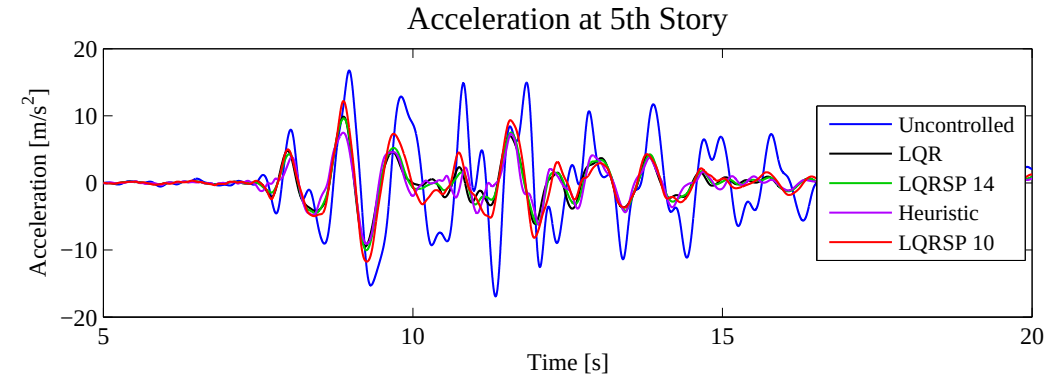

(b) Acceleration of 5th Story during Kobe earthquake simulation

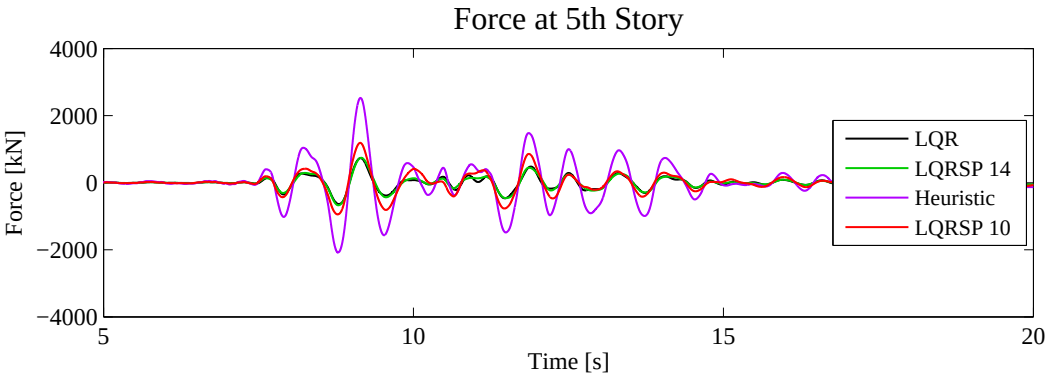

(c) Force of 5th Story actuator during Kobe earthquake simulation

Figure 4.9: Time responses of Kajima-Shizuoka building in Kobe earthquake simulation.

structure. LQRSP 10 has similar problems as the Heuristic system while providing much less control force on the 5^{th} story. To examine these issues more closely, the time history of the 5^{th} story is plotted in Figure 4.9. Again, the LQR and LQRSP 14 methods are almost exactly the same by all three metrics, with the Heuristic and LQRSP 10 systems considerably worse. The Heuristic method overshoots the forces of LQR, leading to increased drift between the 8 and 10 second marks, while the LQRSP 10 system is middling in all three metrics. While both the Heuristic system and LQRSP 10 system have similar difficulties, their problems have different causes. The Heuristic method does not take the $\mathbf{E}$ matrix into account, which leaves the controller unable to anticipate how the external input will enter the system. This is what causes the force and drift overshoots in Figure 4.9. On the other hand, LQRSP 10 lacks velocity state feedback information, which would provide the controller with derivative information useful for making control decisions. When considering the acceleration and force in addition to the interstory drift, it is clear that the earthquake simulations confirm the conclusions of the cost analysis.

While the earthquake records are informative to how the building will behave under transient ground motion, the RMS response of the structure to a more generalized loading, the shaped BLWN, serves as a more comprehensive analysis device in the steady-state response of the building. The Kanai-Tajimi filter is used to shape the BLWN to the frequency range of interest, from which the RMS drift response of the building is evaluated for the different gain matrices. Ultimately, the normalized results presented in Table 4.1 are very similar to those in the earthquake simulations; LQR provides the best interstory drift response, followed very closely by LQRSP 14. The Heuristic Method is worse on Stories 1 and 5, while LQRSP 10 is worst on the lower four stories. Because the RMS response is calculated from a general earthquake with a smooth power spectrum, the results will not reflect the results of more impulsive near-field earthquakes, such as Northridge or Kobe. Indeed, the RMS drift results most closely match the maximum drift results of the Chi-Chi earthquake in Figure 4.8.

To evaluate the effect of the block sparsity and zero diagonal weights in the LQRSP formulation, the second set of gain matrices in Figure 4.7 are compared to the LQR and Heuristic methods. The maximum earthquake results are plotted in Figure 4.10. LQRSP 18 Block only includes local measurements and measurements from the story below, yet exhibits virtually no change from LQR. However, the LQRSP 10 Block

Table 4.1: RMS drift for the Kajima-Shizuoka building under a shaped band-limited white noise, normalized to the RMS drift of the uncontrolled structure.

RMS Drift, Normalized to Uncontrolled				
Story	LQR	LQRSP 14	Heuristic	LQRSP 10
1	0.47	0.48	0.55	0.62
2	0.41	0.42	0.44	0.49
3	0.37	0.37	0.34	0.44
4	0.34	0.34	0.30	0.50
5	0.30	0.30	0.55	0.45

Table 4.2: RMS drift for the Kajima-Shizuoka building under a shaped band-limited white noise, normalized to the RMS drift of the uncontrolled structure.

RMS Drift, Normalized to Uncontrolled				
Story	LQR	LQRSP 18 Block	Heuristic	LQRSP 10 Block
1	0.47	0.47	0.55	0.48
2	0.41	0.41	0.44	0.42
3	0.37	0.38	0.34	0.37
4	0.34	0.34	0.30	0.34
5	0.30	0.30	0.55	0.31

now matches LQR well in all three metrics despite having the same structure as the Heuristic method. LQRSP, unlike the Heuristic method, is able to overcome the lack of non-local information and provide a fully decentralized controller with results similar to the centralized LQR system. This conclusion is also confirmed by the RMS drift calculations in Table 4.2 and the cost calculation results in Section 4.1. After adding a small amount of knowledge of the structure and noting the gain matrix entries that cause the closed-loop cost to increase, the performance of the LQRSP program matches that of centralized LQR at high levels of decentralization.

4.2.2 Active 20-Story Benchmark

The sparse design approaches are extended to the SAC 20-Story benchmark structure with 4 dampers on Stories 1-5, 2 dampers on Stories 6-15, and 1 damper on Stories 16-20 (Section 2.3.2). In this system, the desired sparse feedback structure is less apparent due to the model reduction. Because the full model for the 20-Story benchmark structure has 291 degrees of freedom, with some natural frequencies up to 10^8 Hz, a model reduction for simulation is required. While a lumped-mass system can also be considered, a

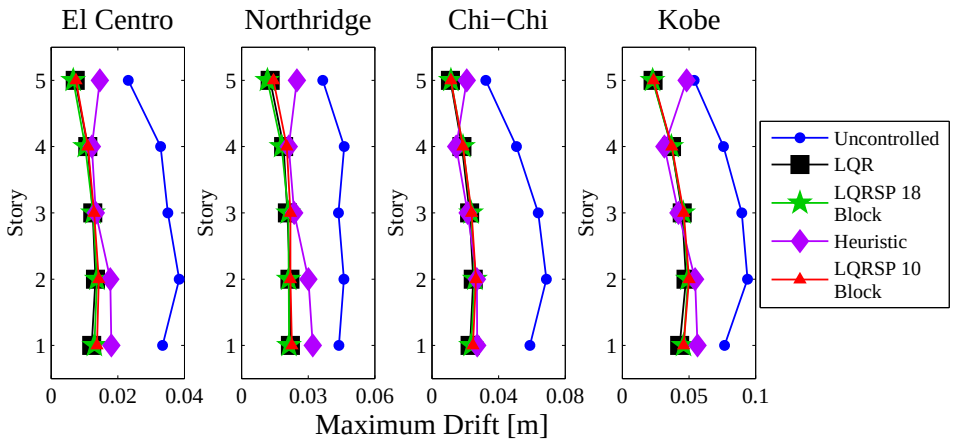

(a) Maximum Drift

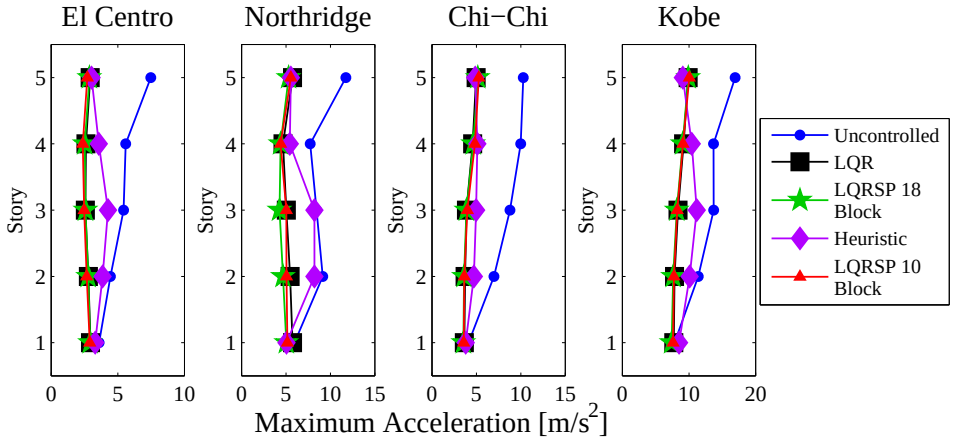

(b) Maximum Acceleration

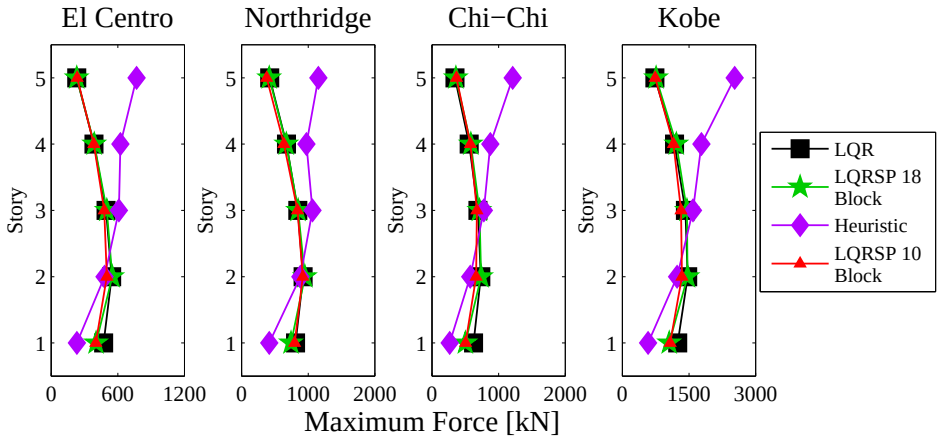

(c) Maximum Force

Figure 4.10: Maximum Responses for Kajima-Shizuoka building with active control during multiple earthquake simulations.

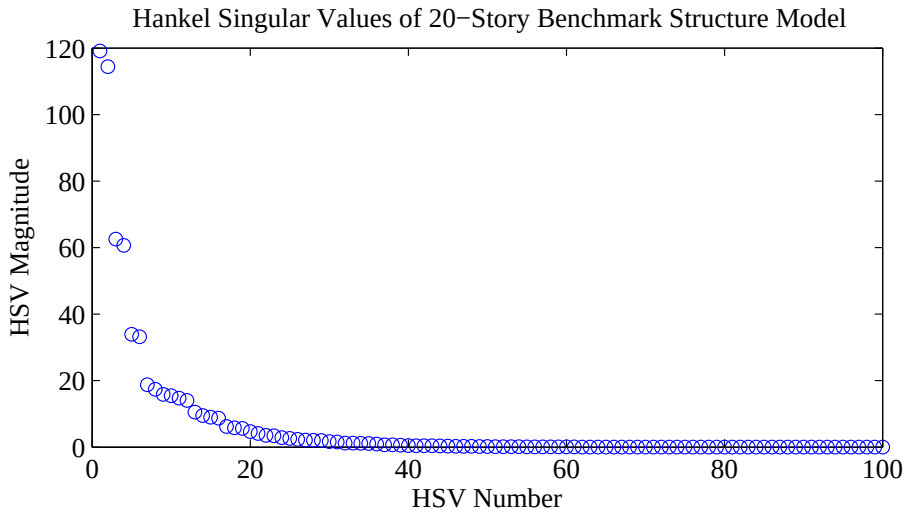

Figure 4.11: Largest 100 Hankel Singular Values for the SAC 20-Story benchmark structure full model.

balanced reduction provided by Ohtori et al. (2000) is chosen for the system model to reduce the system from 582 states to 20 states. The eigenvalues of the product of the controllability Gramian and the observability Gramian give the Hankel Singular Values of the system, which show that the 20 highest-energy states are sufficient to describe the motion of the structure (Figure 4.11). A comparison of the natural frequencies and frequency responses to both ground and control inputs verified that the Ohtori 20 state reduction sufficiently matches the full model in frequencies of interest (Appendix A). The model reduction results in a system model without an easily discernible physical meaning. The states describe the way the structure responds to an earthquake, but the states are not tied to a particular degree of freedom. Therefore, an intuitive Ad-Hoc approach cannot be used in the same way as for the 5-Story structure. LQRSP, on the other hand, is equipped to deal with this situation because it includes the sparsity of the gain matrix in the optimal solution.

The control objective is again to minimize the interstory drifts of the 20-Story benchmark using an LQR/LQRSP approach with idealized active dampers, where $\mathbf{Q}$ is multiplied by 10^3 and $\mathbf{R}$ is multiplied by 10^{-13}. Two different levels of sparsity are chosen for the LQRSP approach. The sparsity levels selected correspond to gain matrices that have approximately 40% (LQRSP 159) and 20% (LQRSP 79) of the information that the full 400 element gain matrix provides. As anticipated, the LQRSP gain matrices

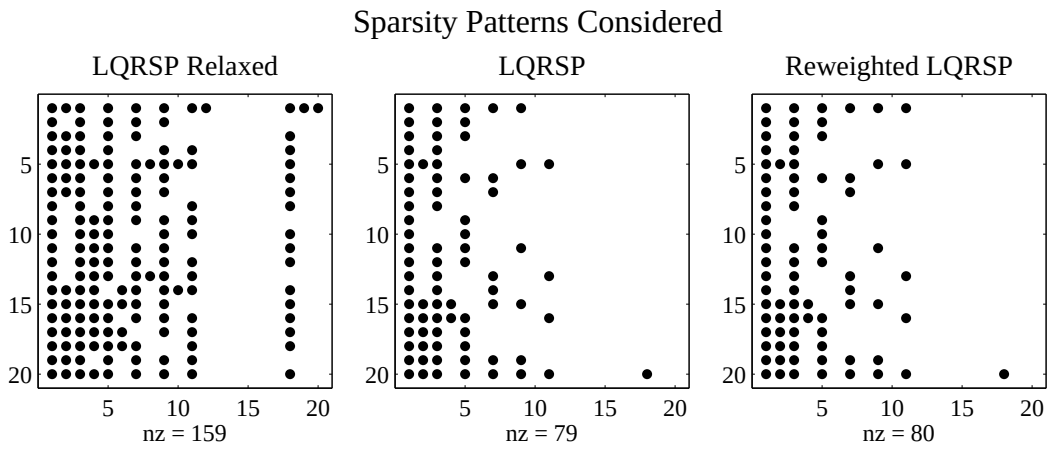

Figure 4.12: Sparsity patterns used for Continuous Time Simulations.

shown in Figure 4.12 reveal unexpected patterns. Some states are important to some dampers and not to others, but the odd numbered states in the left half of the gain matrix seem to be most important. The LQRSP 159 matrix also reveals a strong dependence on state 18. The most important information gleaned from Figure 4.12 is the knowledge of which states need to be estimated at each story. At most, 11 states need to be estimated at each story in the LQRSP 159 gain matrix, which decreases the amount of feedback information required at all stories significantly. In the LQRSP 79 matrix, 11 states can completely be eliminated from the system, and at most, eight states need to be estimated.

When considering the LQRSP 79 system, large drifts are noted in the Kobe earthquake on the first story, so one additional feedback state is added for the first story. The LQRSP sparsity weight $W_{1,11}$ is reweighted to zero in the LQRSP formulation, ensuring additional feedback information at the first story. The LQRSP 80 matrix is then used to examine the effect of one additional feedback state on the system.

The three gain matrix structures are compared to the fully populated LQR gain matrix in the four earthquake ground motion simulations. The maximum drifts, accelerations, and actuator forces at each story for each earthquake are plotted in Figure 4.13. Similar to the 5-Story benchmark structure, all four control control schemes significantly improve the drift of the system, with LQRSP 79 having problems in Stories 1, 7, 8, 12, and 13. As hoped, the reweighting used in LQRSP 80 is able to reduce the first story drift in the Kobe earthquake over the LQRSP 79 system without increasing

drifts on other stories. The first story is considered carefully because it is often the most important story to control due to its interstory height and axial loads. A similar approach of adding feedback information could be extended to the other stories where LQRSP 79 is less effective. For example, Story 12 only has three feedback gain values in the LQRSP 79 gain matrix, so a fourth feedback gain value could be used to decrease the drift on Stories 12 and 13. LQRSP gives an excellent starting gain matrix, but some knowledge of the system can also be used to increase its efficacy.

All feedback gain systems, however, are susceptible to acceleration increases and large accelerations on Stories 5 and 15. This is due to the change in number of dampers between the stories and the poor assumption that the damper is ideal. The forces leading to the large accelerations are not achievable in practice, so the large accelerations should be considered skeptically. If the acceleration increases continue in more realistic simulations, a different weighting in the LQR $\mathbf{Q}$ matrix may be considered to decrease accelerations. In Section 4.2.4, more realistic damping devices are considered where the force gradient needed to produce large accelerations may not be possible.

These observations from the time history maxima are largely confirmed in Tables 4.3, 4.4, and 4.5, which have the maximum, average, and minimum story RMS drift, acceleration, and force, respectively, when the structure is excited by a shaped BLWN. By these results, LQR and LQRSP 159 equally good at limiting interstory drift with LQRSP 79 and LQRSP 80 very close behind. Accelerations are increased in all systems, but the difference between the RMS acceleration and RMS force between all systems is negligible. In all, the LQRSP 159 system has matched the LQR system with 40% of the feedback information, while the LQRSP 79 and LQRSP 80 systems provide similar results but suffer from the loss of feedback information on some stories.

The LQRSP systems for the 5-Story Kajima Shizuoka building and reduced 20-Story SAC structure are seen to provide similar levels of control as the LQR system when ideal actuators are considered. However, because a truly active system cannot be implemented in reality, the following sections explore more realistic semi-active control systems.

4.2.3 Semi-Active 5-Story Benchmark

The ideal actuator case is an excellent tool for exploring the performance of LQRSP; however, for practical applications of feedback control in structural systems, semi-active

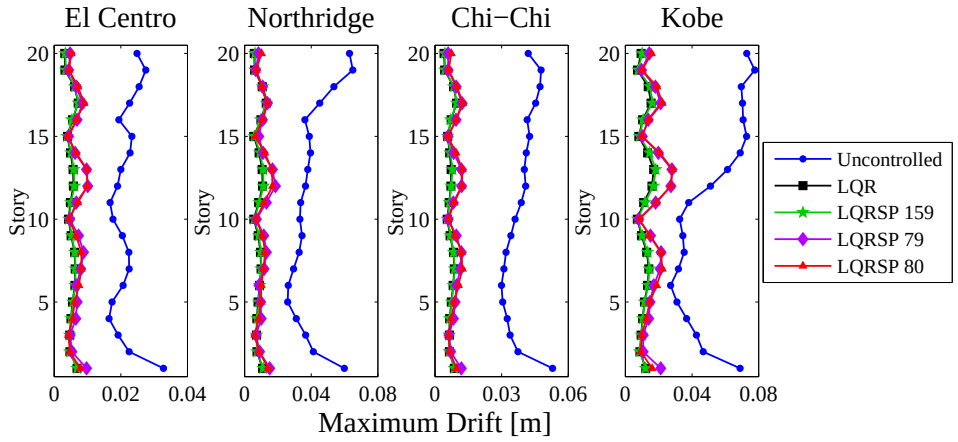

(a) Maximum Drift

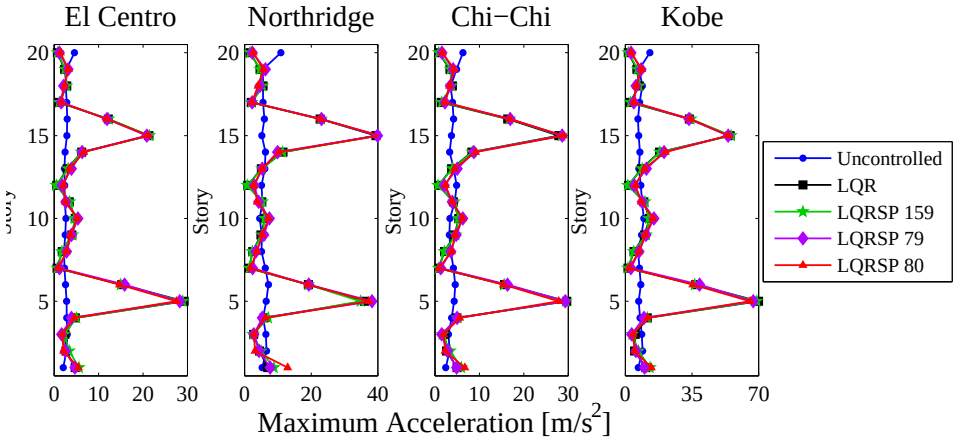

(b) Maximum Acceleration

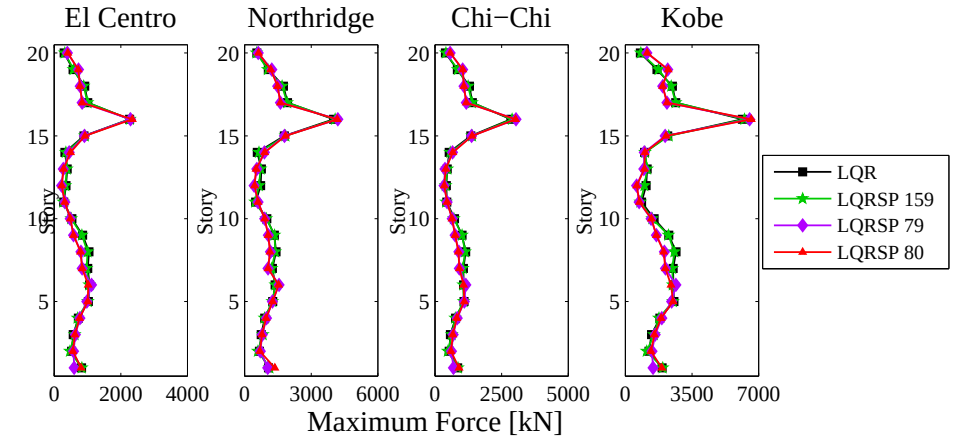

(c) Maximum Force

Figure 4.13: Maximum Responses for 20-Story benchmark building with active control during multiple earthquake simulations.

Table 4.3: RMS drift for the 20-Story benchmark structure under a shaped band-limited white noise, normalized to the RMS drift of the uncontrolled structure.

RMS Drift, Normalized to Uncontrolled				
	LQR	LQRSP 159	LQRSP 79	LQRSP 80
Maximum	0.12	0.12	0.13	0.14
Average	0.08	0.08	0.09	0.09
Minimum	0.05	0.05	0.06	0.06

Table 4.4: RMS acceleration for the 20-Story benchmark structure under a shaped band-limited white noise, normalized to the RMS acceleration of the uncontrolled structure.

RMS Acceleration, Normalized to Uncontrolled				
	LQR	LQRSP 159	LQRSP 79	LQRSP 80
Maximum	5.75	5.64	5.72	5.60
Average	1.35	1.37	1.40	1.40
Minimum	0.09	0.09	0.14	0.15

Table 4.5: RMS force for the 20-Story benchmark structure under a shaped band-limited white noise.

RMS Force in Shaped BLWN [kN (rms)]				
	LQR	LQRSP 159	LQRSP 79	LQRSP 80
Maximum	909	925	955	958
Average	276	275	268	268
Minimum	99	89	96	98

dampers are considered. A Maxwell model is used to model the force in a semi-active hydraulic damper (SHD) (Equation 3.49), and these dampers are included in the control system for the 5-Story Kajima-Shizuoka building. Although these dampers are non-linear and rate-dependent, the control design is still calculated as though active actuators are employed. In order to calculate the desired control force in real time, the dampers are approximated as a dashpot so that the desired damping coefficient c_d can be calculated from the force prescribed by the feedback gain matrix F and the interstory velocity v_{rel}:

$$c_d = \frac{F}{v_{rel}} \tag{4.1}$$

The desired damping coefficient then has saturation limits applied to calculate the actual c_{SHD}, listed in Table 3.1, and there is force saturation inherent in the damper.

Because the fully decentralized LQRSP 10 from the active simulations performed very well, only LQR, LQRSP 10, and Heuristic control designs are considered in the semi-active earthquake simulations. In addition, Passive On and Passive Off systems, where the SHDs are set to maximum and minimum damping coefficients, respectively, are considered in order to guarantee that using a feedback control system is worth the cost of deployment and maintenance.

Despite the difference in dampers considered, the maximum earthquake results seen in Figure 4.14 show LQRSP 10 and LQR controllers perform virtually the same as in the active earthquake simulations. The LQRSP design is based on the assumption of an active system, but it is equally effective with semi-active control on this structure. All systems are also better than the Passive On system, which has difficulty controlling drifts in the Northridge and Kobe earthquakes, while often making accelerations worse than the uncontrolled system. The Heuristic method actually performs better in interstory drift on the 5^{th} story than in the active simulations. However, it is worse on the lower stories than the LQR and LQRSP 10 controllers. Because the lower dampers exert less force for the Heuristic system, the local drifts are increased. This also results in larger forces on upper stories, leading to increased acceleration response on those stories.

While the Heuristic system requires more force toward the top of the structure, the LQR and LQRSP 10 systems are able to balance interstory drift and accelerations with the opposite force distribution. The lack of global information hurts the Heuristic system, as seen in Table 4.6, where the lower stories perform worse in RMS drift in the BLWN than LQR, while the upper stories perform better than LQR. The control goal within the $\mathbf{Q}$ matrix is to minimize the interstory drifts equally on all stories, so the optimal control design should minimize all story drifts as evenly as possible. LQR and LQRSP 10 spread the control fairly evenly over the structure and skewed toward the lower stories (Table 4.8), which keeps drifts low and acceleration (Table 4.7) under control. LQRSP 10 actually improves the RMS acceleration of the system more than LQR. On the other hand, the Heuristic method resembles using Passive Off damper on the 1^{st} story, which improves its RMS acceleration, but does a poor job of preventing energy from traveling to upper stories.

Although the RMS drift in Table 4.6 appears to favor the Passive On system, the large increases in acceleration over the uncontrolled system in Table 4.7 are unacceptable. The shaped BLWN does not have the impulsive content of near-field earthquakes,

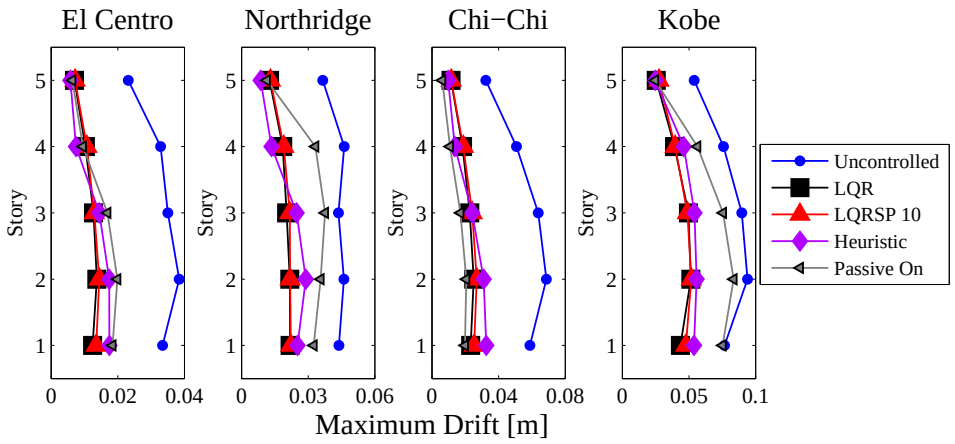

(a) Maximum Drift

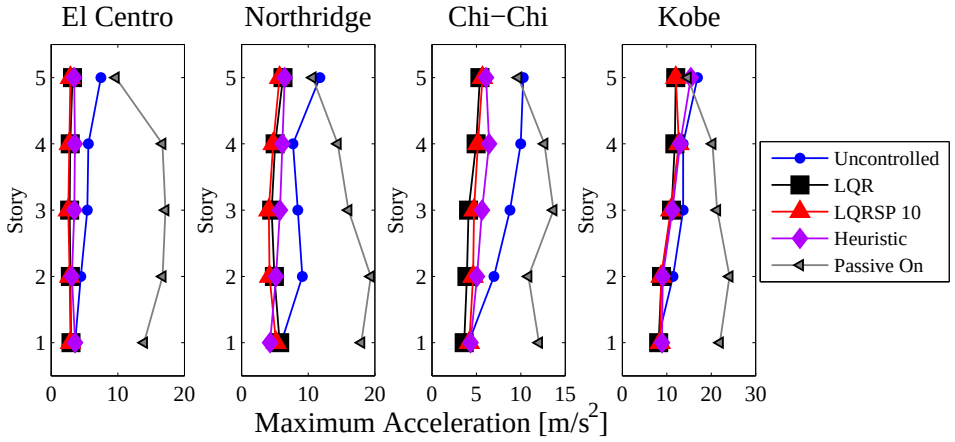

(b) Maximum Acceleration

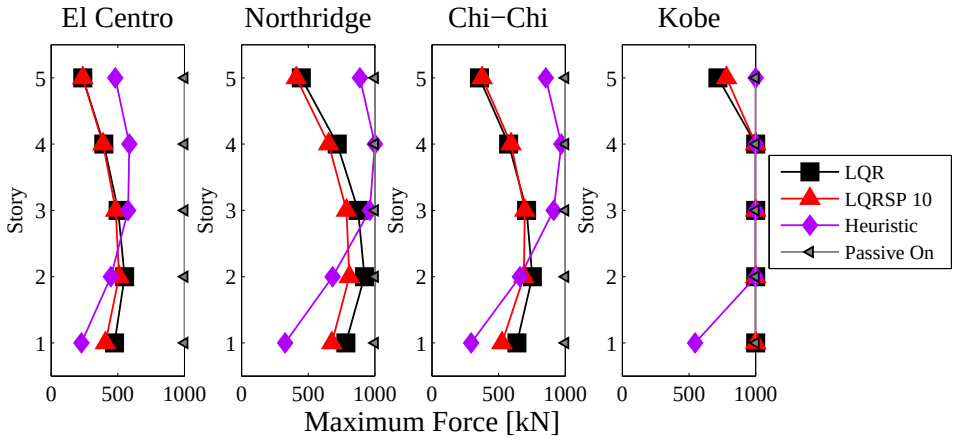

(c) Maximum Force

Figure 4.14: Maximum Responses for Kajima-Shizuoka building with Semi-active control during multiple earthquake simulations.

Table 4.6: RMS drift for the Kajima-Shizuoka building with semi-active control under a shaped band-limited white noise, normalized to the RMS drift of the uncontrolled structure.

RMS Drift, Normalized to Uncontrolled					
Story	LQR	LQRSP 10	Heuristic	Passive On	Passive Off
1	0.49	0.50	0.58	0.39	0.69
2	0.43	0.45	0.49	0.33	0.68
3	0.39	0.41	0.41	0.26	0.67
4	0.36	0.37	0.30	0.21	0.65
5	0.33	0.34	0.23	0.20	0.60

Table 4.7: RMS acceleration for the Kajima-Shizuoka building with semi-active control under a shaped band-limited white noise, normalized to the RMS acceleration of the uncontrolled structure.

RMS Acceleration, Normalized to Uncontrolled					
Story	LQR	LQRSP 10	Heuristic	Passive On	Passive Off
1	0.97	0.84	0.77	2.84	0.74
2	0.67	0.59	0.67	2.71	0.58
3	0.53	0.51	0.67	2.57	0.58
4	0.49	0.50	0.68	2.36	0.62
5	0.44	0.45	0.50	1.29	0.62

Table 4.8: RMS force for the Kajima-Shizuoka building with semi-active control under a shaped band-limited white noise.

RMS Force in Shaped BLWN [kN (rms)]					
Story	LQR	LQRSP 10	Heuristic	Passive On	Passive Off
1	117.7	115.3	61.4	685.8	48.5
2	131.3	125.2	108.3	681.4	52.3
3	118.1	112.3	132.5	626.6	49.4
4	93.6	90.0	133.8	518.5	46.6
5	58.6	56.2	116.5	347.8	34.9

allowing the Passive On system to appear more effective. On the other hand, the Northridge and Kobe earthquakes, shown in Figure 4.14, result in maximum drifts that are not well controlled by the Passive On system. While the RMS drift in a shaped BLWN is useful for describing the steady-state response of a system, a portion of the time history shown in Figure 4.15 indicates the shortcomings of the Passive On system. Passive On minimizes 1^{st} story drift very effectively around the 50-second mark, but

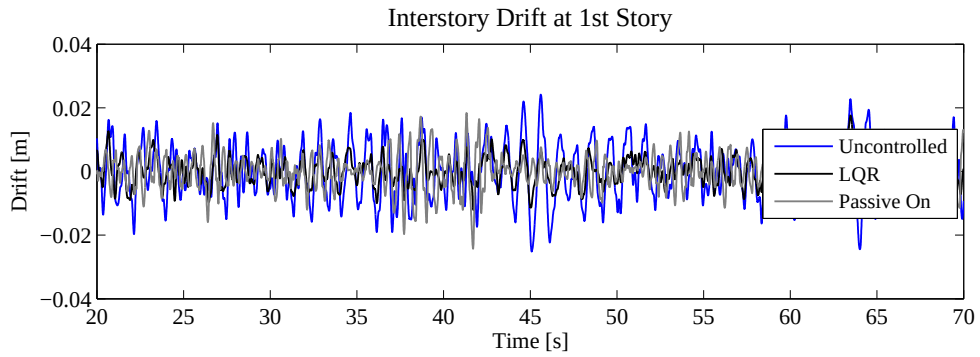

Figure 4.15: Drift of first story of Kajima-Shizuoka building during a portion of shaped BLWN.

it also overshoots the uncontrolled system around the 42-second mark. LQR is able to improve on the uncontrolled system uniformly throughout the entire time history, which leads to the RMS drift discrepancy. Though not plotted in Figure 4.15 for clarity, the LQRSP 10 system has very similar time response to the LQR system. In addition, the first story accelerations of the Passive On system throughout the Kobe earthquake are shown in Figure 4.16 to be much higher than both LQR and the uncontrolled system, even for the earthquake time periods of lower intensity, *e.g.* after the 15-second mark. The ability of LQR and LQRSP to improve drift and acceleration response throughout the time histories of both earthquakes and shaped BLWN indicates that they are better controllers over a broad range of frequency content, while the Passive On system is a better controller for narrow ranges of frequency content. As all earthquakes contain varying frequency content, LQR and LQRSP will be more consistently effective than a Passive On controller.

The frequency response of the first story drift with ground input in each control system is considered in Figure 4.17. The Passive On system has a higher predominant natural frequency than the uncontrolled and closed-loop systems. The large forces provided by the dampers make the building stiffer, driving the first natural frequency from 1 Hz to about 1.75 Hz. In addition, Figure 4.18 shows the inability of the Passive On system to control accelerations between 1 and 2 Hz, which is often where a large portion of earthquake frequency content lies. The Passive On system also has increased gains at frequencies beyond 6 Hz, further increasing the acceleration response of the system. Furthermore, the Heuristic system does not reduce the peaks of the first natural

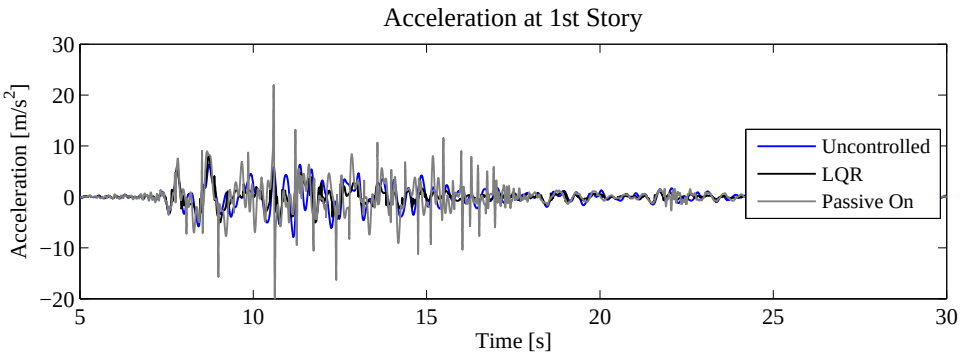

Figure 4.16: Acceleration of first story of Kajima-Shizuoka building during the Kobe earthquake.

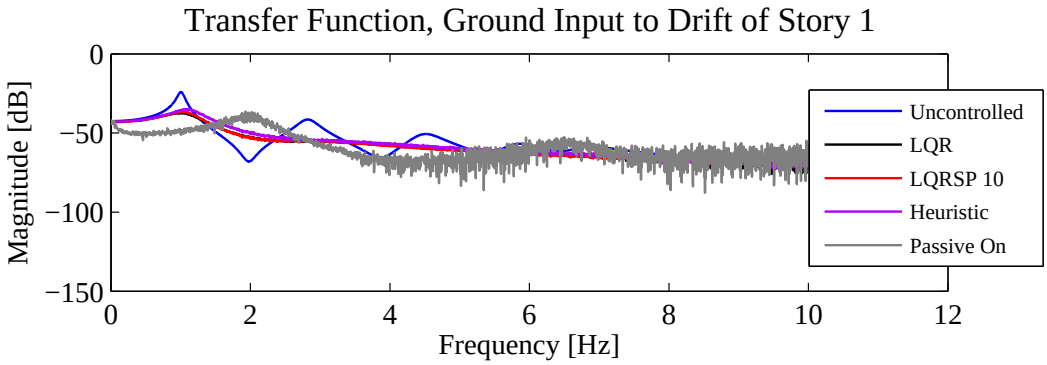

Figure 4.17: Transfer function from ground motion to first story drift of the Kajima-Shizuoka building.

frequency as well as LQR or LQRSP 10.

The Passive Off system, on the other hand, does not have problems with increasing accelerations, but it also does not meet the control goal of minimizing interstory drifts. The RMS Tables 4.17 and 4.18 consistently show Passive Off leading to a marginal improvements over the uncontrolled system. Therefore, the feedback control systems provide more consistent control over broader ranges of earthquake frequencies and magnitudes than the passive systems.

The semi-active analysis has also made it clear that LQRSP provides a better controller than the Heuristic method for fully decentralized control, as was determined previously in closed-loop cost and active control comparisons. All feedback control systems are also clearly better than the Passive On and Passive Off systems, justifying the

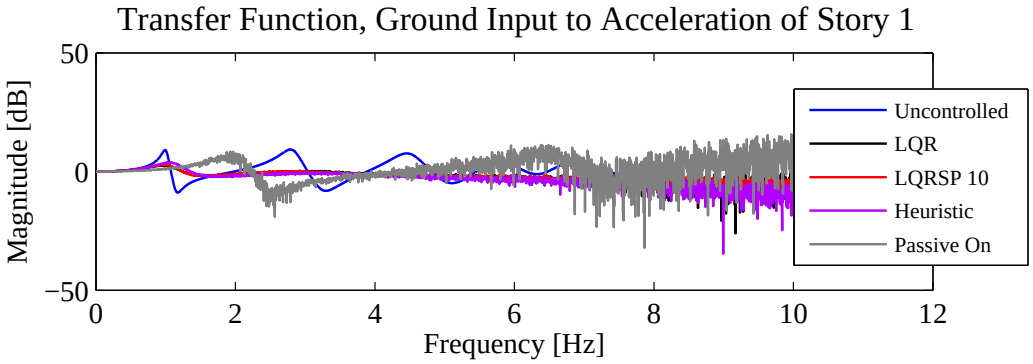

Figure 4.18: Transfer function from ground motion to first story acceleration of the Kajima-Shizuoka building.

use of a feedback control system on the 5-Story Kajima-Shizuoka building.

4.2.4 Semi-Active 20-Story Benchmark

The SHDs with the same parameters (Table 3.1) are now deployed on the 20-Story benchmark structure. Similar to the active simulations, the first five stores are given four SHDs, the sixth to 15^{th} stories are given two SHDs, and the remaining stories are given one SHD each. Because of the control improvements of the reweighted LQRSP 80 system over the LQRSP 79 system in the actively controlled structure, only LQRSP 80 and LQRSP 159 are compared to LQR control for the semi-active systems.

The three control methods are almost identical across maximum drift, acceleration, and force calculations in the four earthquakes considered (Figure 4.19). All three controllers minimize interstory drift effectively, with the LQRSP 80 system almost equaling the LQR and LQRSP 159 systems. The maximum acceleration and force profiles also have very similar shapes among the three controllers. Additionally, the large acceleration increases seen in the active simulations are not present in the semi-active simulations, demonstrating the ability of the semi-active devices to prevent extreme control efforts. The larger forces and the number of dampers on the lower stories lead to some expected acceleration increases, but above Story 5, the accelerations remain similar to those experienced by the uncontrolled structure. In all, it appears the LQRSP 80 system successfully eliminates 11 states from the feedback control system without any decrease in performance.

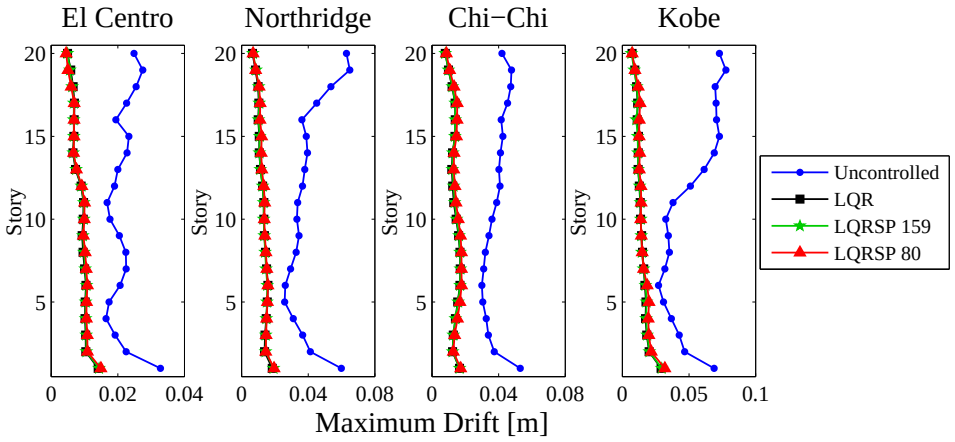

(a) Maximum Drift

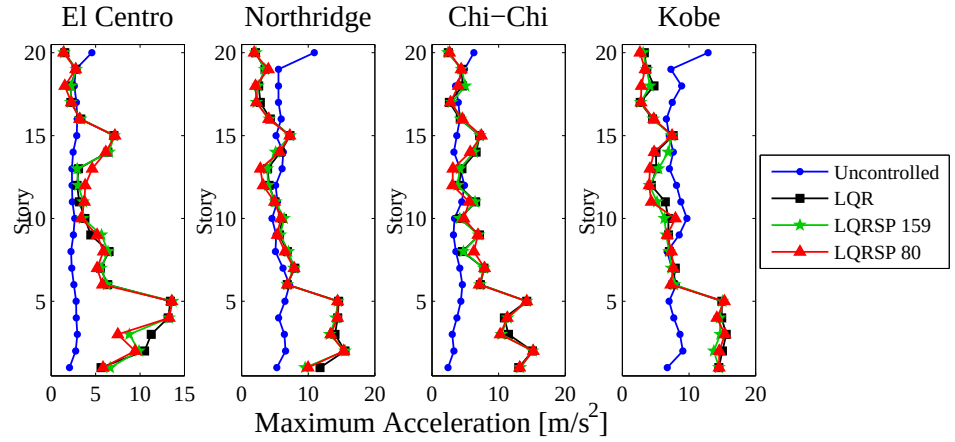

(b) Maximum Acceleration

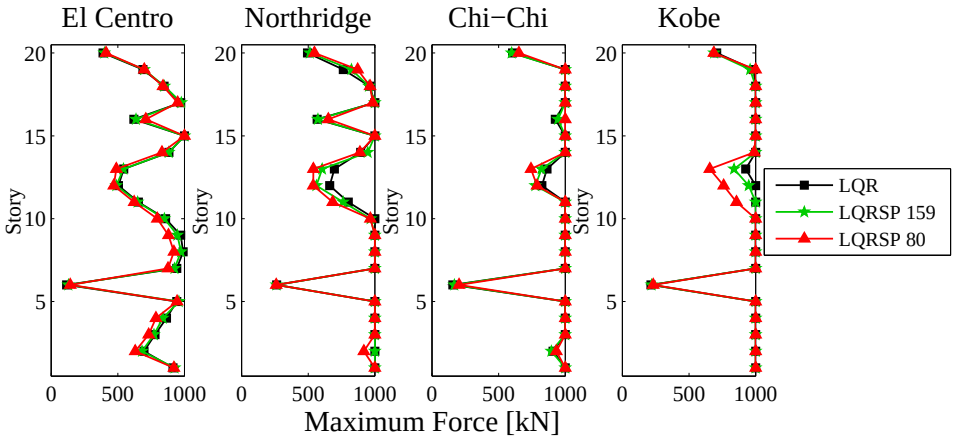

(c) Maximum Force

Figure 4.19: Maximum Responses for Kajima-Shizuoka building with Semi-active control during multiple earthquake simulations.

Passive On and Passive Off systems are also considered in the 20-Story system, but they are much less effective than the feedback control systems, even in RMS metrics calculated during the shaped BLWN. As is seen in Tables 4.9 to 4.11, the LQR, LQRSP 159, and LQRSP 80 feedback control systems are very similar across all RMS results. The Passive On system approaches the feedback control systems in RMS drift, but increases the RMS accelerations of all stories significantly and provides very high levels of force, while the Passive Off system only decreases RMS drift and RMS acceleration very slightly with correspondingly low force levels.

Table 4.9: RMS drift for the 20-Story benchmark structure with semi-active control under a shaped band-limited white noise, normalized to the RMS drift of the uncontrolled structure.

RMS Drift, Normalized to Uncontrolled					
	LQR	LQRSP 159	LQRSP 80	Passive On	Passive Off
Maximum	0.22	0.22	0.23	0.32	0.83
Average	0.19	0.19	0.20	0.25	0.80
Minimum	0.12	0.12	0.12	0.17	0.71

Table 4.10: RMS acceleration for the 20-Story benchmark structure with semi-active control under a shaped band-limited white noise, normalized to the RMS acceleration of the uncontrolled structure.

RMS Acceleration, Normalized to Uncontrolled					
	LQR	LQRSP 159	LQRSP 80	Passive On	Passive Off
Maximum	6.32	6.32	6.46	6.94	0.88
Average	2.96	2.97	2.95	2.98	0.66
Minimum	0.43	0.44	0.45	1.41	0.57

Table 4.11: RMS force for the 20-Story benchmark structure with semi-active control under a shaped band-limited white noise.

RMS Force in Shaped BLWN [kN (rms)]					
	LQR	LQRSP 159	LQRSP 80	Passive On	Passive Off
Maximum	456	456	464	817	74
Average	303	302	298	737	51
Minimum	42	44	48	504	45

The decentralized systems computed by LQRSP, therefore, are shown to be as effective as the centralized LQR control system on the 20-Story benchmark structure with a fraction of the feedback control measurements. The LQRSP algorithm is shown to

easily compute sparse feedback gains for an unintuitive gain matrix structure, which could be extended to non-collocated systems as well as systems involving input-output models.

4.3 Reformulation of Heuristic Algorithm

The implementation of the ADMM is what allows LQRSP to identify desired sparse gain matrix structures and calculate a good starting guess for the the LQRSP polishing step. In addition, LQRSP allows the control designer to compare gain matrices at various sparsity levels and discern which gain matrix entries are most important. Figures 4.4 and 4.6 also show that the LQRSP polishing step leads to better decentralized gain matrices than similarly structured Heuristic gain matrices, and these results are confirmed with the results of the various continuous time simulations. Upon closer examination, the largest difference between the two algorithms is the calculation of the matrix $\mathbf{L}$ in Equations 3.22 and 3.45. Because the $\mathbf{C}$ matrix is an identity for the benchmark structures considered, the two equations only differ with the inclusion of the ground input matrix $\mathbf{E}$. The Heuristic method does not include $\mathbf{E}$ and minimizes cost as $trace(\mathbf{P})$ instead of $trace(\mathbf{E}^T\mathbf{P}\mathbf{E})$. Comparing $trace(\mathbf{P})$ calculated by the Heuristic method and LQRSP for the same gain matrices previously considered in Section 4.1 in Figure 4.20 shows that the Heuristic method is capable of minimizing its objective function, *i.e.* $trace(\mathbf{P})$ in this case.

If the nature of the external excitations were of unknown origin and assumed to be random, the $\mathbf{E}$ matrix would become an identity matrix and not factor in to the closed-loop cost in $trace(\mathbf{E}^T\mathbf{P}\mathbf{E})$. Therefore, the cost equation would reduce to $trace(\mathbf{P})$, which the Heuristic method minimizes by default, and the two methods would converge. However, the way the external inputs enter the system is known, so the $\mathbf{E}$ matrix is not an identity. Using this knowledge by default allows LQRSP to compute more effective decentralized feedback gain matrices, as shown in the continuous time simulations. The Heuristic method can be reformulated to include the input information in $\mathbf{E}$. After the reformulation, the $trace(\mathbf{E}^T\mathbf{P}\mathbf{E})$, shown in Figure 4.21, has very little difference between LQRSP and the Heuristic polishing. However, the initial guess and step size sometimes lead the Heuristic method to find local minima not found by the LQRSP method. For example, the Heuristic method has a small jump in its cost around $nz = 32$ not seen in

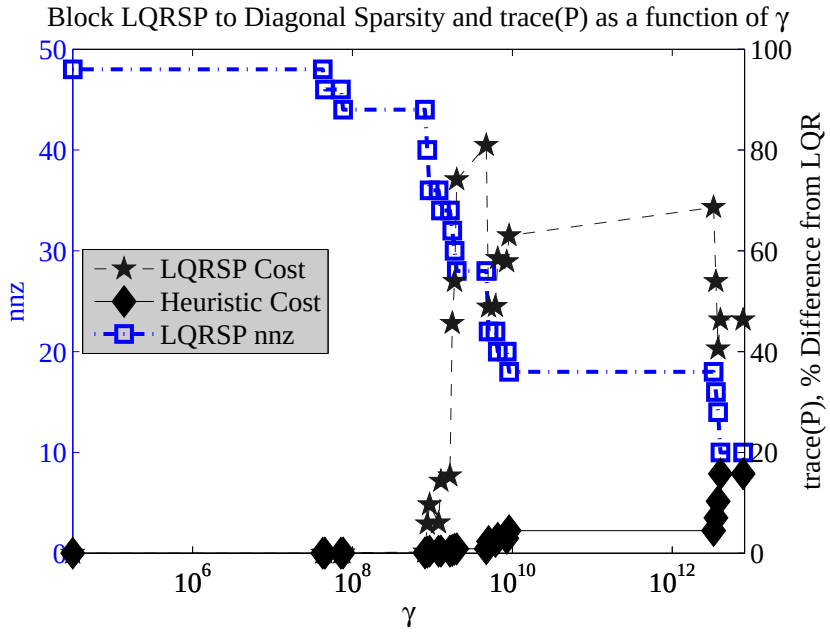

Figure 4.20: Number of non-zero elements in the gain matrix decreasing as γ and the cost of the trace($\mathbf{P}$) increases.

the LQRSP method.

To ensure the reformulated Heuristic method is computing the optimal decentralized feedback gain matrices, the fully decentralized gain matrix values from the 5-Story Kajima-Shizuoka benchmark structure are compared in Equation 4.2 for (a) LQRSP, (b) the reformulated Heuristic method including the $\mathbf{E}$ matrix, and (c) the original Heuristic method. The reformulated Heuristic method is able to calculate virtually the same final gain matrix as the LQRSP polishing step despite starting at a worse initial guess, while the Heuristic algorithm where input from $\mathbf{E}$ is not considered has a much different form. The gain matrix values for velocity states and lower stories tend to be larger for the methods that include the $\mathbf{E}$ matrix, while the gain matrix values for displacement states and upper stories tend to be larger for the non-$\mathbf{E}$ Heuristic method. This discrepancy shows why the Heuristic method called for more control on the upper story in the simulations, while the LQRSP control was more uniform throughout the structure.

While the Heuristic method can be reformulated to mostly match the LQRSP polishing step, there are still many advantages to the LQRSP algorithm.

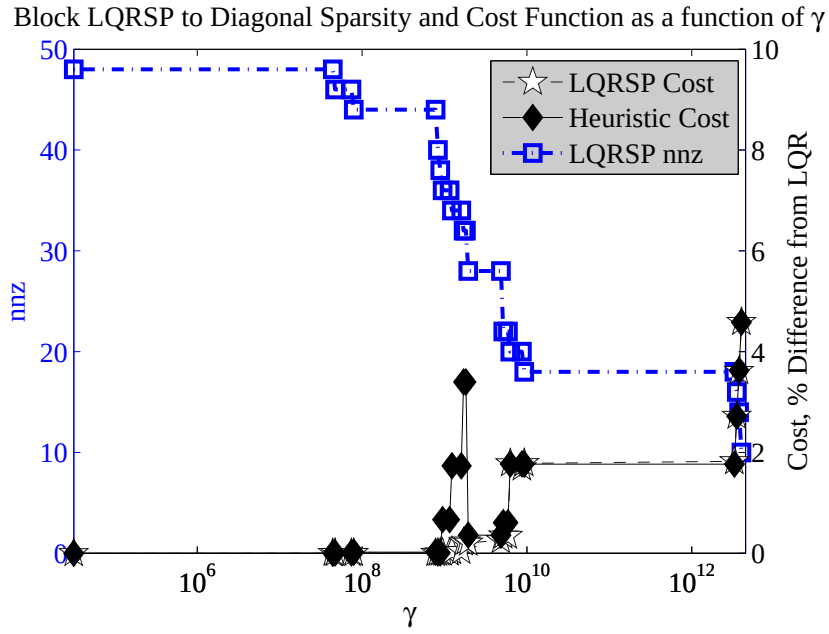

Figure 4.21: Number of non-zero elements in the gain matrix decreasing as γ and the cost of the objective function increases. The Heuristic algorithm is reformulated for this computation.

- LQRSP is better equipped to deal with non-collocated systems or systems that have a non-intuitive gain matrix structure, as was seen in the control of the 20-Story benchmark structure.
- The use of ADMM in LQRSP allows for better initial guesses for the polishing of structured gain matrices, which results in a higher likelihood of calculating the global minimum instead of a local minimum.
- Calculating a large family of gain matrices for increasing sparsity parameters γ also allows for better initial guesses for the polishing step. In addition, with the closed-loop cost evaluated for every gain matrix, the large increases in cost due to the loss of particular feedback gain values can be traced and those values can be preserved. This was seen to improve the control effort in both benchmark structures considered.
- LQRSP is able to lump state feedback information together, which will be useful for considering wireless systems where state estimation results are lumped together and time delay is a factor. Coupled with the large family of gain matrices

$$\begin{bmatrix} -8.06 & & & & & -2.79 & & & & \\ & -5.97 & & & & & -1.71 & & & \\ & & -4.34 & & & & & -1.15 & & \\ & & & -3.13 & & & & & -0.77 & \\ & & & & -1.77 & & & & & -0.43 \end{bmatrix} \times 10^6 \tag{4.2a}$$

$$\begin{bmatrix} -8.21 & & & & & -2.79 & & & & \\ & -5.97 & & & & & -1.71 & & & \\ & & -4.34 & & & & & -1.16 & & \\ & & & -3.09 & & & & & -0.77 & \\ & & & & -1.79 & & & & & -0.43 \end{bmatrix} \times 10^6 \tag{4.2b}$$

$$\begin{bmatrix} -6.93 & & & & & -0.92 & & & & \\ & -7.83 & & & & & -0.98 & & & \\ & & -7.25 & & & & & -1.02 & & \\ & & & -6.59 & & & & & -1.05 & \\ & & & & -6.15 & & & & & -1.77 \end{bmatrix} \times 10^6 \tag{4.2c}$$

Equation 4.1: Diagonal gain matrices for the Kajima-Shizuoka building calculated by (a) LQRSP, (b) Heuristic with **E** matrix included, and (c) Original Heuristic formulation.

considered, various control schemes with different sampling rates can be compared easily in the LQRSP framework.

In this chapter, LQRSP has been demonstrated to calculate decentralized feedback gains for both intuitive and non-intuitive gain structures in the continuous time domain with good results. In the next chapter, the LQRSP algorithm will be extended to the discrete time domain to examine its efficacy in systems where time delay and noise is considered.

Chapter 5

Discrete Time Comparison

In this chapter, the LQRSP control algorithm is extended to the discrete time domain, in which time delay can be taken into account for more realistic simulations of wireless feedback control.

5.1 Simulation Parameters

While the continuous time simulations are useful for general comparison of control schemes, discrete time simulations can include the time delay inherent in some physical control systems. At very fast sampling rates, the discrete time feedback control gain matrix approaches the continuous time gain matrix. Therefore, for wired systems, the continuous time feedback gain matrix can be used with little error due to time delay. If wireless controllers and sensors are used, an associated time step for each communication link must be considered along with a time step for each control force calculation.

The modified 5-Story Kajima-Shizuoka benchmark structure (Figure 2.1) outfitted with collocated wireless controllers and sensors is considered for the discrete time control simulations. The three discrete time control gain matrix structures considered in the wireless system are shown in Figure 5.1. The LQR gain matrix is fully populated, and two LQRSP gain matrices are considered: one gain matrix that lumps displacement and velocity state feedback information together and has lower stories send their local information to the story above, and one gain matrix that only requires local information. The discrete-time LQRSP software, though not currently available for download, is provided by the same research group that provided the continuous-time software—`http:`

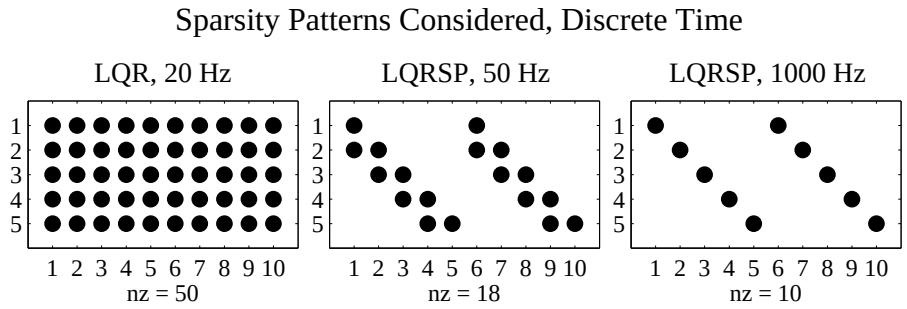

Figure 5.1: Sparsity patterns used for Discrete Time Simulations.

`//www.ece.umn.edu/users/mihailo/software/lqrsp/`. The corresponding sampling rates listed in Figure 5.1 are calculated with the following assumptions:

- The controllers can use feedback gain measurements and prescribe damper coefficient c every 1 ms, i.e. they can run at a maximum of 1000 Hz.
- If only local information is required, no wireless communication is required because the sensor and local controller are collocated and linked.
- At least 8 ms is required for each packet of wireless communication sent between stories.
- All sensors sample at the same time, starting at time $t = 0$.

With these assumptions, the sampling rates of each controller can be calculated. In the calculation of the LQR gain matrix, each story broadcasts its local measurements from time $t = 0$ to all stories in turn:

1. Story 1 broadcasts measurements (8 ms)
2. Story 2 broadcasts measurements (8 ms)
3. Story 3 broadcasts measurements (8 ms)
4. Story 4 broadcasts measurements (8 ms)
5. Story 5 broadcasts measurements (8 ms)
6. Update c and measure again (1 ms)

Minimum time required: 41 ms

There are five separate communication steps of 8 ms and one update step of 1 ms, leading to an absolute maximum sampling rate of 24 Hz. The sampling rate is lowered to 20 Hz both for conservatism of the feedback communication in the control design and for ease of implementation.

In the partially decentralized LQRSP gain matrix with nz = 18, the communication of the local measurements from time $t = 0$ is only required to the story above:

1. Stories 1 and 3 send their local measurements to Stories 2 and 4 (8 ms)
2. Stories 2 and 4 send their local measurements to Stories 3 and 5 (8 ms)
3. Update c and measure again (1 ms)

Minimum time required: 17 ms

The sampling could be done at 58 Hz, but the sampling rate is again lowered to 50 Hz for conservatism of the feedback communication and ease of implementation.

The fully decentralized LQRSP gain matrix with nz = 10 is assumed to measure and update every 1 ms, and because no non-local information is required, this is the only associated time delay. The sampling rate is therefore 1000 Hz, and the continuous time LQRSP 10 feedback control gain matrix is used. The LQR and LQRSP 18 gain matrices are computed with the discrete time extensions of their continuous time counterparts (see Section 3.5).

In addition to including the sample time in the feedback control system, the discrete time simulations have sensor noise added to the feedback control loop. Displacements and velocities relative to the ground are difficult to measure in practice, but the accelerations at each story can be easily measured with accelerometers, and interstory displacements could be measured where the damper connects two adjacent stories. From these measurements, the states needed for the feedback control calculations can be estimated in addition to the interstory velocities needed to calculate the desired damping coefficient c_{SHD}. Ideally, noise would be included in the sensor signal and reflected in the final estimation in the feedback loop, but estimator design is not considered in this thesis; thus, only noise has been added to the system. The frequency content of the noise from the estimations will be dependent on the sampling rate of the control system, so the assumed noise is added to the simulation as a band-limited white noise

(BLWN) with the control system sample time oversampled to the sampling rate of the simulation. The noise power of the BLWN is adjusted such that each sensor has RMS noise at approximately 5% of the actual RMS signal. In addition, the noise seed for each measurement is changed to ensure that there is no correlation between the different measurements when noise is included.

5.2 Simulation Results

Examining the earthquake simulation results for the discrete time controllers and Passive On system on the Kajima-Shizuoka building in Figure 5.2 shows many trends similar to the continuous-time control simulations. All three feedback control systems —LQR, LQRSP 18, and LQRSP 10 —clearly improve the drift of the structure in the four considered earthquakes while also improving on the maximum acceleration reached by the structure despite the addition of noise and delay. The maximum forces rarely saturate for the feedback control systems, but the control forces are slightly larger in the upper stories of the discrete time LQR system than they are in the continuous system of Figure 4.14c. This can easily be explained by the delay inherent in the discrete time system and the noise added to the system; the discrete time LQR calculation can compensate for some delay in the system, but at some time steps more force is needed to compensate for the slower sampling rate combined with the assumed sensor noise. The LQRSP 10 accelerations are also increased slightly in the Chi-Chi earthquake because of the added noise in the system.

Because the results mirror those of the continuous time simulations, the feedback controllers are shown to be more effective than the Passive On controller. The passive systems considered in the discrete-time control simulations are unchanged from the continuous-time simulations because there is no effect on passive results due to time delay or noise. The Passive On system again remains effective in some earthquakes but not in others.

The similarities in discrete-time earthquake simulation results extend to the RMS responses to the BLWN shaped by the Kanai-Tajimi filter. Tables 5.1 and 5.2 compare very similarly to Tables 4.6 and 4.7, with LQRSP 10 now slightly better than LQR in RMS drift but slightly worse than LQR in RMS acceleration. The LQR system is shown in Table 5.3 to have consistently larger RMS forces on the upper stories than the

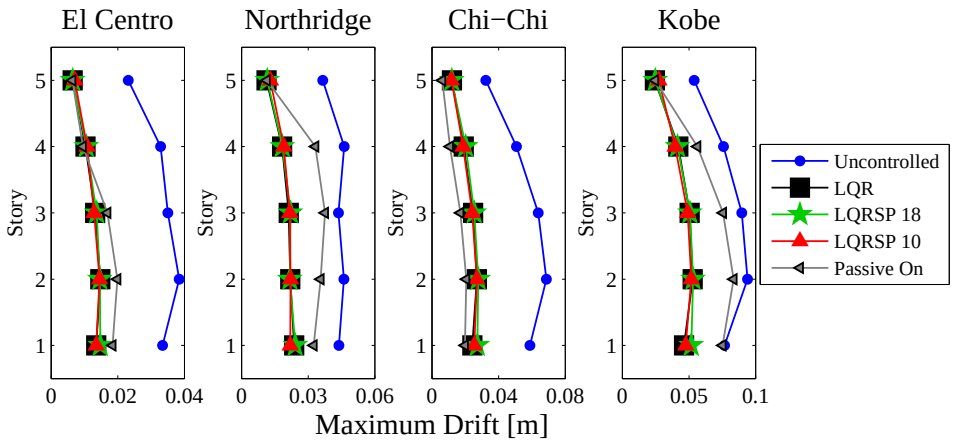

(a) Maximum Drift

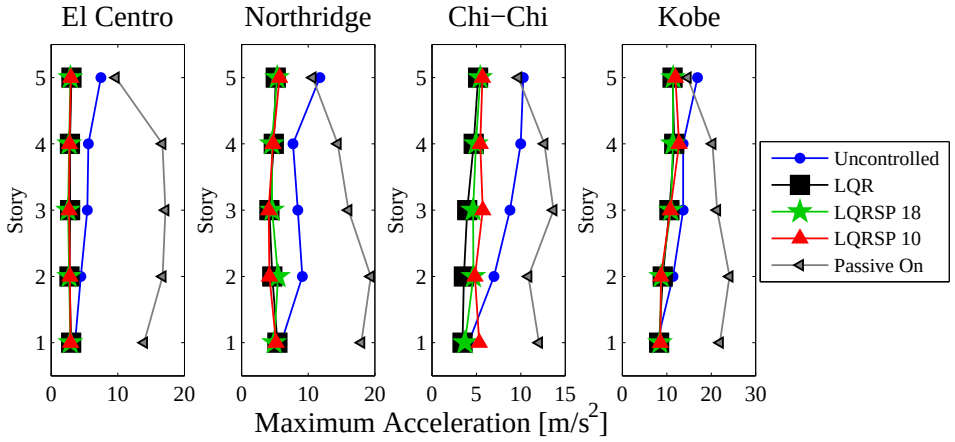

(b) Maximum Acceleration

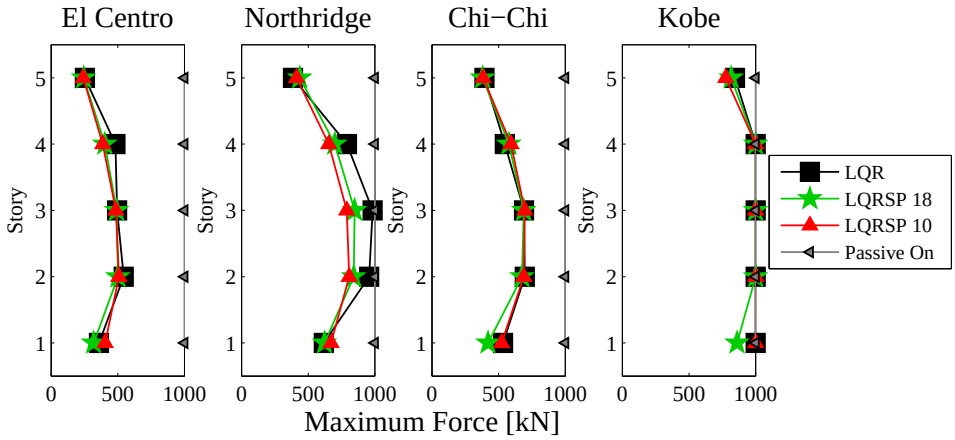

(c) Maximum Force

Figure 5.2: Maximum Responses for Kajima-Shizuoka building with discrete-time semi-active control during multiple earthquake simulations.

continuous time system in Table 4.8 due to time delay and noise, while the LQRSP 10 system has virtually the same RMS force as in the continuous time simulations. The LQRSP 18 controller is seen to be a compromise of the LQR and LQRSP 10 controllers; it runs faster than LQR, resulting in smaller RMS forces, and it has more information than LQRSP 10, resulting in lower RMS accelerations. The RMS values also reinforce the results of the feedback controllers seen in the earthquake maxima in Figure 5.2, which show a close similarity between the drift, acceleration, and force results of all systems. It is clear that all three controllers effectively control the drift response of the Kajima-Shizuoka building when time delay and noise are considered. Because the highest natural frequency of the Kajima-Shizuoka building is 6.77 Hz, it is not surprising that the three controllers are effective —even the 20 Hz LQR controller —and can improve the response of the system without negative consequences.

5.3 Loss of Information

Given the similar results between the LQR, partially decentralized LQRSP, and fully decentralized LQRSP in the discrete time simulations, there are four advantages to the fully decentralized LQRSP system:

1. A fully decentralized wireless system requires less effort to install and program.
2. Synchronization of wireless communication links can be difficult to implement.
3. By only relying on local information, the fully decentralized system can run much faster than the wireless LQR system, making up for a loss of information in the system.
4. A fully decentralized system is potentially less vulnerable to sensor or controller failure.

The first, second, and third advantages are easy to deduce, but the fourth can be tested within the discrete time simulation. For example, the third story controller is assumed to be dead on arrival of the earthquake, unable to calculate control forces or send local measurements to the other controllers. As a result, the third story damper becomes a Passive Off damper, and the other stories that require state measurements from the third story assume that the states at the third story are zero.

Table 5.1: RMS drift for the 5-Story Kajima-Shizuoka building with discrete-time semi-active control under a shaped band-limited white noise, normalized to the RMS drift of the uncontrolled structure.

RMS Drift, Normalized to Uncontrolled					
Story	LQR	LQRSP 18	LQRSP 10	Passive On	Passive Off
1	0.52	0.54	0.50	0.39	0.69
2	0.45	0.45	0.45	0.33	0.68
3	0.41	0.42	0.41	0.26	0.67
4	0.37	0.38	0.38	0.21	0.65
5	0.33	0.33	0.34	0.20	0.60

Table 5.2: RMS acceleration for the 5-Story Kajima-Shizuoka building with discrete-time semi-active control under a shaped band-limited white noise, normalized to the RMS acceleration of the uncontrolled structure.

RMS Acceleration, Normalized to Uncontrolled					
Story	LQR	LQRSP 18	LQRSP 10	Passive On	Passive Off
1	0.82	0.73	0.91	2.91	0.74
2	0.57	0.55	0.64	2.72	0.58
3	0.52	0.50	0.56	2.61	0.58
4	0.51	0.50	0.53	2.42	0.62
5	0.45	0.45	0.46	1.29	0.62

Table 5.3: RMS force for the 5-Story Kajima-Shizuoka building with discrete-time semi-active control under a shaped band-limited white noise.

RMS Force in Shaped BLWN [kN (rms)]					
Story	LQR	LQRSP 18	LQRSP 10	Passive On	Passive Off
1	94.6	97.2	116.6	691.9	48.8
2	137.7	129.6	127.8	687.2	52.6
3	127.9	119.9	115.3	633.4	50.0
4	102.4	97.2	92.4	525.2	47.1
5	63.2	60.5	57.2	352.6	35.3

Earthquakes are simulated on the Kajima-Shizuoka structure with no third story sensor or controller, and the maximum drifts show slight increases among the feedback control systems in Figure 5.3. The LQR system is affected by the loss of information on the third story with increased drifts and forces on the second and fourth stories. The LQRSP 10 system only has increased drifts on the third story, because that is the only controller that is affected by the information loss. This feedback information structure

also allows LQRSP 10 the smallest maximum drifts of the feedback control systems on the second and fourth stories. LQRSP 18 is somewhat of a compromise between the LQR and LQRSP 10 systems due to its partial decentralization and somewhat faster sampling rate. Again, each control scheme outperforms the Passive On system, showing that all are good choices to decrease interstory drifts.

The systems that require feedback information from a story that is unable to provide it are more susceptible to both drift increases and large force and acceleration increases. This conclusion from the maximum earthquake results is corroborated by the general RMS results obtained from the Kanai-Tajimi shaped BLWN simulations in Tables 5.4 through 5.6. The LQRSP 10 system has very little change from the full discrete systems in Tables 5.1 through 5.3, except for the increase in RMS drift on the local story with no control. The LQR system has increased RMS drifts on the second, third, and fourth stories, which all rely heavily on the third story for feedback information. Additionally, the RMS accelerations on the third and fourth stories are increased with the forces on the fourth and fifth stories. As can be expected, the larger amount of third story feedback information required changes many more results in the LQR system than in the LQRSP 10 system. The LQRSP 18 system is still a compromise, only increasing the third story RMS drift and RMS acceleration and fourth story RMS acceleration and force.

All three systems are not greatly affected by a loss of information, but it is also important to note that this contingency would have to be programmed into the LQR and LQRSP 18 feedback systems, whereas the LQRSP 10 system would do it by default. LQR remains effective due to the sampling rate of the system; the 20 Hz controller is able to control all modes of the Kajima-Shizuoka building. The LQR and LQRSP 18 systems are also helped by the sizing of dampers in the system—when information is lost, extra damper capacity is very helpful to keep the systems from losing effectiveness. Regardless, the LQRSP 10 system has shown to provide the required control even when the system loses information, in addition to its advantages of simpler installation and programming efforts and lack of synchronization required.

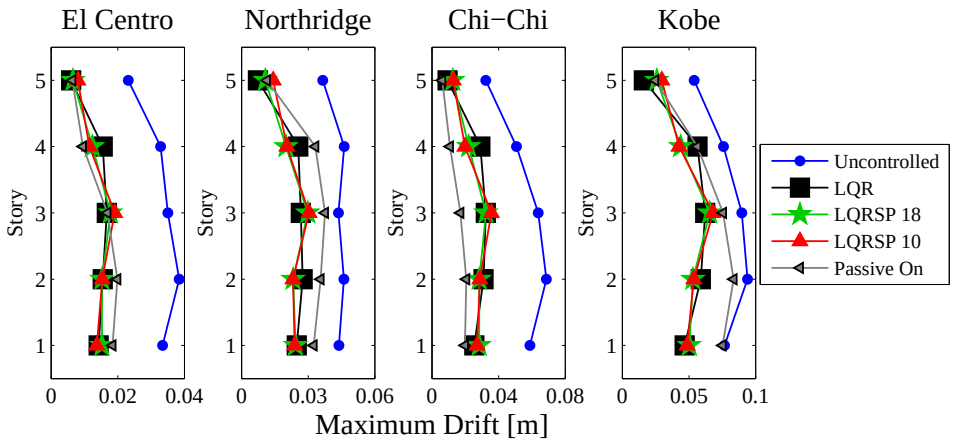

(a) Maximum Drift

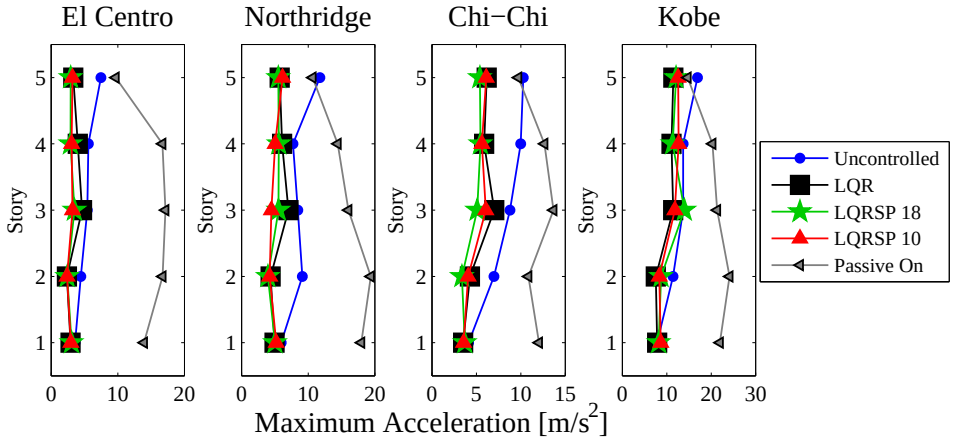

(b) Maximum Acceleration

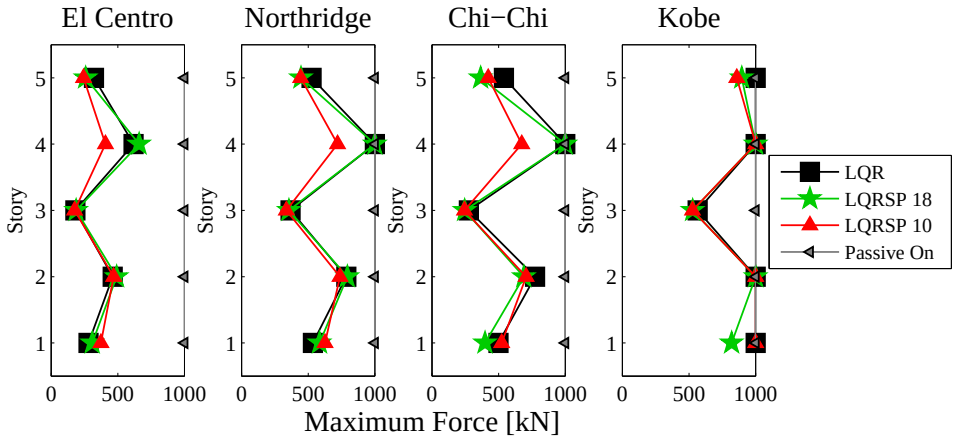

(c) Maximum Force

Figure 5.3: Maximum Responses for Kajima-Shizuoka building with discrete-time semi-active controlwith no 3^{rd} Story sensor or controller during multiple earthquake simulations.

Table 5.4: RMS drift for the 5-Story Kajima-Shizuoka building with discrete-time semi-active control with no 3^{rd} Story sensor or controller under a shaped band-limited white noise, normalized to the RMS drift of the uncontrolled structure.

RMS Drift, Normalized to Uncontrolled					
Story	LQR	LQRSP 18	LQRSP 10	Passive On	Passive Off
1	0.54	0.54	0.52	0.39	0.69
2	0.52	0.46	0.47	0.33	0.68
3	0.52	0.52	0.55	0.26	0.67
4	0.53	0.38	0.41	0.21	0.65
5	0.27	0.34	0.37	0.20	0.60

Table 5.5: RMS acceleration for the 5-Story Kajima-Shizuoka building with discrete-time semi-active control with no 3^{rd} Story sensor or controller under a shaped band-limited white noise, normalized to the RMS acceleration of the uncontrolled structure.

RMS Acceleration, Normalized to Uncontrolled					
Story	LQR	LQRSP 18	LQRSP 10	Passive On	Passive Off
1	0.83	0.75	0.94	2.91	0.74
2	0.56	0.54	0.58	2.72	0.58
3	0.68	0.63	0.56	2.61	0.58
4	0.69	0.59	0.57	2.42	0.62
5	0.47	0.46	0.49	1.29	0.62

Table 5.6: RMS force for the 5-Story Kajima-Shizuoka building with discrete-time semi-active control with no 3^{rd} Story sensor or controller under a shaped band-limited white noise.

RMS Force in Shaped BLWN [kN (rms)]					
Story	LQR	LQRSP 18	LQRSP 10	Passive On	Passive Off
1	83.3	93.4	112.8	691.9	48.8
2	113.4	125.1	123.2	687.2	52.6
3	47.4	48.7	46.7	633.4	50.0
4	141.8	161.4	99.5	525.2	47.1
5	74.9	60.4	61.5	352.6	35.3

5.4 Summary

Between all theoretical, continuous-time simulation, and discrete-time simulation comparisons, the LQRSP method has proven to create decentralized controllers capable of providing similar results as a centralized LQR system without the potential shortcomings of centralized control. However, physical testing should be explored to implement

the LQRSP controller on a scaled specimen. In the next section, a specmien similar to the Kajima-Shizuoka building is designed for physical dynamic testing to compare to simulation results.

Chapter 6

Specimen Design

In this chapter, a specimen similar to the Kajima-Shizuoka building with one bay in each frame direction is designed to test the control techniques explored in this thesis. In order to design the specimen for physical dynamic testing of the wireless LQR, LQRSP, and Heuristic control feedback gain matrices, a number of factors going into the specimen design must be considered.

6.1 Similitude

Ideally, a full scale model of the Kajima-Shizuoka building would be built and tested, but as that is prohibitively expensive, it cannot be considered. Thus, an approximate 1/10 scale model of the Kajima-Shizuoka building is designed for physical testing of feedback control designs and for future testing of wireless sensing and estimation techniques. Because of the scaling of the structure, dynamic similitude must be considered.

The first step to creating a suitable scale model should be to match the eigenvalues and eigenvectors of the system. With the 5 story Kajima-Shizuoka steel structure, the system is analyzed as a lumped-mass system, and the natural frequencies are: 1.01, 2.82, 4.49, 5.80, and 6.77 Hz. In a true replica model (Harris and Sabnis 1999), the time-scale factor will be the square root of the length-scale factor. The natural frequencies of the model would also scale linearly with the time-scaling, so if the length scale is decreased by a factor of 10, the time scale is decreased by a factor of 3.16, and the first natural frequency of the model would be 3.16 Hz. If such a large time-scaling is applied, only two of the five natural frequencies of the specimen remain below 10 Hz, and it will be

difficult to use wireless sensors effectively for frequencies above 10 Hz.

In addition to the wireless sensor difficulty, the response of the system will change based on the time scaling. The inertial accelerations will remain consistent as long as the natural frequencies of the system scale with the time scaling. However, the velocities decrease by a factor of the time scaling and the displacements decrease by a factor of the time scaling squared. As the time scaling decreases, the shake table aims to achieve the same accelerations over a shorter period of time, which decreases the amount of time over which the specimen reacts. The velocity and displacement are calculated by integrating the acceleration record, so as the acceleration record duration decreases, the velocity and displacement must also decrease at each time step. Due to the compression in time scaling, higher mode effects may also not propagate into the structure in the same way as they would for the full scale structure.

Time-scaling the earthquakes is not desirable for research that includes sensors, controllers, and rate-dependent dampers. With nonlinear semi-active hydraulic dampers (SHDs) or magnetorheological (MR) dampers, the velocities must be large enough for the dampers to dissipate energy and introduce a countering force into the system. In addition, the control algorithms implemented with these SHDs or MR dampers will look to alter their damping characteristics in real time, and in the future, a wireless network with an associated sampling rate may also be used on the building. If the time scale is compressed, the desired sampling or controlling rates may not be achievable.

However, if the natural frequencies of the benchmark structure are matched exactly with those of the specimen and the time scale remains unchanged, the specimen columns become too soft and are unable to support the structure in the unscaled earthquakes. Wang (2007) and Wang et al. (2006) verified their control algorithm through physical testing by scaling the earthquake ground records to a peak ground acceleration (PGA) of 1 m/s^2. In keeping with this approach, the scale model considered in this thesis will match the natural frequencies of the Kajima-Shizuoka building, resulting in a very soft structure. To guarantee the safety of the structure when no control is applied, the earthquake records will be scaled to 1 m/s^2.

6.2 Specimen Considerations

As outlined above, the main consideration for the shake table specimen is to match the natural frequencies and mode shapes of the true Kajima-Shizuoka structure. Because the natural frequencies and mode shapes are the eigenvalues and eigenvectors of

$$[v, \omega_n^2] = eig(\mathbf{M}^{-1}\mathbf{K}) \tag{6.1}$$

and the eigenvalues are unique for any system of $\mathbf{M}$ and $\mathbf{K}$, the mass and stiffness of the specimen should be proportional to the mass and stiffness of the benchmark structure. However, to simplify the design, the exact proportionality is relaxed to make the system easier to design and assemble. The columns are divided into three sizes, one for the first story, one for the second and third stories, and one for the fourth and fifth stories. The story masses are then finely tuned for a set of column sizes to match the first natural frequency as closely as possible, while keeping the remaining natural frequencies of the specimen within 5% of those of the benchmark structure. The stiffness of each column with modulus E, moment of inertia I, and length L is calculated as:

$$k_i = \frac{12EI}{L^3} \tag{6.2}$$

With displacement compatibility at each story, the columns are considered to be in parallel, meaning their stiffnesses are additive. In addition, the geometric stiffness of the columns are considered, where the geometric stiffness at a column is calculated from the axial force on the column P from the weight of the stories above, the length of the column L, and a constant that depends on the assumed end fixity conditions α:

$$k_g = \frac{\alpha P}{L} \tag{6.3}$$

For the specimen, the ends are assumed to be rotationally fixed but able to translate, resulting in $\alpha = \frac{6}{5}$. Finally, the stiffness of each column k_{col} becomes

$$k_{col} = k_i - k_g \tag{6.4}$$

With four columns per story, the column stiffness is multiplied by four on each story to obtain the resulting story stiffness.

The next consideration for the specimen design is the limits of the shake table. A 1.5

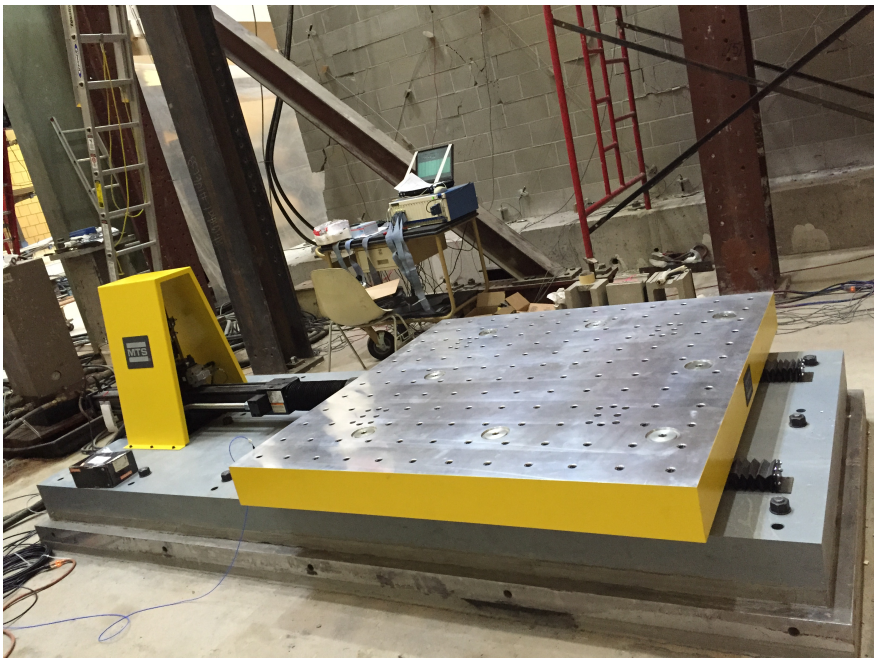

Figure 6.1: MTS Shake Table.

meter by 1.5 meter uniaxial shake table (Figure 6.1), built by MTS Systems Corporation, is used for dynamic excitation. Figure 6.2 shows the tripartite performance curve for sinusoidal loading. The dotted blue line is the curve for the bare table, which has displacement limits of ±0.2 m at low frequencies and acceleration limits of 3.5 g at high frequencies. The orange and red dotted lines refer to the limits guaranteed at the order of the table, which were ±0.08 m at 1 Hz, and ±0.02 m and 3.5 g at 8 Hz for the bare table. The solid blue line is the curve for the table with a 2 ton specimen, which is the payload of the shake table. The displacement controlled region is unchanged, while the acceleration limit is dropped to 1 g. At frequencies above 40 Hz, the acceleration limit is decreased further; however, this should not affect any testing because that is well beyond any frequency of interest. These performance limits are also dependent on the performance of the hydraulic oil and hydraulic pump. If the oil is not sufficiently warm or the pump is not running at full capacity, the shake table limits may be diminished.

With a maximum specimen mass of 2 tons, or 1,800 kg, the next step taken to design the specimen is to determine the desired column dimensions in coordination with the story masses and the control MR dampers. To ensure the columns act as springs that stay within the linear elastic range, spring steel columns of at least 60 ksi yield

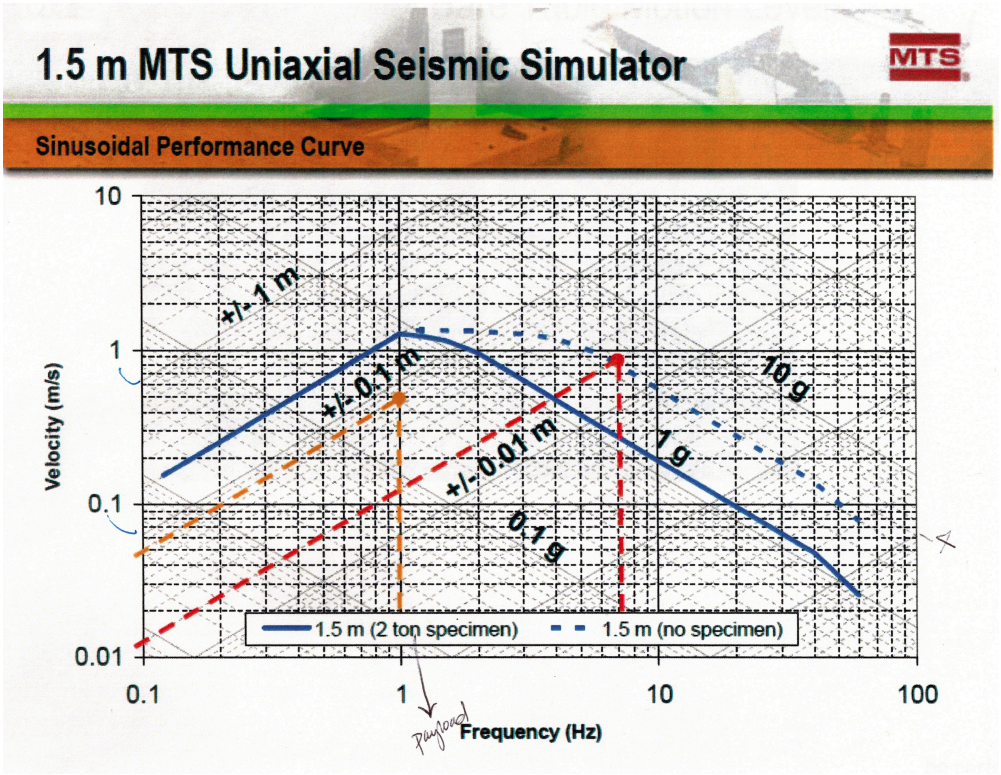

Figure 6.2: MTS Shake Table limits.

strength with rectangular cross sections are chosen. The cross sections are oriented such that the columns bend about their weak axis in the one-dimensional ground excitation. The column weak axis is designed to be much softer than the strong axis in order to encourage response in the desired direction and to eliminate torsion from the system. Steel plates are designed for each story to provide the mass for the lumped-mass system and attachments for the columns, dampers, extra mass for natural frequency tuning, and sensors. In addition to the steel plates, mass is also provided by the columns, dampers, damper mounts, miscellaneous hardware, and any necessary extra steel. As the specimen column size is increased and the columns become stiffer, more mass is required to keep the frequency characteristics of the structure constant, and then larger dampers are required to control the structure. An iterative process is outlined for the design:

1. Choose column depth, width, and length for each story. The depth is kept constant for all stories, the width is increased for the bottom story if required for strength,

and the length is changed on each story to help tune the natural frequencies of the structure.

2. Determine required story masses and approximate steel plate size required to supply that mass by solving the eigenvalue problem.

3. Set up a state-space system for the specimen design with 2% modal damping and simulate the four earthquakes considered, scaled to a PGA of 1 m/s^2. From the acceleration time histories and heights of each story, calculate the overturning moment and base shear at each time step.

4. Use the Direct Stiffness Method to calculate the internal axial, shear, and bending forces in each column at the times of maximum base shear and maximum overturning moment.

5. Determine the axial load/bending moment interaction value for each story column at maximum overturning moment in all earthquakes based on the AISC Manual of Steel Construction (2010) procedure:

$$\frac{P_u}{P_n} + \frac{8}{9}\left(\frac{M_u}{M_n}\right) \leq 1 \tag{6.5}$$

   where P_u is the axial force in the column, P_n is the nominal axial column strength, M_u is the bending moment in the column, and M_n is the nominal bending moment capacity of the column. Buckling considerations decrease the critical steel stress limit, and the B_2 approach is used for moment magnification.

6. Verify the shear capacity of the column is sufficient.

7. If the interaction is met and the shear capacity is sufficient, determine the damper size by multiplying the specimen weight by 10%. This percentage is an approximation drawn from literature, where Kurata et al. (1999) used 2 SHDs per story with force capacites 9% of the total 10,800 kN weight of the 5 Story structure, Wang (2007) used one MR damper per story with force capacity 14% of the total 177 kN weight of the 3 Story structure, and Yi et al. (2001) used MR dampers on the first two of six stories with force capacities 1.6% of the total 1.4 kN structure. If the interaction is not met, increase column widths to increase capacity or increase column lengths to decrease the mass in the structure.

Two conflicting directions arise with the iterative procedure. Ideally, the MR dampers used in the structure would be stock dampers to avoid having to make the dampers. On the other hand, the ability to move the story plates or easily change the structural configuration without a structural crane was considered. The smallest available MR damper through the Lord Corporation has a capacity of 1.25 kN at 0.05 m/s. The largest available spring steel columns have depths of 0.187", requiring a specimen weight of approximately 7 kN and a height of 2.9 m by the eigenvalue analysis. With story masses of approximately 150 kg each, the crane would be necessary for any assembly of or changes to the structure. In addition, the 1.25 kN stock dampers, at 18% of the specimen weight, are too large for the system. If the dampers are sized too large, the acceleration increases in the structure become undesirable, and the control techniques start to resemble a Passive Off damper. Therefore, lower capacity dampers must be considered along with a lighter overall structure.

Instead of using stock dampers, smaller MR paddle dampers with a similar design to those presented by Yi et al. (2001) and detailed in Figure 6.3 are designed. The 1"x1.75"x0.75" damper has an electromagnetic coil on one end of the damper, and a steel paddle sliding in between two MR fluid saturated foam sheets on the other. A set screw is used to attach the paddle to a rod that connects to the brace of the story below, and holes are drilled on the coil end to connect the damper to the story above. The detailing of damper thickness and foam thickness can also be altered to change the range of force available in the damper. The MR paddle dampers are then used to design the final structure.

6.3 Final Design and Drawings

With the smaller MR paddle dampers, a lighter structure is designed. When 30 N dampers and 0.062" deep columns are considered for the specimen design, the story masses are approximately 15 kg each, leading to dampers with force capacity of 4% of the total structure weight, similar to the ratio listed by Yi et al. (2001). This approximate force capacity, combined with the easier constructability and alterability of 15 kg plates, provides a better design for the research goals of this specimen. Therefore, the smaller paddle dampers are chosen, the story plate thickness is chosen to be 3/8", and the spring steel columns with 0.062" thickness are chosen. The first story columns

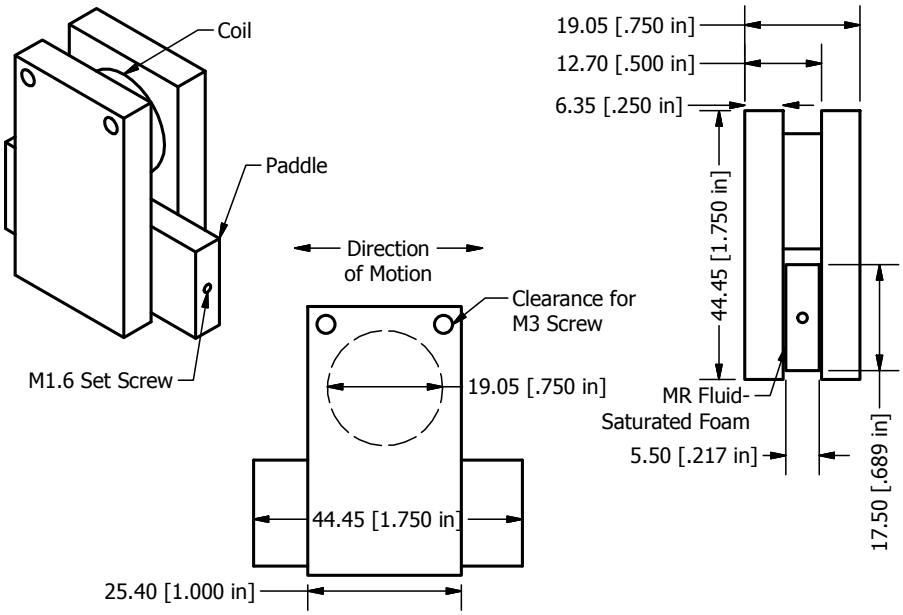

Figure 6.3: Isometric (Left), Front (Center), and Side (Right) views of the damper proposed for control of the shake table specimen.

are wider to provide additional capacity, while the column lengths increase for the upper stories to more closely follow the natural frequencies of the Kajima-Shizuoka building.

The parts used for the damper and brace assembly are shown in Figure 6.4. Aluminum is chosen over steel to decrease the weight on the structure, and welds are used to increase stiffness and constructability. Figure 6.4 (L) shows the 1"x1"x1/8" aluminum tube that is used as a brace in between the stories. Despite using aluminum instead of steel, the geometry of the aluminum tube leads to an interstory stiffness of a factor of 3 greater than the steel columns provide. To ensure the assumed base fixity in the tube, the tube is welded to a 1/4" aluminum plate on all sides. The aluminum plate is then attached through the center four holes of the steel story plate. A similar process is used for the damper mount in Figure 6.4 (R). An aluminum angle is welded to a 1/4" aluminum plate, which is then attached to the underside of the same four holes of the steel story plate. The holes in the alumium angle line up to attach to the holes on the MR damper in Figure 6.3, while the holes at the end of the aluminum tube are at a height to attach to the MR damper paddle and an LVDT.

Similar to the 6-Story steel test structure of Yi et al. (2001), a brace system for the damper and LVDT is used. The story plates have through holes drilled in order to

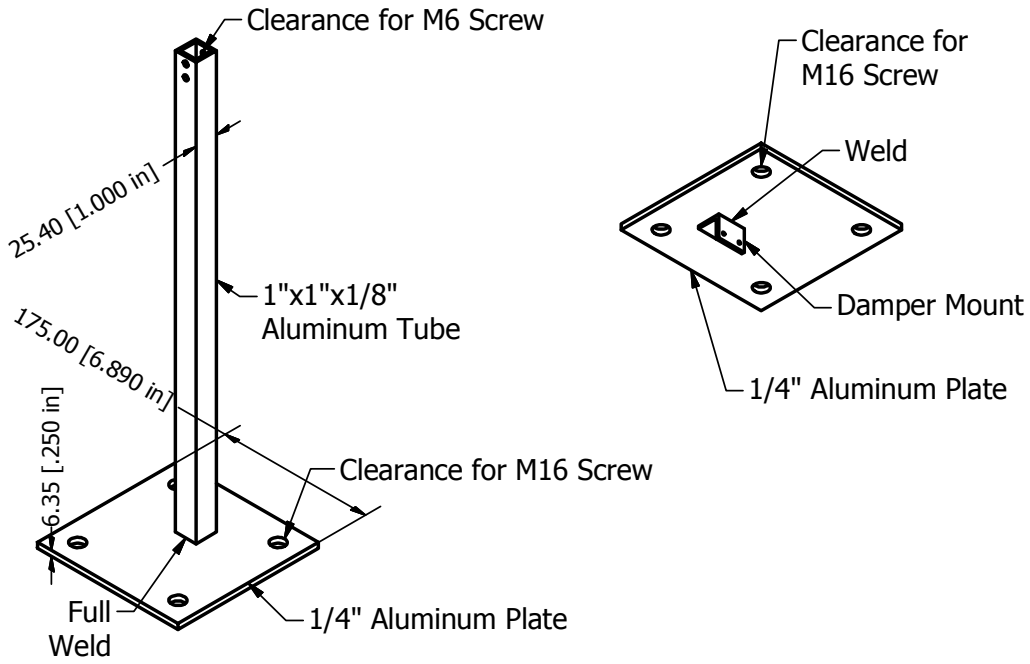

Figure 6.4: Isometric views of the interior brace (L) and damper mount (R) used for control of the specimen.

attach a brace on the top of the lower story and a damper and LVDT on the bottom of the story above. In addition to the use of the MR paddle dampers, these schematics from the 6-Story test structure are used and modified for the 5-Story specimen design. The mounting hole pattern of the shake table is adopted for the through holes of the story plates, and additional through holes are specified for column and LVDT mount attachments. All specimen detailing is done to maximize constructability and ease of testing.

The final drawings of the assembled first story are seen in Figure 6.5. The base plate will be attached to the shake table mounting holes with 8 socket head cap screws. The aluminum tube extends nearly up to the first story, where the MR paddle damper is attached to its left and the LVDT is attached to its right. The distance between the LVDT and the aluminum tube is variable, while the distance between the MR damper and the aluminum tube is 0.025 m. With interstory drifts smaller than 0.025 m for the earthquakes considered, the spacing is sufficient. Detailed drawings and limits achieved during the earthquakes and samples of the specimen response are found in Appendix B.

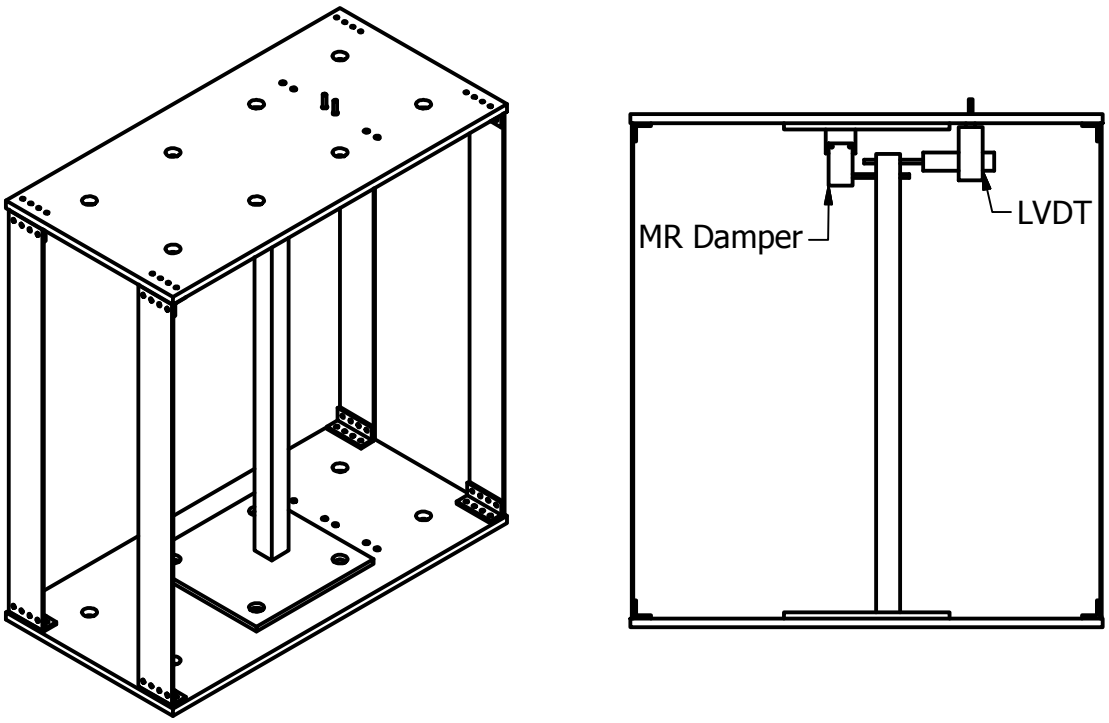

Figure 6.5: Drawings for the first story assembly of the shake table specimen.

Table 6.1: Mass and length parameters of specimen

Story	Desired Mass [kg]	Hardware Mass [kg]	Plate Mass [kg]	Extra Mass [kg]	Column Length [m]	Column Width [m]
1	15.4	4	9	2.4	0.520	0.0508
2	14	4	9	1	0.555	0.0381
3	13.4	4	9	0.4	0.555	0.0381
4	13.2	4	9	0.2	0.585	0.0381
5	17	2	9	6	0.585	0.0381

The final design variables are found in Table 6.1. The column depth is 0.062" (0.00157 m) for all columns. Multiple iterations tuning the natural frequencies of the system lead to the desired mass values found in the table. Between the columns, angles, socket head cap screws, dampers, braces, and aluminum plates, the additional mass is approximated as 4 kg per story, except for the top story, which has half of the miscellaneous hardware lumped into its story mass. The steel plate used for each story is approximately 9 kg, and extra mass can be added to the system to reach the desired mass. This can be achieved in the form of steel masses with through holes mounted on the steel story plates. In the case of stories 2-4, extra mass may not be required if the specimen system ID is sufficiently close to the desired system ID. The column lengths listed in the table are the total length of the columns, where there is a 0.01 m spacing to the center of the through holes used for the column connection. The center-on-center spacing between holes is used for effective length and stiffness calcultions.

The variables used in Table 6.1 lead to the natural frequencies seen in Table 6.2. The difference between the desired natural frequency from the Kajima-Shizuoka building and the calculated natural frequency for the proposed specimen design are listed. As was desired, the first mode has almost the exact same natural frequency, while the remaining natural frequencies stay within 3%. As the structure is built and the true structural characteristics, including actual mass and stiffness, are observed, the natural frequencies will change slightly. However, the specimen is designed to easily add more mass to tune the natural frequencies. In addition to the eigenvalues, the eigenvectors are examined in Figure 6.6, where the mode shapes for the five modes are normalized to a value of unity at the top story and compared. The specimen design very closely resembles the Kajima-Shizuoka mode shapes for the first three modes. Modes 4 and 5 appear to be further apart than they truly are due to the normalization; the fifth story magnitude is

Table 6.2: Natural Frequencies of specimen using mass values from Table 6.1

Mode	Desired ω_n	Calculated ω_n	% Difference
1	1.01	1.01	0.3
2	2.82	2.87	1.7
3	4.49	4.62	2.7
4	5.80	5.77	0.6
5	6.77	6.59	2.8

much smaller in Modes 4 and 5 than it is in the first three modes. It is also important to note the majority of building response will be from the lower modes.

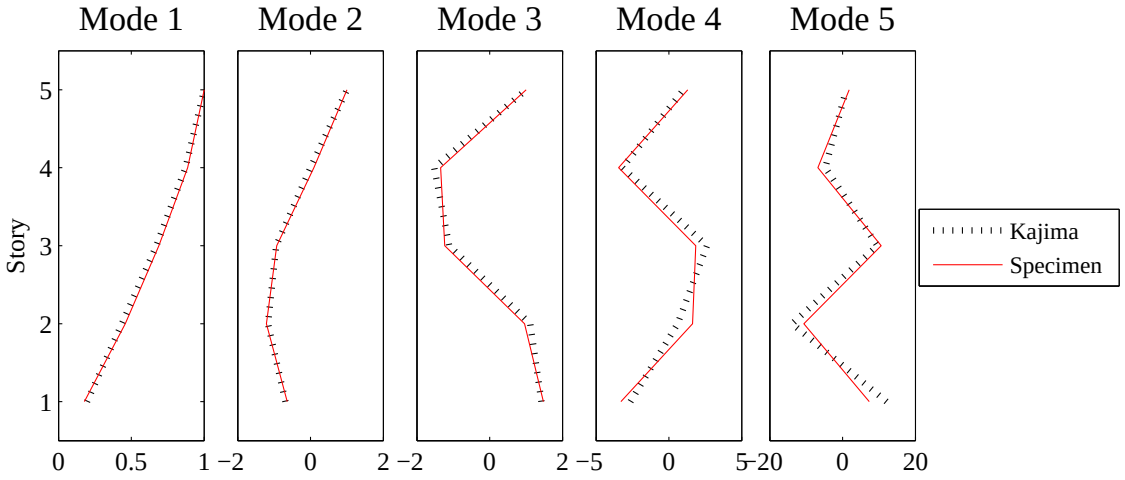

Figure 6.6: Mode shapes of Kajima-Shizuoka building and proposed specimen, normalized to 1 at Story 5.

Finally, the axial load/bending moment interaction results are tabulated in Table 6.3 for each story in each earthquake at the time of maximum overturning moment. The earthquakes are scaled to a PGA of 1 m/s^s. All stories meet the interaction requirement of 1.0 for compressive forces and moments. No complete overturning leading to tensile forces in columns occurs in any earthquake, so tensile forces in connections were not considered. Shear forces were considered, but the interaction controlled in all cases.

Table 6.3: Axial load/bending moment interaction results for the proposed shake table specimen in the four ground motions considered.

Interaction Results				
Story	El Centro	Northridge	Chi-Chi	Kobe
1	0.49	0.41	0.67	0.54
2	0.56	0.52	0.79	0.66
3	0.38	0.42	0.50	0.46
4	0.26	0.31	0.33	0.31
5	0.13	0.15	0.15	0.15

6.4 Summary

With the proposed specimen, the structural control techniques investigated in this thesis can be physically verified in conjunction with sparse estimation techniquies. The specimen will be assembled and instrumented with accelerometers and LVDTs while the MR dampers are fabricated and assembled. The specimen will undergo a system identification to determine its frequency response characteristics, while the dampers will be characterized by determining their hysteresis loops. Once the specimen and the damper are characterized, their time response to earthquake ground motions can be simulated within the same MATLAB and Simulink framework as the Kajima-Shizuoka building in Chapter 4. When wireless sensors and controllers are also added to the system, the framework from Chapter 5 will be utilized.

Chapter 7

Conclusion and Future Research

7.1 Conclusions

This research presents the application of sparse feedback control techniques on civil structural systems. The LQRSP method presented by Lin et al. (2013) is shown to effectively balance the sparsity of the feedback gain matrix with the control performance of two benchmark structures subjected to earthquake ground motions and shaped BLWN. The 5-Story Kajima-Shizuoka structure is used to verify the LQRSP method on a structure with a clear feedback gain structure, and the 20-Story SAC benchmark structure is used to test the LQRSP algorithm on a feedback gain matrix without an immediately apparent optimal decentralized structure. A study of LQRSP has produced the following conclusions:

- The LQRSP method efficiently calculates feedback gain matrix structures for growing levels of sparsity, creating a family of γ-parameterized gain matrices to easily determine the most important feedback measurements in each decentralized controller.
- After computing the optimal feedback gain structure, the LQRSP polishing step takes the controllability gramian into account when solving for the optimal sparse feedback gain matrix. This is shown to be a marked improvement over the previously considered Heuristic method as presented by Lunze (1992) in both closed-loop cost calculations and in ground motion simulations.

- While the Heuristic method can be reformulated to match the gain matrices produced by LQRSP, there are still a number of advantages in the LQRSP program:
  - LQRSP can efficiently compute optimal feedback gain structures for non-intuitive gain matrices or for very large gain matrices, while the Heuristic method requires an Ad-Hoc approach to choose the gain matrix structure. LQRSP therefore leads to better structures in much less computation and control design time.
  - LQRSP utilizes ADMM to provide better guesses for the polishing step than a similar Ad-Hoc process would, leading to the global cost minimum instead of a local cost minimum in some cases.
  - LQRSP illuminates the most important feedback measurements in the system and provides the control designer with the ability to keep those measurements, while the Heuristic algorithm relies on an Ad-Hoc approach to observe such trends and alter the feedback gain structure.
  - LQRSP is able to lump feedback information together, allowing a more intuitive approach to systems where state information will be lumped together.
- In both continuous-time and discrete-time, the sparse feedback gains computed by LQRSP are able to match the performance of the LQR controller with only local feedback information. This allows for a number of practical advantages:
  - Installation and programming times are decreased drastically.
  - No wireless or wired communication is required, reducing hardware requirements and installation costs.
  - No synchronization is required between wireless controllers at the beginning of an event.
  - Loss of control feedback information does not cause significant loss of control performance.
  - Fewer communication links make the system less vulnerable to sensor or controller failure.

A 5-Story steel specimen similar to the Kajima-Shizuoka building is designed with the intent of verifying the simulation results of the LQRSP method. The system is

designed with spring steel columns, steel plate stories, and MR control dampers. The specimen will allow for the testing of sensing, estimation, and control designs.

7.2 Future Research

This research has provided a simulation framework to test the performance of LQR and decentralized LQRSP control designs in continuous and discrete time. The 5-Story specimen is designed with the purpose of verifying the results found in the simulation results. In addition, the specimen can be used for estimator design and testing of sensor deployment techniques.

A number of other future research directions can be explored based on this research:

- Although time delay and sensor noise is examined in the discrete-time simulations, estimator designs with similar sparse feedback structures and sampling rates can be explored. The sparser systems should be tested to see if their fast sampling rates make up for the lack of global system information and anticipated estimator limitations.

- Because the closed-loop H_2 norm cannot be directly compared between discrete-time controllers with different sampling rates due to the change in state-space matrices, the discrete-time LQRSP design could consider an alternative way to compare the H_2 norm.

- In systems with reduced models, the LQRSP method can be extended to minimize the feedback information in the physical domain instead of the states of the reduced order model.

References

American Institute of Steel Construction (2005). *Manual of Steel Construction,14th Edition*. Chicago: AISC.

Dörfler, F., Jovanović, M. R., Chertkov, M., and Bullo, F. (2013). Sparse and optimal wide-area damping control in power networks. *American Control Conference (ACC), 2013*, IEEE, 4295-4300.

Dörfler, F., Jovanović, M. R., Chertkov, M., and Bullo, F. (2014). Sparsity-promoting optimal wide-area control of power networks. *IEEE Trans. Power Syst.*, 29(5), 2281-2291.

Dhingra, N. K., Jovanović, M. R., and Luo, Z.Q. (2014). An ADMM algorithm for optimal sensor and actuator selection. *Proceedings of the 53rd IEEE Conference on Decision and Control*, 4039-4044.

Dyke, S. J., Spencer, B. F., Sain, M. K., and Carlson, J. D. (1996). Modeling and control of magnetorheological dampers for seismic response reduction. *Smart Materials and Structures*, 5(5), 565-575.

Fardad, M., Lin, F., and Jovanović, M. R. (2009). On the optimal design of structured feedback gains for interconnected systems. *Proceedings of the 48th IEEE Conference on Decision and Control*, 978-983.

Fardad, M., Lin, F., and Jovanović, M. R. (2011). Sparsity-promoting optimal control for a class of distributed systems. *American Control Conference (ACC), 2011*, IEEE, 2050-2055.

Guyan, R. J. (1965). Reduction of Stiffness and Mass Matrices. *AIAA Journal*, 3(2), 380.

Harris, H. G., and Sabnis, G. M. (1999). *Structural Modeling and Experimental Techniques*. CRC, Boca Raton.

Hatada, T., Kobori, T., Ishida, M., and Niwa, N. (2000). "Dynamic analysis of structures with Maxwell model." *Earthquake engineering & structural dynamics*, 29(2), 159-176.

Housner, G. W., Bergman, L. A., Caughey, T. K., Chassiakos, A. G., Claus, R. O., Masri, S. F., Skelton, R. E., Soong, T. T., Spencer, B. F., and Yao, J. T. P. (1997). Structural Control: Past, Present, and Future. *Journal of Engineering Mechanics*.

Kobori, T. (1990). Technology Development and Forecast of Dynamical Intelligent Building (DIB). *Journal of Intelligent Material Systems and Structures*, 1(4), 391-407.

Kurata, N., Kobori, T., Takahashi, M., Niwa, N., and Midorikawa, H. (1999). Actual seismic response controlled building with semi-active damper system. *Earthquake Engineering & Structural Dynamics*, 28(11), 1427-1447.

Lei, Y., Kiremidjian, A. S., Nair, K. K., Lynch, J. P., and Law, K. H. (2005). Algorithms for time synchronization of wireless structural monitoring sensors. *Earthquake engineering & structural dynamics*, 34(6), 555-573.

Linderman, L. E., and Spencer Jr, B. F. (2014). *Smart wireless control of civil structures*. Newmark Structural Engineering Laboratory. University of Illinois at Urbana-Champaign.

Lin, F., Fardad, M., and Jovanović, M. R. (2011). Augmented Lagrangian approach to design of structured optimal state feedback gains. *IEEE Transactions on Automatic Control*, 56(12), 2923-2929.

Lin, F., Fardad, M., and Jovanović, M. R. (2013). Design of Optimal Sparse Feedback Gains via the Alternating Direction Method of Multipliers. *IEEE Transactions on Automatic Control*, 58(9), 2426-2431.

Lunze, J. (1992). *Feedback control of large scale systems*. Prentice Hall PTR.

Lynch, J. P., Law, K. H., and others. (2002). Decentralized control techniques for large-scale civil structural systems. *Proc. of the 20th Int. Modal Analysis Conference (IMAC XX)*.

Lynch, J. P., Sundararajan, A., Law, K. H., Kiremidjian, A. S., and Carryer, E. (2004). Embedding damage detection algorithms in a wireless sensing unit for operational power efficiency. *Smart Materials and Structures*, 13(4), 800.

Lynch, J., Wang, Y., Swartz, R., Lu, K., and Loh, C. (2008). Implementation of a closed-loop structural control system using wireless sensor networks. *Structural Control and Health Monitoring*, 15(4), 518-539.

Ohtori, Y., Christenson, R. E., Spencer, Jr., B. F., and Dyke, S. J. (2000). Benchmark Control Problems for Seismically Excited Nonlinear Buildings.

Sandell Jr, N. R., Varaiya, P., Athans, M., and Safonov, M. G. (1978). Survey of Decentralized Control Methods for Large Scale Systems. *IEEE Transactions on Automatic Control*, 23(2), 108-128.

Soong, T. T., and Chen, W. F. (1990). *Active structural control*. Longman Scientific and Technical, New York.

Spencer Jr, B. F., Christenson, R. E., and Dyke, S. J. (1998). Next generation benchmark control problem for seismically excited buildings. *Proceedings of the Second World Conference on Structural Control*, 1135-1360.

Spencer Jr, B., and Nagarajaiah, S. (2003). State of the art of structural control. *Journal of structural engineering*.

Wang, Y. (2007). Wireless sensing and decentralized control for civil structures: theory and implementation. Stanford University.

Wang, Y. (2011). Time-delayed dynamic output feedback H∞ controller design for civil structures: A decentralized approach through homotopic transformation. *Structural Control and Health Monitoring*, 18(2), 121-139.

Wang, Y., and Law, K. (2011). Structural control with multi-subnet wireless sensing feedback: experimental validation of time-delayed decentralized H ∞ control design. *Advances in Structural Engineering*, 14(1), 25-39.

Wang, Y., Lynch, J. P., and Law, K. H. (2009). Decentralized H∞ controller design for large-scale civil structures. *Earthquake Engineering & Structural Dynamics*, 38(3), 377-401.

Wang, Y., Swartz, R. A., Lynch, J. P., Law, K. H., Lu, K. C., and Loh, C. H. (2006). Decentralized civil structural control using a real-time wireless sensing and control system. *Proc. of the 4th World Conf. on Structural Control and Monitoring (4WCSCM)*, 11-13.

Williams, M. S., and Blakeborough, A. (2001). Laboratory testing of structures under dynamic loads: an introductory review. *Phil. Trans. R. Soc. Lond.*, The Royal Society, 16511669.

Wu, X., Dörfler, F., and Jovanović, M. R. (2016). Input-output analysis and decentralized optimal control of inter-area oscillations in power systems. *IEEE Trans. Power Syst.*, 31(3), 2434-2444.

Yao, J. T. (1972). Concept of structural control. *Journal of the Structural Division*, 98(7), 1567-1574.

Yi, F., Dyke, S. J., Caicedo, J. M., and Carlson, J. D. (2001). "Experimental verification of multiinput seismic control strategies for smart dampers." *Journal of Engineering Mechanics*, 127(11), 1152-1164.

Appendix A

Model Reduction

In this appendix, the process for verifying the behavior of the model reduction for the 20-Story SAC benchmark structure is outlined. As originally explained in Section 4.2.2, the sparse design approaches are used on the 20-Story benchmark structure, but because the original model has 582 states with natural frequencies up to 10^8 Hz, a model reduction for simulation is required. The model reduction included with the paper by Ohtori et al. (2000) is considered alongside the unreduced system and a lumped mass model to provide a simple model example. The methods for verification of input-output behavior are outlined below.

In order to determine the number of states needed for a reasonable model reduction, the observability and controllability Gramians of the state-space system are used. The Hankel singular values (HSVs) of the system are calculated as the eigenvalues of the product of the Gramians, where the HSV of a state gives a measure of the energy the state has in the input-output behavior. The HSV values for the first 100 states for horizontal state outputs are seen in Figure A.1. It is clear that most of the energy is contained in the first few states, decaying exponentially to nearly zero energy after 40 states. While a 40 state reduction would capture 99% of the behavior of the system according to the HSVs, the 93% captured by the first 20 states is more than sufficient to accurately model the behavior of the system. Some of the 21-40 states also have associated natural frequencies beyond the desired limit of 10^2 Hz, where little earthquake content lies.

To illustrate the similarities of the 20 state Ohtori reduction to the unreduced original model, the first ten natural frequencies for each system are plotted in Figure A.2

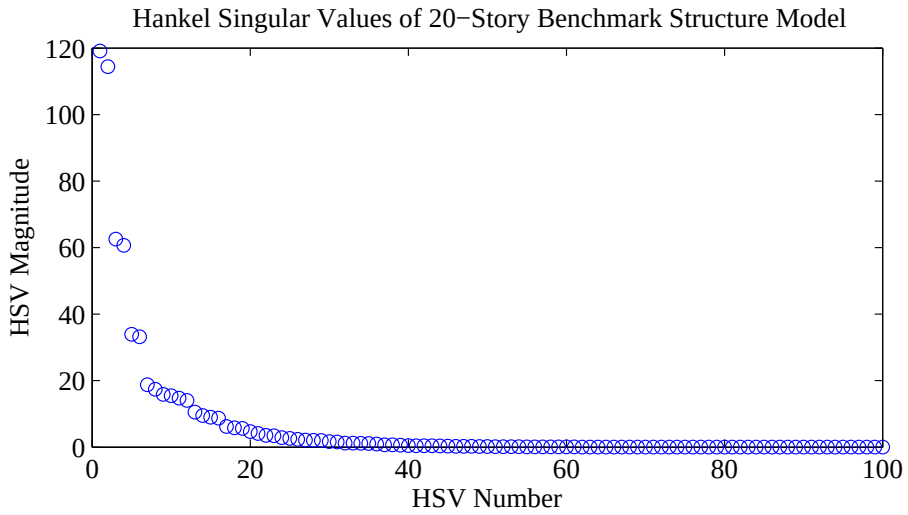

Figure A.1: Hankel Singular Values for the 20-Story benchmark structure model. 93% of total HSV data is contained in the first 20 states, and 99% of total HSV data is contained in the first 40 states.

along with a lumped mass model for comparison. The Ohtori reduction is the same for nine of its ten natural frequencies, while the lumped mass model is slightly different from both of the other systems. The mode shapes normalized to unity at the 20^{th} story for the first seven modes are also plotted in Figure A.3. The unreduced system and Ohtori reduction have the same first five mode shapes, starting to deviate slightly in the highest modes, and the lumped mass model is again slightly different. It is clear that the modal properties of the Ohtori reduction are similar to the unreduced system, while the lumped mass system, which does not take vertical and rotational degrees of freedom into account for simplicity, characterizes the building differently.

In addition to the modal behavior of the systems, the input-output behavior of the systems can be examined through a frequency response calculation. For an input U, the reponse Y of the system is given by

$$\frac{Y}{U} = C(sI - A)^{-1}B + D \tag{A.1}$$

where (A, B, C, D) are state space matrices that capture the desired input-output behavior of the system. Calculating the frequency response for a shaped BLWN at a variety of frequencies yields magnitude and phase angle plots for any story input to any story output, like those found in Figures A.6 through A.13. The ground input to

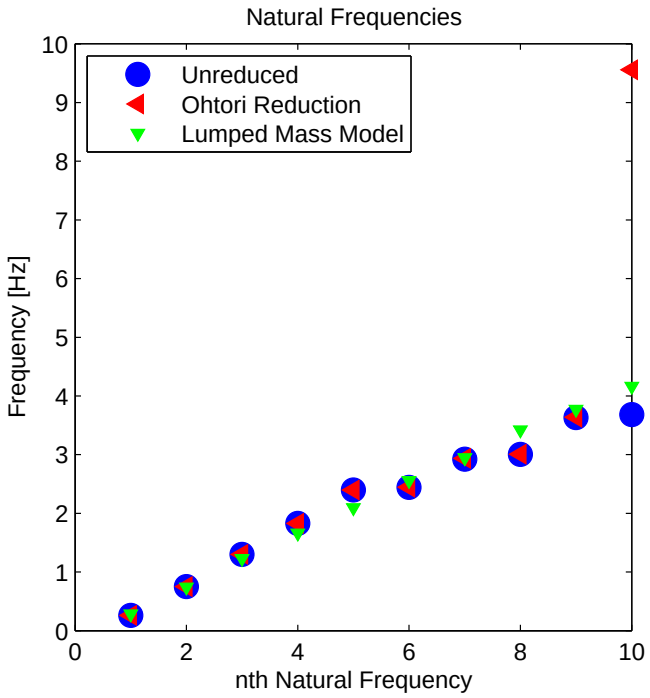

Figure A.2: First 10 natural frequencies of the various models for the 20-Story benchmark structure.

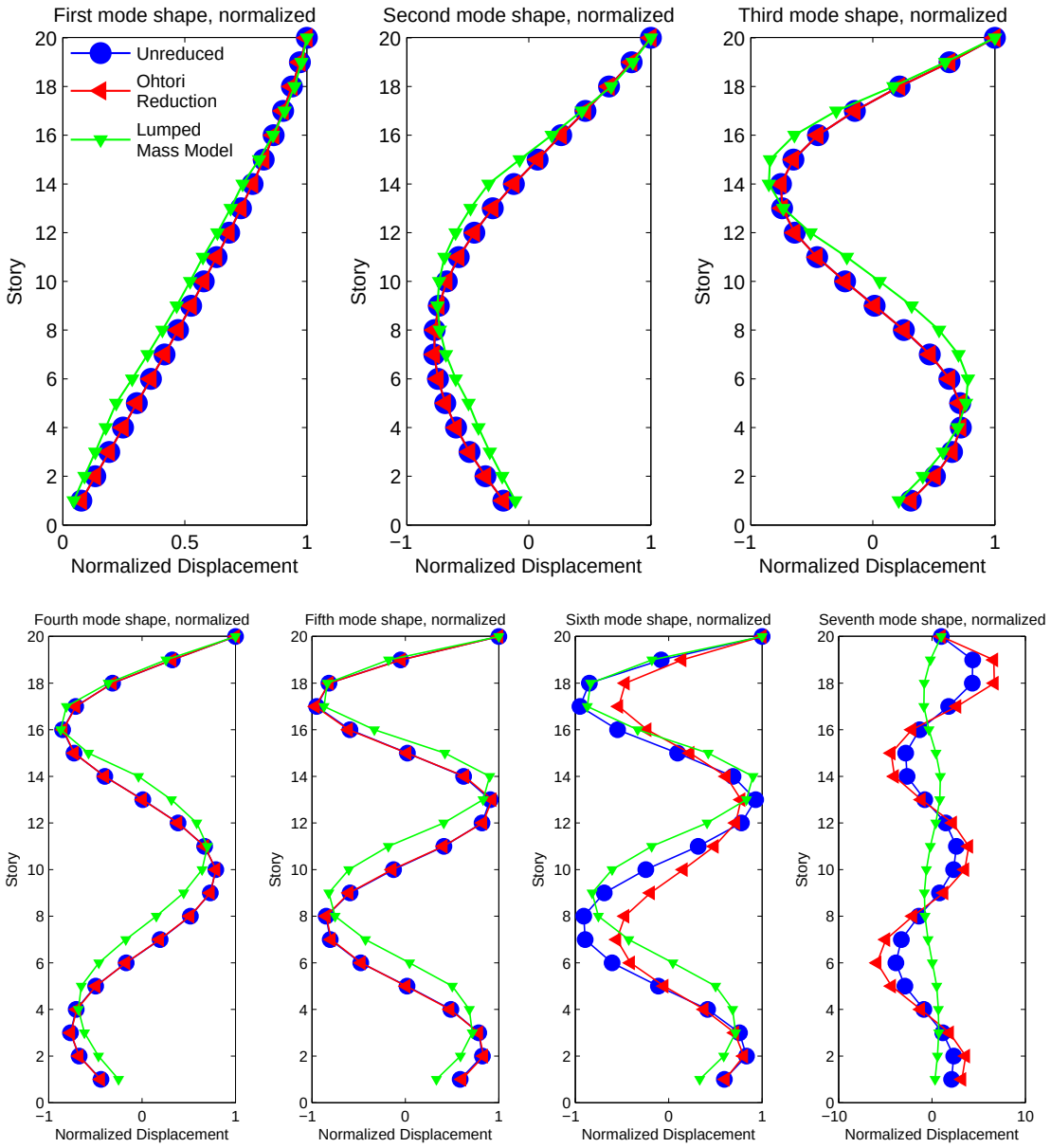

Figure A.3: Mode Shapes of the various models for the 20-Story benchmark structure.

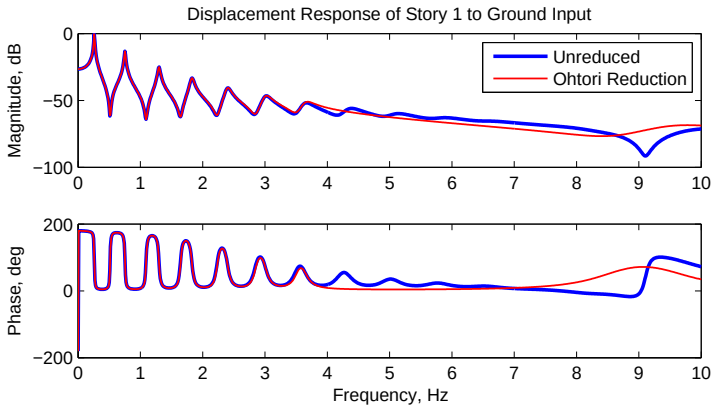

Figure A.4: Frequency response, ground input to 1^{st} story displacement for the 20-Story benchmark structure.

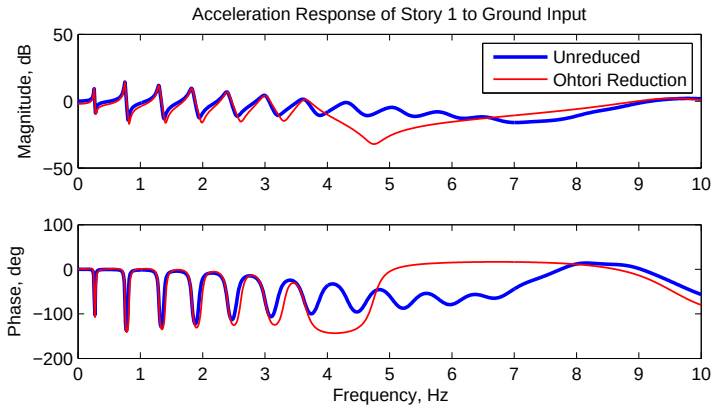

Figure A.5: Frequency response, ground input to 1^{st} story acceleration for the 20-Story benchmark structure.

first and 20th story displacement and acceleration in Figures A.4 through A.7 show the uncontrolled behavior of the first and 20^{th} stories. The similarities end at about 4 Hz, but it is important to note that the gains above 4 Hz are very small compared to the peaks found at the first five natural frequencies. Therefore, the matching lower frequency modes will dominate the uncontrolled response of the structure.

The input-output behavior for a structure with inputs at each story, like dampers, can also be examined. input-output at the first (Figures A.8 and A.9), seventh (Figures A.10 and A.11), and 20th (Figures A.12 and A.13) stories are examined more closely. There is generally good agreement among magnitude plots, though some acceleration magnitudes become quite flat. The reduction sacrifices capturing some acceleration

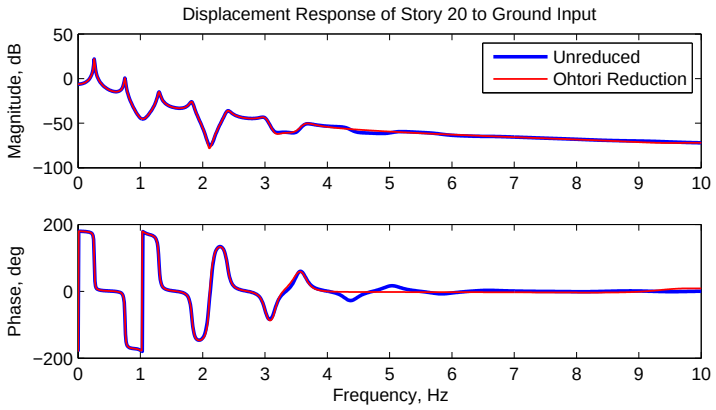

Figure A.6: Frequency response, ground input to 20^{th} story displacement for the 20-Story benchmark structure.

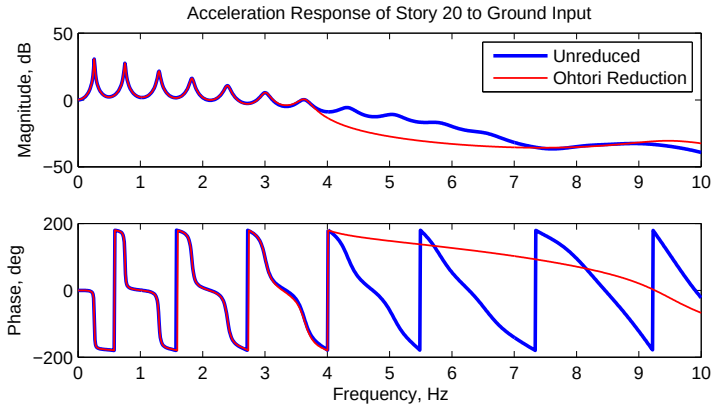

Figure A.7: Frequency response, ground input to 20^{th} story acceleration for the 20-Story benchmark structure.

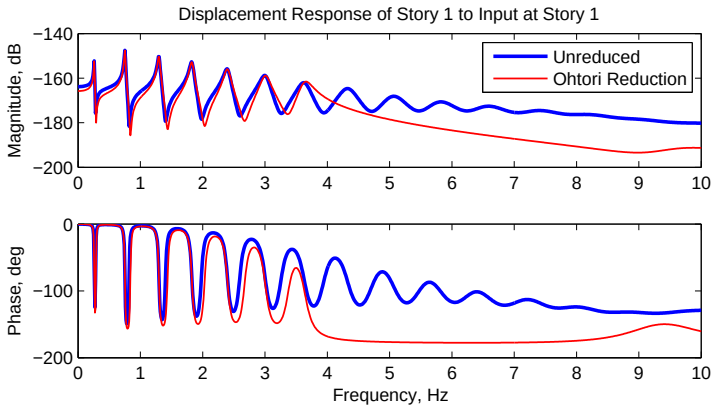

Figure A.8: Frequency response, 1^{st} story input to 1^{st} story displacement for the 20-Story benchmark structure.

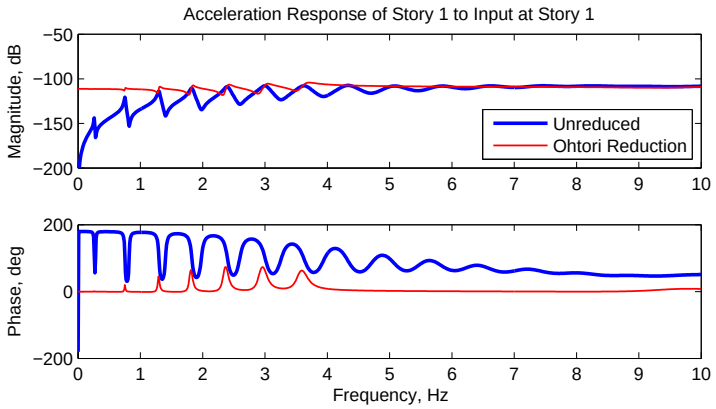

Figure A.9: Frequency response, 1^{st} story input to 1^{st} story acceleration for the 20-Story benchmark structure.

response near the origin to capture the ground input and displacement responses more accurately. The Ohtori reduction acceleration phase angle plots also are out of phase for low frequencies on some stories due to the elimination of zeros at the origin.

The uncontrolled response is further examined in Figure A.14, where a Lyapunov equation is used to calculate the RMS displacement, velocity, and acceleration response of the systems excited by a shaped BLWN at the base. The unreduced and reduced system responses are nearly the same, highlighting the preservation of open loop input-output behavior in all states in the Ohtori reduction. The lumped mass model remains slightly different from both systems.

Between the modal, frequency response, and RMS analyses, the 20 state reduction

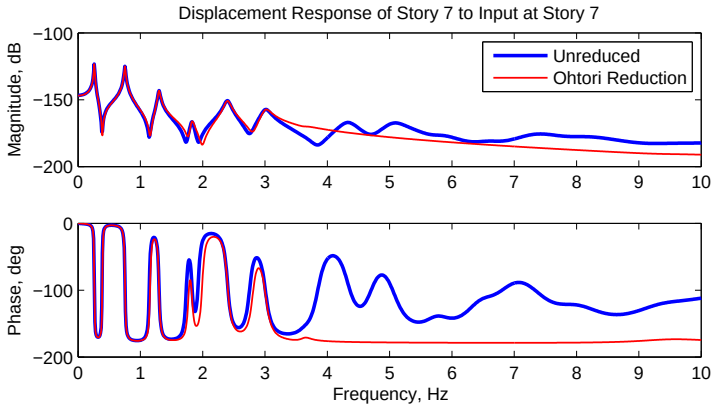

Figure A.10: Frequency response, 7^{th} story input to 7^{th} story displacement for the 20-Story benchmark structure.

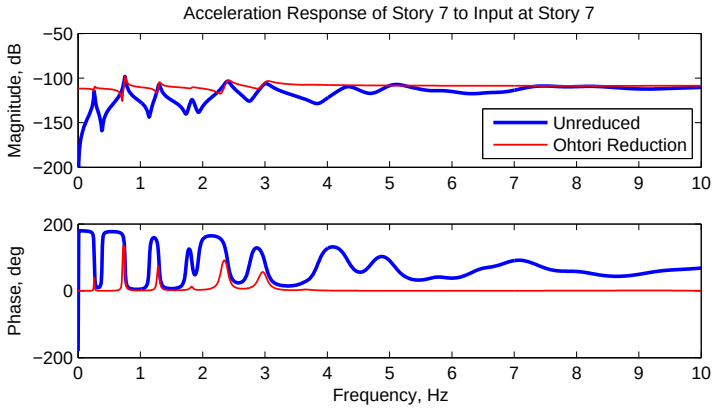

Figure A.11: Frequency response, 7^{th} story input to 7^{th} story acceleration for the 20-Story benchmark structure.

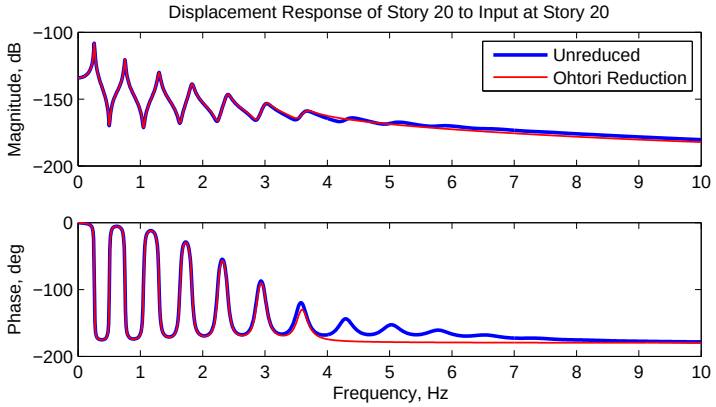

Figure A.12: Frequency response, 20^{th} story input to 20^{th} story displacement for the 20-Story benchmark structure.

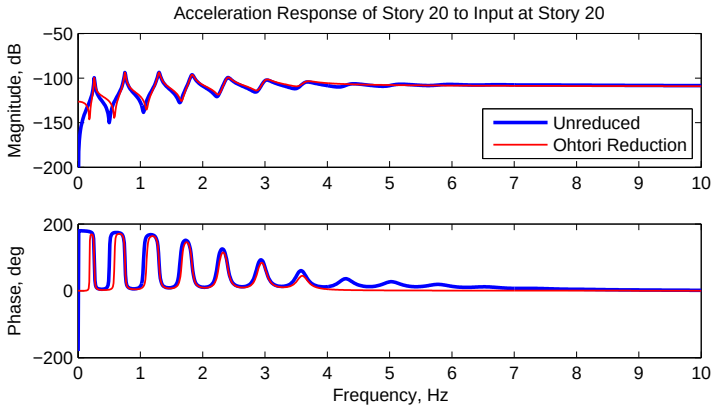

Figure A.13: Frequency response, 20^{th} story input to 20^{th} story acceleration for the 20-Story benchmark structure.

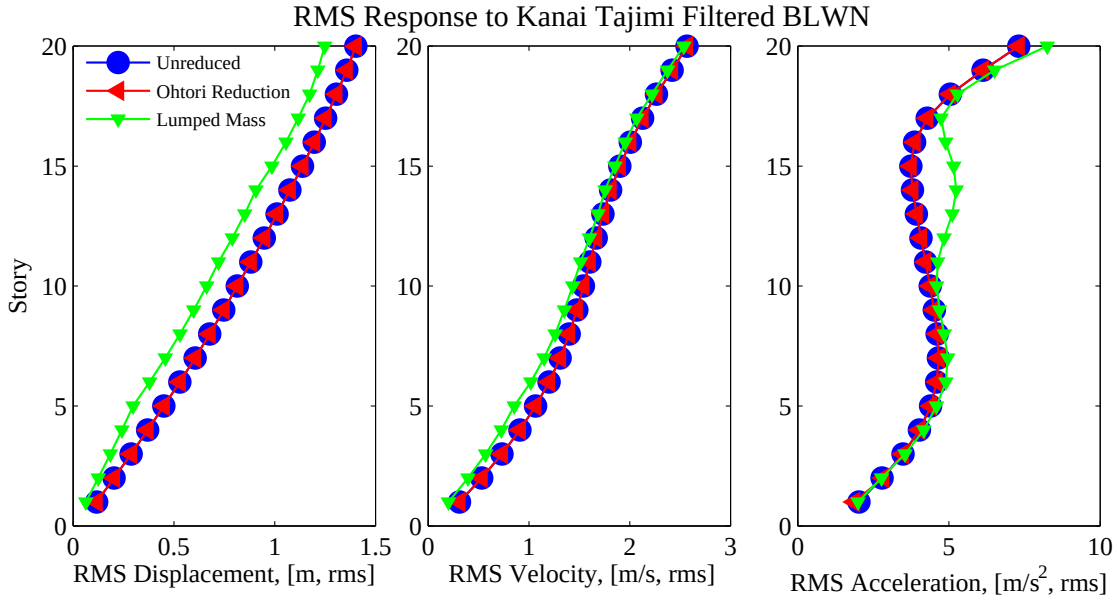

Figure A.14: RMS displacement of each story in a Kanai-Tajimi shaped BLWN for various models of the uncontrolled 20-Story benchmark structure.

provided by Ohtori is seen to provide excellent agreement with the 582 state unreduced system, while both systems resemble a lumped mass model used to ensure the approximate accuracy of the systems. As a result, the Ohtori reduction is chosen to compare the various control algorithms. This will allow the computation of sparse gain matrices on a feedback gain matrix without an immediately apparent feedback gain structure.

Appendix B

Specimen Design

In this appendix, a brief overview of the process for determining the design loads and maximum responses of the proposed 5-Story specimen is outlined. Four earthquakes, all scaled to 1 m/s^2, are used as design earthquakes. The response of the specimen is simulated within MATLAB and Simulink for each earthquake, and the overturning moment is calculated at each time step by multiplying the story inertial forces by their respective heights. At the time step of maximum overturning moment, the internal forces are calculated using the Direct Stiffness Method. An example of the force equilibrium considered is given in Figure B.1. One bay of the total frame is considered, so while the story accelerations remain the same, the story masses, listed along the right side of the plots, are divided in half, essentially halving both the lateral forces generated by the earthquake and the gravitational forces from the mass of the structure. The displaced shape at maximum overturning (solid line) is also superimposed over the static structure (dotted line). Base shear [N] and overturning moment [N-m] for force equilibrium are printed at the bottom of the plot.

It is also important to consider the maximum displacement, velocity, and acceleration responses in order to ensure the structural response is on the correct order of magnitude, as seen in Tables B.1, B.2, and B.3. The maximum displacements are on the order of 2% drift per story, enough to be noticeable in testing, while not too much to cause overt second order effects. In addition to displacements, the maximum interstory drift achieved in the four earthquakes is 0.015 m, well below the maximum of 0.025 m required for the structural constraints of the damper assembly. The velocities reach above 0.05 m/s for the first story in all earthquakes, which is the velocity required to

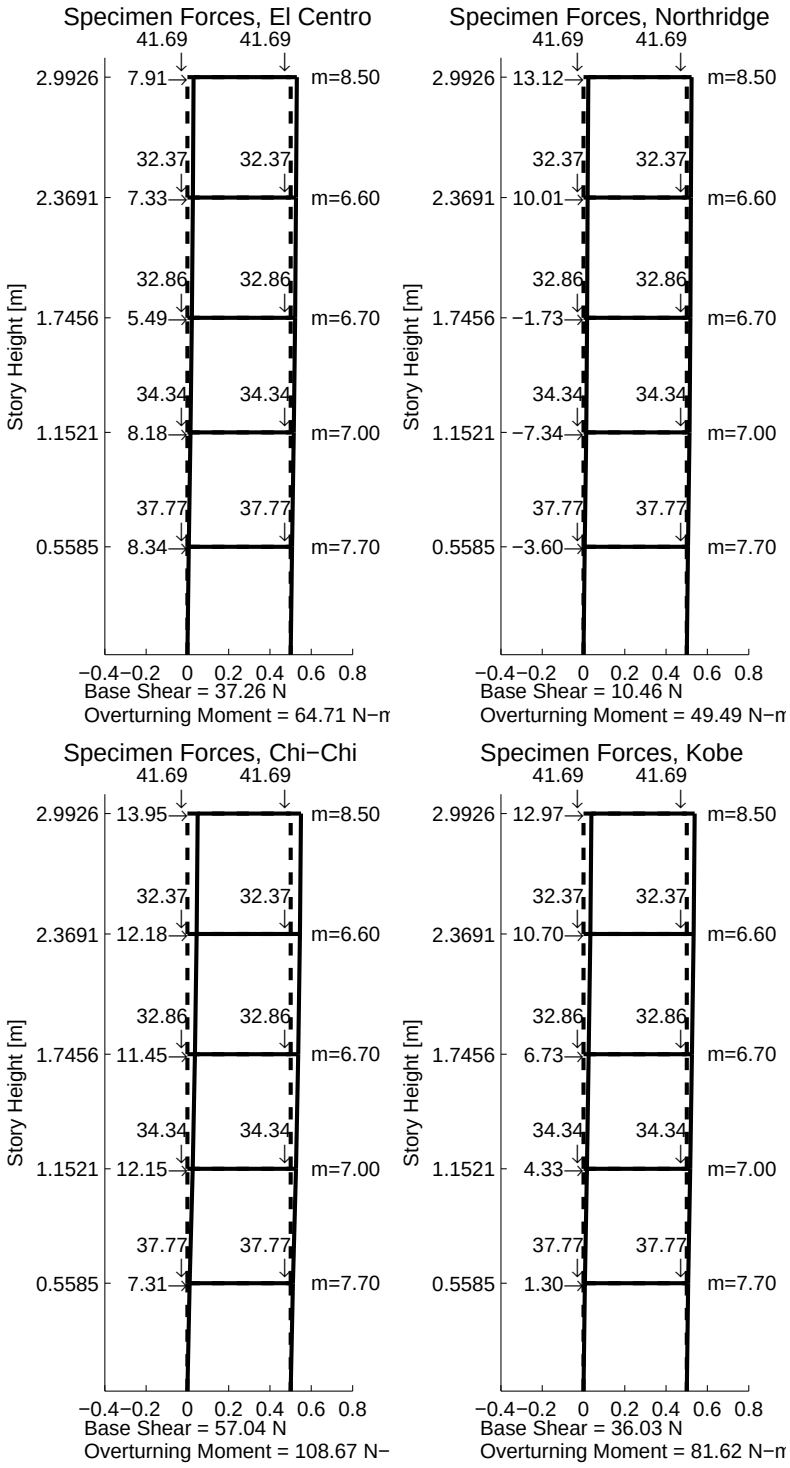

Figure B.1: Forces and drifts of Specimen plotted at maximum overturning moment during various earthquakes scaled to 1 m/s/s.

Table B.1: Maximum displacement of specimen during various earthquakes scaled to 1 m/s/s.

Maximum Displacement [m]				
Story	El Centro	Northridge	Chi-Chi	Kobe
1	0.0067	0.0062	0.0109	0.0065
2	0.0152	0.0133	0.0259	0.0169
3	0.0216	0.0173	0.0366	0.0253
4	0.0263	0.0203	0.0452	0.0331
5	0.0302	0.0237	0.0497	0.0382

Table B.2: Maximum velocity of specimen during various earthquakes scaled to 1 m/s/s.

Maximum Velocity [m/s]				
Story	El Centro	Northridge	Chi-Chi	Kobe
1	0.0582	0.0699	0.0636	0.0617
2	0.1072	0.1208	0.1368	0.1315
3	0.1566	0.1771	0.2137	0.1754
4	0.2108	0.1922	0.2715	0.2614
5	0.2583	0.2257	0.3329	0.2894

Table B.3: Acceleration of specimen at maximum overturning moment during various earthquakes scaled to 1 m/s/s.

Acceleration at Maximum Overturning [m/sˆ2]				
Story	El Centro	Northridge	Chi-Chi	Kobe
1	1.0836	-0.4674	0.9488	0.1690
2	1.1684	-1.0489	1.7364	0.6185
3	0.8191	-0.2577	1.7091	1.0048
4	1.1113	1.5170	1.8455	1.6205
5	0.9306	1.5430	1.6408	1.5261

reach the maximum damper force. It is also noted that the interstory velocities will generally be larger on the upper stories than they are on the first story. The rest of the maximum story velocities listed in Table B.2 do not give any reason for concern. For completeness, the story accelerations at the maximum overturning moment in each earthquake are listed in Table B.3. These accelerations correspond to the forces and masses seen in Figure B.1.

The listed values and plotted structures are used to verify the safety of the specimen design as well as ensure the ability of the control system to control the specimen during

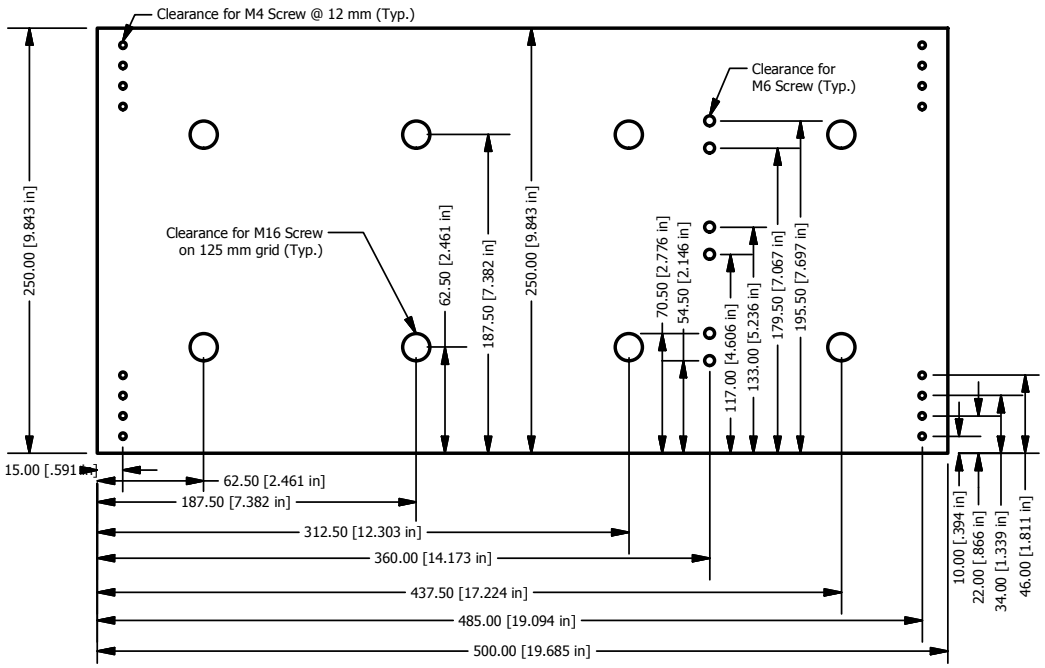

Figure B.2: Drawing for the 3/8" thickness steel story plates of the shake table specimen.

the considered earthquakes. BLWN excitations scaled to PGA of 1 m/s^2 will also be considered, but the maximum overturning moments calculated in the BLWN simulations are less than those in the earthquake ground motions. For each different BLWN ground motion generated, the interaction should be verified to guarantee safety of the specimen.

B.1 Specimen Drawings

For completeness, the specimen steel plate and column drawings for fabrication are seen in Figures B.2 and B.3.

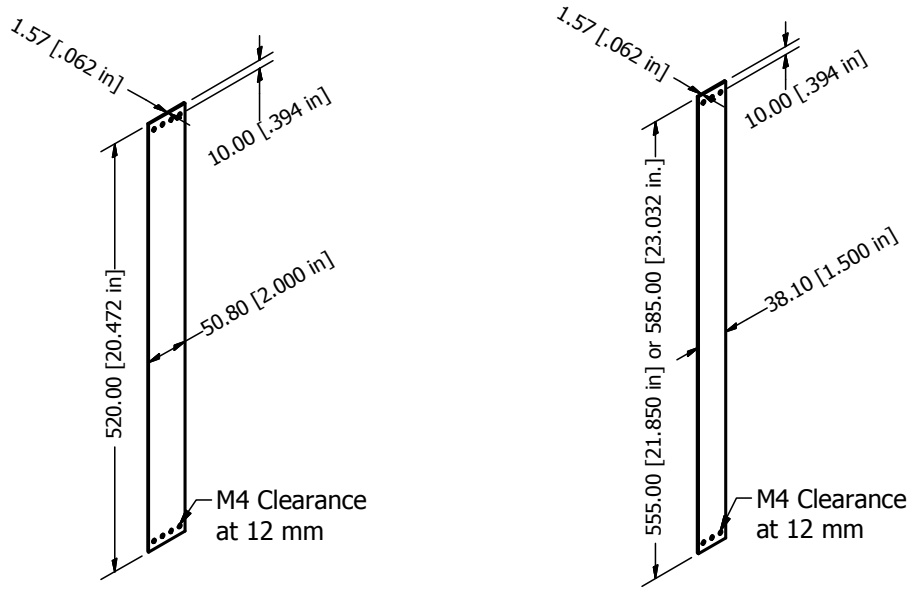

Figure B.3: Isometric views of the spring steel columns for Story 1 (L) and Stories 2 and 3 or Stories 4 and 5 (R) of the shake table specimen.